The Effect of Long-Term Exercise on Neurotransmission

THE EFFECT OF LONG-TERM EXERCISE ON NEUROTRANSMISSION

BY

DIANA HARASYM, B.Eng.

A THESIS

SUBMITTED TO THE SCHOOL OF BIOMEDICAL ENGINEERING

AND THE SCHOOL OF GRADUATE STUDIES

OF MCMASTER UNIVERSITY

IN PARTIAL FULFILMENT OF THE REQUIREMENTS

FOR THE DEGREE OF

MASTER OF APPLIED SCIENCE

Master of Applied Science (2018) McMaster University

(School of Biomedical Engineering) Hamilton, Ontario, Canada

TITLE: The Effect of Long-Term Exercise on Neurotransmission

AUTHOR: Diana HARASYM

B.Eng., (Electrical and Biomedical Engineering)

McMaster University, Hamilton, Canada

SUPERVISORS: Dr. Michael NOSEWORTHY

Dr. Aimee NELSON

NUMBER OF PAGES: xviii, 137

Lay Abstract

Aerobic exercise, such as running, cycling or swimming, is an excellent way to preserve the health of the body and brain in ageing. However, most adults do not meet the recommended daily amount of physical activity. The goal of this work was to determine how and to what extent fitness changes the structure and function of the brain. Aspects of the communication between neurons were evaluated, as well as the thickness of brain regions and integrity of connections between brain structures. Results revealed that fitness improves the connections in areas of the brain devoted to movement, sensation and memory. This suggests that aerobic exercise can preserve these functions during ageing.

Abstract

Aerobic exercise is recognized for its many benefits to the cardiorespiratory system, as well as the brain. For this reason, aerobic exercise has been extensively investigated over the last decade to understand the mechanisms involved in its beneficial effects. However, the model of fitness-related neural plasticity remains incomplete. **Purpose:** The primary goal of this thesis was to investigate the effect of long-term aerobic exercise, in the form of cardiorespiratory fitness, on neurotransmission. In order to achieve this goal, methodological validation was required. The secondary goal was to investigate commonly assessed structural changes associated with exercise, to compare with previous literature. **Materials and Methods:** The first experiment involved phantom and human validation of measures of the neurotransmitter γ-aminobutyric acid (GABA) using magnetic resonance spectroscopy (MRS). Following this objective, the second experiments recruited a total of thirty-five healthy post-menopausal women to investigate the effect of fitness on neurophysiological and structural measures. Transcranial magnetic stimulation (TMS) and MRS were used to evaluate GABA and glutamate (Glu) concentrations and receptor function in the primary motor cortex (M1). Magnetic resonance imaging (MRI) was used to assess cortical thickness (CT) and the microstructure of white matter (WM) tracts. **Results:** Regression analysis found that

fitness improved the microstructure in pre-motor and sensory tracts, as well as the hippocampal cingulum in post-menopausal women. There was no effect of fitness on CT nor neurotransmission. This suggests cardiorespiratory fitness may preserve motor control and tactile acuity, as well as memory in post-menopausal women via improvements in WM microstructure. **Conclusion:** The results provided in this thesis can improve our understanding of how aerobic exercise and cardiorespiratory fitness achieve their benefits in order to create efficient training programs to prevent age-related decline and improve prognosis of age-related disease.

Acknowledgements

I would first like to thank my supervisors, Dr. Michael Noseworthy and Dr. Aimee Nelson, for the opportunity to work in both their labs and their constant support and guidance through the learning processes that is a master's degree. I would also like to thank Dr. Hubert deBruin for his advice and encouragement throughout my time as an undergrad and as a member of my thesis committee. This work would not have been possible without the help of Norm Konyer and the IRC technologists; Carol Awde, Julie Lecomte, and Toni DiLeonardo. I also really appreciate all of the hard work put in by Madi Jenkins to conduct the fitness testing. A huge thanks to all of my lab mates (from both labs) for help with data collections, writing, brainstorming, and the occasional beer; Claudia Turco, Chiara Nicolini, Jenin El-Sayes, Mitch Locke, Stephen Toepp, Mitch Savoie, Patrick Dans, Alejandro Santos Diaz, Nick Simard, Paul Polak, Amy Harrison, Olga Dona Lemus, Evan McNabb, Michael Behr, Mitch Doughty, Neil MacPhee, Aravinthan Jegatheesan, Ethan Danielli, Ashley Gilbank, Cameron Nowikow, and Jimmy Nguyen. It has been a pleasure getting to know every one of you! Finally, I must express my gratitude to my family and friends for providing me with unfailing support and continuous motivation through the process of researching and writing this thesis. This accomplishment would not have been possible without them.

Table of Contents

List of Figures

List of Tables

Notation and Abbreviations

AD	Axial diffusivity
AMPA	α-amino-3-hydroxy-5-methyl-4-isoxazolepropionic acid
AMT	Active motor threshold
BDNF	Brain-derived neurotrophic factor
CNS	Central nervous system
CS	Conditioning stimulus
CSF	Cerebrospinal fluid
DTI	Diffusion tensor imaging
DWI	Diffusion weighted imaging
EMG	Electromyography
EPI	Echo-planar imaging
EPSP	Excitatory post-synaptic potential
FA	Fractional anisotropy
FID	Free induction decay
FT	Fourier transform
GABA	Gamma-aminobutyric acid
Gln	Glutamine

Glu	Glutamate
GM	Gray matter
ICF	Intracortical facilitation
IPSP	Inhibitory post-synaptic potential
LAI	Long-latency afferent inhibition
LICI	Long-latency intracortical inhibition
LIHI	Long-latency interhemispheric inhibition
MD	Mean diffusivity
MEGA-PRESS	Meshcher-Garwoord point resolved spectroscopy
MEP	Muscle evoked potential
MRI	Magnetic resonance imaging
MRS	Magnetic resonance spectroscopy
NMDA	N-Methyl-D-aspartate
PRESS	Point resolved Spectroscopy
RD	Radial diffusivity
RF	Radio frequency
RMT	Resting motor threshold
ROI	Region of interest
SAI	Short-latency afferent inhibition
SICI	Short-interval intracortical inhibition
SIHI	Short-latency interhemispheric inhibition
SNR	Signal-to-noise

STEAM	Stimulated echo acquisition mode
T1	Spin-lattice relaxation time
T2	Spin-spin relaxation time
TE	Echo time
TMS	Transcranial magnetic stimulation
TR	Repetition time
TS	Test stimulus
VOI	Voxel of interest
WM	White matter

Chapter 1: Introduction

1.1 Goal of Thesis

Exercise is planned and structured physical activity aimed at improving and maintaining physical fitness. It is widely implicated in improving overall health and lowering the risk of chronic diseases [1]. Aerobic exercise is a subgroup of exercise aimed at supporting cardiorespiratory fitness and has been extensively investigated for its role in promoting and preserving brain health and function. Specifically, it has been involved in improving learning, memory and executive function, and delaying age-related cognitive decline [2]–[4]. Not only does aerobic exercise have beneficial effects on cognition, it also has beneficial effects on neuropsychiatric disorders such as depression [5], [6]. Additionally, exercise can help curb age-related diseases such as stroke, dementia and Alzheimer's disease by accelerating rehabilitation [7], [8]. However, as of 2013 only about 2 out of 10 Canadian adults actually meet the Canadian Physical Activity Guidelines [9]. The rise in technology and screen time over the next few years are inevitably going to exacerbate these statistics, adding to sedentary lifestyles and poor health outcomes [10].

Despite the large body of evidence indicating the broad benefits of exercise on the brain, the model of how neural plasticity mediates the beneficial effects of long-term exercise remains incomplete [11]. Exercise related improvements in behavioral outcomes are associated with structural changes, including greater gray matter (GM) and white matter (WM) volume [12], greater neural integrity, density and myelination [13], as well as greater perfusion [14] and number of small blood vessels [15]. On a cellular level, these structural changes may be attributed to neurogenesis, synaptogenesis, gliogenesis, and angiogenesis [16], likely mediated by neurotrophic factors acting on the central nervous system (CNS) [11].

Exercise-induced improvements in behavioral outcomes are also associated with change in neural function [17], that can possibly be mediated by changes in underlying structure or changes to molecular aspects of neuronal activity, such as energy metabolism and neurotransmission [18], [19]. Neuronal function is primarily centered around neurotransmission, which allows for the communication between neurons. However, this is one of the least studied mechanisms of long-term aerobic exercise, even though it has large implication in the way the brain functions. Neurotrophic factors, which are linked to the structural changes associated with long-term exercise, also have a large role in synaptic transmission [20]. Raising the question whether long-term exercise does in fact change aspects of neurotransmission.

The primary goal of this thesis was to investigate the effects of long-term aerobic exercise on neurotransmission. Although many neurotransmitter systems exist, the focus was on the most prevalent inhibitory and excitatory neurotransmitters, γ-aminobutyric acid (GABA) and glutamate (Glu), respectively. This thesis tested measures of neurotransmission in sedentary and long-term physically active/ cardiorespiratory fit individuals using *in vivo* non-invasive techniques such as transcranial magnetic stimulation (TMS) and proton magnetic resonance spectroscopy (1H-MRS). Specifically, TMS was used to assess corticospinal excitability, as well as Glutamatergic and GABAergic receptors function indirectly. Multiple TMS circuits were assessed, including intracortical, interhemispheric and afferent, to determine if fitness preferentially affects certain circuits. Finally, the concentration of GABA and Glu were measured via 1H-MRS.

Due to the low concentration of GABA in the brain, as well as the technological difficulty in resolving its spectrum from other more abundant metabolites using 1H-MRS, it is necessary to ensure precise, consistent and reliable measurements. Therefore, to achieve the primary goal of this thesis, two objectives needed to be met. First, phantom validation was required to ensure measured GABA concentrations are consistent over time. This was achieved by constructing a MRS phantom and measuring GABA concentrations randomly over multiple sessions. Next, human validation was necessary to ensure GABA concentrations are comparable with other literature. This

objective was achieved by measuring GABA concentrations in healthy participants in specific regions described in the literature.

The secondary goal of this thesis was to evaluate exercise-induced structural changes in commonly assessed regions of interest. As such, cortical thickness (CT) and WM microstructure were evaluated to compare with previous findings.

1.2 Significance

This research will determine if neurotransmission can be used as a biomarker for fitness related changes in the brain and will contribute to the developing model of neuroplasticity related to exercise [11]. Improving our understanding of the mechanisms by which aerobic exercise promotes brain function is crucial to exploit its neuroprotective and neurorehabilitative effects to the fullest for both healthy and patient populations. The research obtained from this thesis will contribute to basic neuroscience and will have future application to special populations.

Chapter 2: Background

2.1 Magnetic Resonance Imaging

MRI is a non-invasive and non-ionizing medical imaging technique that using magnetic fields and radiofrequency (RF) electromagnetic energy to create a variety of images that provide structural, functional and metabolic information from within the body. Participants are positioned inside the bore of the MRI, where a large external static magnetic field (B_0) is present for the duration of the scan. An RF pulse if applied to modify the quantum properties of different tissues and a signal is measured from tissues reverting back to their original characteristics. This signal is digitized and Fourier transformed (FT) to reconstruct a two-dimensional image. A set of multiple 2D slices can be acquired to represent an area in 3D.

2.1.1 Signal Generation

The MR signal is generated by altering the quantum properties of different nuclei within tissues. Although multi-nuclear MRI is possible with other atoms that possess a quantum spin property and follow the Pauli exclusion principle (^{13}C, ^{15}N, ^{19}F, ^{31}P, ^{23}Na,

etc.), ^{1}H-MRI is still the most common method as ^{1}H is the most organically abundant (99.98%) and receptive (100%) atom. In a classical physics sense, the ^{1}H nucleus can be thought of as a spinning charged particle with an angular momentum (J) and a magnetic moment (μ). In the absence of B_0 the magnetic moment of the nuclei are pointing in random directions, resulting in a tissue net magnetization vector equal to zero. However, in the presence of B_0, some of the magnetic moments align parallel to the field, while others align anti-parallel. Essentially, B_0 causes the splitting of ^{1}H nuclear spin energy levels into two states (+1/2 and -1/2) based on the Zeeman effect. There are always slightly more magnetic moments aligning with the field due to the lower energy level, resulting in a non-zero tissue net magnetization vector. The difference in energy states due to the presence of B_0 creates a torque on the magnetic moment, which causes a secondary spin of the magnetic moment around B_0 referred to as the resonance frequency (ω_0) given by the Larmor equation:

$$\omega_0 = \gamma B_0$$

γ is a constant known as the gyromagnetic ratio, which is the ratio between μ and J. For protons, the gyromagnetic ratio is equal to 42.58 MHz/Tesla which results in a resonant frequency of 128 MHz at 3T. In order to measure a MR signal the tissue net magnetization vector needs to be rotated from the equilibrium position or longitudinal plane, that is in line with B_0 (z-axis), to the transverse plane (x-y plane) using an RF

pulse. This is because the net magnetization vector is virtually impossible to differentiate from B_0, when it is in line with B_0. Usually, the RF pulse produces a 90° flip of the net magnetization vector into the transverse plane, but other angles can be achieved by altering the duration or amplitude of the pulse. The RF pulse creates a magnetic field (B_1) perpendicular to B_0 oscillating at the Larmor frequency using an RF transmitter coil. The net magnetization vector in the transverse plane then induces current in the RF receiver coils and results in an MR signal. A pulse sequence with a single RF pulse produces an MR signal referred to as a free induction decay (FID). However, other more complex pulse sequences exist that create MR signals known as echoes.

2.1.2 Imaging Contrast

Following the RF pulse the MR signal decays while the net magnetization vector precesses back to equilibrium. This decay in the MR signal is a result of two mechanisms that occur simultaneously and determine the contrast of tissues in an image. The first mechanism being the loss of phase coherence of spins or dephasing, which is referred to as transverse or spin-spin T2 relaxation. Specifically, interactions between spins within a tissue (i.e. spin-spin interaction) reduces the magnitude of the transverse component of the net magnetization vector. Spin dephasing is also affected by inhomogeneity in B_0 and magnetic susceptibility effects, which is denoted as T2*. T2 is directly related to tissue properties and is not affected by the strength of B_0, while

T2* will vary as it is dependent on external factors including the uniformity and strength of B_0 and subject composition.

The second mechanism is known as longitudinal or spin-lattice T1 relaxation. This is a result of the longitudinal component of the net magnetization vector recovering to equilibrium as all the spins slowly start re-aligning to B_0 by releasing the energy gained from the RF pulse through interaction with surrounding tissues (i.e. spin-lattice interaction). T1 is affected by both the magnetic field strength of B_0 and tissue properties.

T1 relaxation is much slower than T2 and it can take up to several seconds before the longitudinal magnetization vector is fully restored. This can be seen for fluids which generally have long T1s (e.g. 1500–2000 ms) and T2s (e.g. 700–1200 ms), and in fat-based tissues that have shorter T1s (e.g. 100–150 ms) and T2s (e.g. 10–100 ms). Controlling the timing of pulse sequences allows MR imaging to produce a wide range on contrasts to be able to see the boundaries between tissues. For example, in T1-weighted images fluids are very dark and fat-based tissues are very bright, while in T2-weighted images fluids are bright and fat-based tissues are dark.

2.1.3 Localization

In order to construct an image of a specific area, the MR signals need to be localized

by selectively exciting only ^{1}H in that region. Spatial localization is performed by selecting specific slices in a certain imaging plane (axial, sagittal, coronal) using gradient fields produced by 3 orthogonal gradient coils (Gx, Gy and Gz). For example, axial slices use gradients in the z-direction (G_z), while sagittal slices use G_x and coronal slices use G_y. Gradients fields provide short-term linear gradations of B_0 for a given direction, where one side has a magnetic field strength less than B_0, the opposite greater than B_0 and the isocentre equal to B_0. This can be seen in the following equations:

$$G_x = \frac{\partial B_z}{\partial x}, \qquad G_y = \frac{\partial B_z}{\partial y}, \qquad G_z = \frac{\partial B_z}{\partial z}$$

$$B(i) = B_0 + iG_i$$

As a results the Larmor equation for a given direction becomes:

$$\omega_0 = \gamma B(i)$$

Each slice, for a given imaging plane, is then selectively excited by an RF pulse with a center frequency at this new Larmor frequency, based on its location from the isocentre of the bore. The thickness of the slice is determined by the bandwidth of the RF pulse and the size of the gradient. Thus, the larger the gradient or the smaller the RF bandwidth the thinner the slice.

2.1.4 K-space and Image Reconstruction

Once a slice is selectively excited, the resulting MR signals needs to be sampled or encoded in k-space, in order to reconstruct an image. The peripheral regions of k-space contain the high frequency components of the image, which define the edges and detail of the image (i.e. resolution). While the center of k-space contains low frequency components that define the general shapes and contrast of the image (i.e. signal-to-noise). There are numerous encoding methods that trade-off between resolution, signal-to-noise and acquisition time by altering the encoding trajectory and the number of points sampled in k-space. Traditional cartesian encoding trajectories occurs line by line going from left-to-right, while more complex trajectories include spiral (moving outward from the center of k-space), radial (outward spokes from the center of k- space) and echo planar imaging (EPI; line by line alternating between left-to-right and right-to-left).

The horizontal axis of k-space is commonly denoted as k_x and represents frequency-encoding, while and vertical axis is known as k_y and represent phase-encoding. Gradient fields are also used for frequency- and phase-encoding. For example, if images are acquired in the axial plane, then slice selection occurs in the z-direction using G_z, frequency-encoding occurs in the x-direction using G_x, and phase-encoding occurs in the y-direction using G_y. The number of MR signals acquired equal the number of phase-encoding steps, meaning MR signals are acquired using the same

frequency-encoding gradient but multiple different phase-encoding gradients. However, in EPI imaging all phase-encoding steps are acquired in a single MR signal allowing for ultrafast acquisition of multiple slices and volumes. Once all the MR signals are encoded into k-space it is then 2D FT transformed to reconstruct the image.

2.1.5 Diffusion Imaging

Diffusion weighted imaging (DWI) is an MRI technique that is able to map the diffusion rate of water within tissue in a certain direction. Diffusion of water generates contrast in an image that varies with tissue type, morphology, and integrity. Diffusion tensor imaging (DTI) uses DWI in multiple directions to model a 2^{nd}-order tensor representing the net diffusion of a specific voxel. Components of the modelled diffusion tensor are related to the microstructural properties of white matter (WM) tracts within the brain, since the diffusion of water tends to be restricted along the axon (anisotropic). Whereas the diffusion in gray matter (GM) is less restricted, hence less anisotropic. Diffusion within cerebrospinal fluid (CSF) is isotropic or completely unrestricted. Below (**Figure 1)** is an ellipsoid model of the diffusion tensors, with eigenvectors and corresponding eigenvalues for all 3 directions:

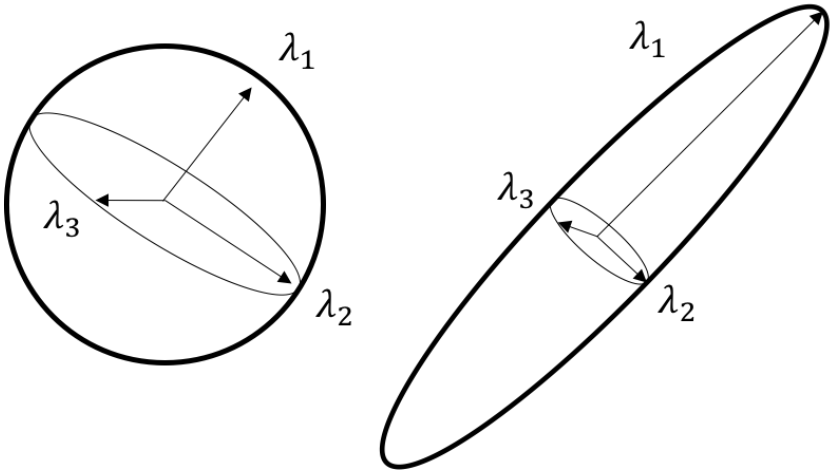

Figure 1: *Ellipsoid model of diffusion tensors. The image on the left depicts completely unrestricted or isotropic diffusion, while the image on the depicts anisotropic or restricted diffusion in two directions.*

Fractional anisotropy (FA) is a measure of the anisotropy of a given tensor and represents the general integrity of WM tracts. A measure of zero indicating isotropic diffusion in all directions and a measure of one indicating anisotropic diffusion along one direction only [21]. The following is the formula to quantify FA using the different tensor components:

$$FA = \frac{\sqrt{3}}{\sqrt{2}} \frac{\sqrt{(\lambda_1 - MD)^2 + (\lambda_2 - MD)^2 + (\lambda_3 - MD)^2}}{\sqrt{{\lambda_1}^2 + {\lambda_2}^2 + {\lambda_3}^2}}$$

Other measures quantified using the tensor model include axial diffusivity (AD), radial

diffusivity (RD) and mean diffusivity (MD). AD measures the diffusion along the principle eigenvector, such that AD = λ_1 and may reflect axonal loss or degradation [22]. RD measures diffusion in the outward direction and appears to reflect the myelination of axons [22]. The following equation represents RD [21]:

$$RD = \frac{\lambda_2 + \lambda_3}{2}$$

Finally, MD measure the average diffusion of all three eigenvectors [21] as follows:

$$MD = \frac{\lambda_1 + \lambda_2 + \lambda_3}{3}$$

It is assumed the value of MD is negatively related to the density of cells [22]. However, the interpretation of FA, AD, RD and MD should be taken with a grain of salt, as crossing fibers may affect the values of FA, AD and RD [21].

2.1.6 Spectroscopy

Magnetic resonance spectroscopy (MRS) is an MRI technique that can evaluate and quantify tissue metabolites *in vivo*. Essentially, it is an *in vivo* application of nuclear magnetic resonance (NMR) spectroscopy. The MR signal described earlier, an FID, can actually provide information on the chemical environment of ^{1}H nuclei based on their

T2 and T1 relaxation. The FID is collected in the time domain and is FT to the frequency domain to show the specific resonance frequency associated with each ^{1}H environment. This spectrum is depicted as signal intensity (amplitude) against chemical shift (frequency peak position). The chemical shift is field strength dependent and is usually reported in field-independent units: parts-per million of the proton frequency (ppm). An example ^{1}H-NMR spectrum of ethanol is depicted in **Figure 2**.

The number of distinct peaks represents the number of chemically distinct ^{1}H environments. Electronegative atoms like oxygen and aromatic rings withdraw electron density from attached protons altering their local magnetic field. This is known as de-shielding and causes protons to oppose B_0 as they are returning back to equilibrium, which results in a downfield shift of their peaks to lower frequencies (greater ppm). The splitting or multiplicity of each peak in a spectrum is associated with the chemical environment of neighboring nuclei, and are caused by either homonuclear (^{1}H-^{1}H) or heteronuclear (^{1}H-^{13}C) J-coupling. Specifically, it is the coupling between the spins of a proton and neighbouring nuclei that alters the protons local magnetic field into several possible states. These states each have a slightly different shift in frequency. Regardless of the strength of B_0, J-coupling causes the same absolute degree of separation (in Hz) between peaks.

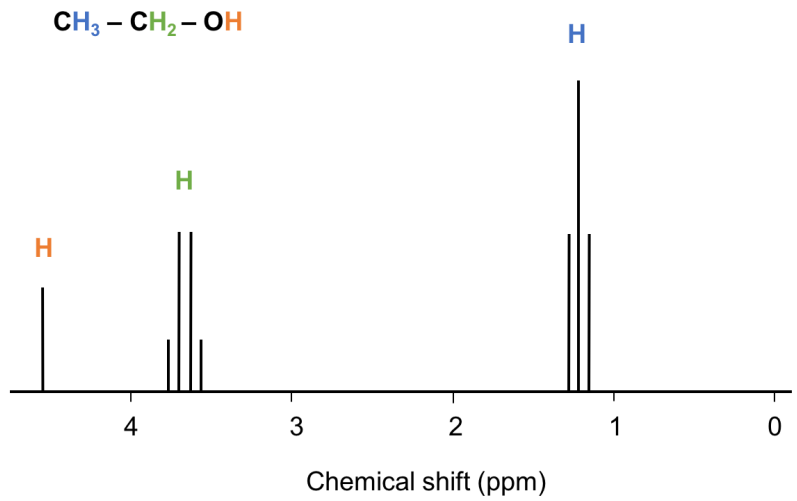

Figure 2: *Example 1H-NMR spectra of ethanol. Each proton environment affects the chemical shift (ppm) and splitting of the spectra, while the integration of peaks represents the number of atoms.*

In NMR, peak intensity or the integral (area under the curve) is associated with the nuclear count (number of atoms). Because MRS in tissues is a combination of spectra from multiple metabolites, the area under the spectra for a given metabolite is considered to be the concentration of that metabolite. This concentration can be expressed as an area or a ratio with reference to another metabolite. Concentration in institutional units (mM/L) can also be estimated by using water as a reference and assuming a certain water contribution in the tissue being measured [23], usually around 55M but this can vary between tissue types. These spectra can be easily quantified using fitting tools that linearly combine basis spectra or fit Lorentzian functions to metabolite peaks, such as LCModel [24], [25], Tarquin [26], JMRUi [27].

MRS signals are localized to specific regions of the body or volumes of interest (VOI) using gradients to sequentially select three orthogonal slices. This technique is usually referred to as single voxel spectroscopy (SVS) or single-voxel acquisition (SVA). Single-voxel sequences can be used to acquire data from multiple voxels using chemical shift imaging (CSI) or MRS imaging (MRSI). Although CSI has the advantage of obtaining multiple VOIs, SVS is still that method of choice to obtain consistent and high quality spectra [28]. Point RESolved Spectroscopy (PRESS) and Stimulated Echo Acquisition Mode (STEAM) are the most common sequences used to localize and acquire single-voxel spectra [29]. PRESS uses a slice selective 90° pulse followed by two slice-selective 180° refocusing pulses. STEAM forms a stimulated echo from a single voxel using three slice selective 90° pulses. Compared to PRESS, STEAM can achieve a shorter echo time (TE), which avoids signal loss for metabolites with short T_2, spectral distortion from J-coupling, as well as superior water suppression. It can also attain better voxel profiles with lower outer volume lipid contamination and baseline distortion. However, STEAM theoretically obtains only half the available signal (SNR) that PRESS does and is more sensitive to spin displacement effects due to macroscopic motion and diffusion [28], [30].

Signal-to-noise (SNR) of each spectrum is dependent on voxel size and acquisition time. Common voxel sizes used for MRS in the brain are between 8 cm^3 and 27 cm^3. Increasing voxel size and acquisition time, would increase the SNR of most

metabolites. However, large voxels are susceptible to partial volume affects due to the different composition of tissue (tissue heterogeneity), including lipid and macromolecule contamination. Large voxels also suffer from poor homogeneity of B_0 due to magnetic susceptibility affects near tissue boundaries, as it is difficult to shim large and non-cubic voxels resulting in signal loss.

Due to the large concentration of water *in vivo*, the water (H_2O) resonance at around 4.6 ppm is the predominant signal in ^{1}H-MRS. Since the FT of an FID is a Lorentzian function, it is common to assess spectral quality by determining the line-width or the full-width at half max (FWHM) of the water peak (in Hz). The line width is primarily associated with the homogeneity of the magnetic field, which affects T2*. Shimming coils are used to help homogenize the magnetic field and narrow the line-width. A well shimmed spectrum will have a maximum line-width of 5 Hz for phantoms and 12 Hz for subjects. However, this is also dependent on voxel size and placement. In order to get information from the rest of the spectra, the dominant water peak needs to be effectively suppressed. CHEmical-Shift-Selective pulse (CHESS) sequences are used for this purpose, and avoid unwanted echoes and interference with the localization [31].

Temperature and pH variations can also affect the chemical shift of the MR spectra making it difficult to fit using basis sets. Specifically, the resonance frequency of water is sensitive to temperature and shifts the entire spectra by about -0.01 ppm/ºC [28]. pH

variations in ^{1}H-MRS are only known to alter the resonance of lactate. However, these factors rarely affect MRS in humans, as the physiological temperate and pH range is quite narrow.

Due to the low concentration of neurometabolites such as GABA, and its spectral overlap with other more abundant metabolites it is necessary to use specialized methods to accurately and reliably measure GABA *in vivo*. The most widely used method for detecting GABA at 3T is MEshcher-GArwoord Point RESolved Spectroscopy (MEGA-PRESS) [32], [33], which is a J-difference edited version of PRESS. Meaning this technique subtracts PRESS sequences with 2 different frequency selective pulses as seen in **Figure 3**. This allows the GABA spectrum signal at 1.9 ppm, which is coupled to the signals at 3.0 ppm, to be separated from the remaining signals at 3.0 ppm that are not directly coupled to the GABA signal at 1.9ppm [34].

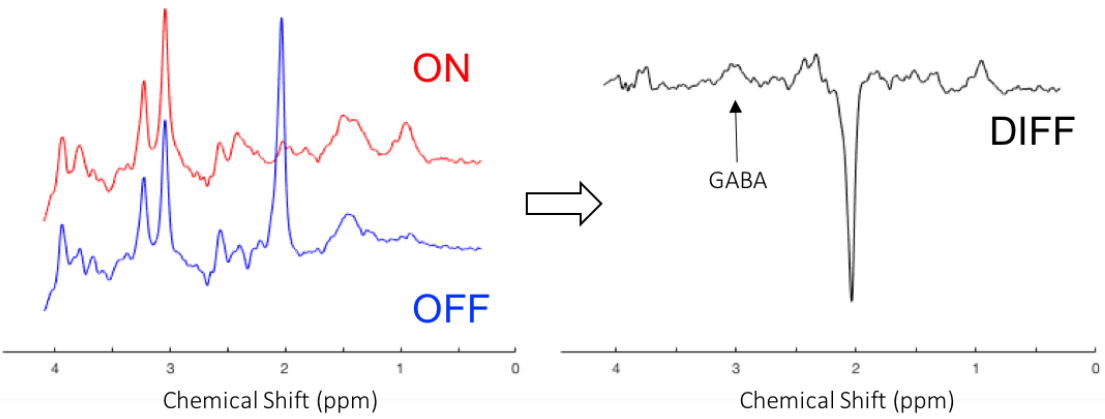

Figure 3: *Depiction of MEGA-PRESS spectra. The OFF spectra is subtracted from the ON spectra to create the difference spectra (DIFF), which enables better detection of GABA at 3.0ppm.*

Other options to help differentiate GABA from the rest of the spectra include using systems with higher field strengths or two-dimensional MRS. Higher field strengths (4T-7T) disperse the signals along the chemical axis (i.e. better field resolution). Hence, acquiring spectra of GABA and Glu at higher field strengths would allow for more accurate measurements of neurotransmitter concentrations. Although high field sequences and 2D MRS show more promise for the detection of both GABA and Glu, and are likely to be used more often in the future, they are not yet widely applied [35]. Another option is to use sequences that have been optimized to measure certain metabolites, such as a STEAM sequence with a specific acquisition parameters that are able to adequately separate GABA, Glu and Gln [36].

2.2 Transcranial Magnetic Stimulation

Transcranial magnetic stimulation (TMS) is a non-invasive method of probing corticospinal function. Although, transcranial electrical stimulation (TES) can also be used to assess the function of neural pathways, it uses high-voltage which is far more uncomfortable than TMS. Faraday's law of electromagnetic induction is the basic principle explaining the ability of TMS to activate neurons in the cortex. TMS is comprised of a coil of wound copper wire connected to a large capacitor that produces a peak magnetic field in the coil similar to that of B_0 for an MRI, around 1-2T, but only for a short period of less than 1ms [37]. The coil itself can be circular or a figure-of-eight shape, although the shape of the coil impacts the intensity and specificity of stimulation. Specifically, a figure-of-eight shape produces a much more intense and focal magnetic field than a circular coil.

2.2.1 Physiology

The magnetic field produced is perpendicular to the coil, and can pass through the skull when the coil is placed tangentially to the scalp. This induces electric fields within the cortex parallel to the coil. With the necessary current produced by the induced electric field it can depolarize the axon of a neuron, generating an action potential. Stimulation can be applied to various region of the cortex but the primary motor area (M1) is most commonly investigated. The physiological basis of TMS was first investigated through spinal cord epidural recordings after TES [38]. Following TES, it was proposed that

there is an initial descending volley related to the direct activation of the corticospinal axons, termed the D-wave. Following the D-wave, there are indirect descending volleys approximately 1.5ms apart called I-waves, which are believed to be interneurons that are synapsed to corticospinal neurons. This is depicted in **Figure 4.** I-waves are numbered based on their latency in the recordings, with the I1-wave being an interneuron that is in closest proximity to the corticospinal neuron. However, for TMS the recordings were highly dependent on coil orientation such that a posterior-anterior orientation produced an initial epidural volley representing an I1-wave, an anterior-posterior orientation produces an I3-wave, and a lateral-medial orientation produced a D-wave [38]. Although, at very high TMS intensities the D-wave can be elicited [38].

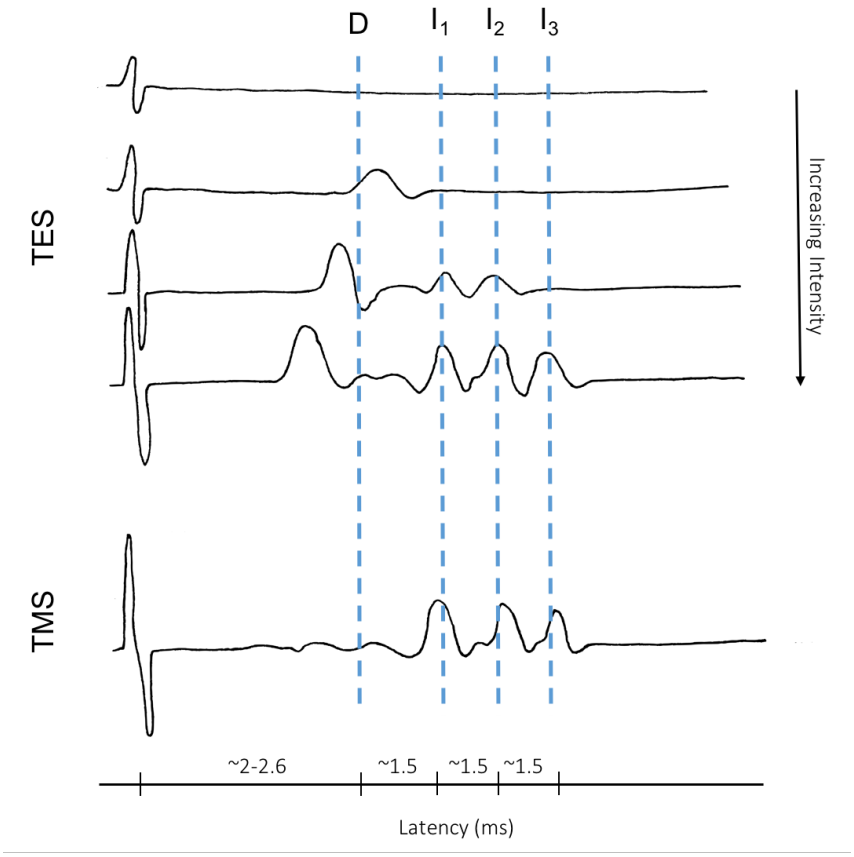

Figure 4: *Example of epidural spinal recordings after TES (top)and TMS (bottom). TES elicits a D-wave followed by I-waves, which increase in number with increasing stimulator intensity. TMS does not easily elicit the D-wave and is mainly comprised of I-waves.*

It is speculated that TMS activates the axons of interneurons parallel to the coil in layers II and III of M1 that tans-synaptically activate corticospinal neurons in layer V, producing I-waves [39]. In most TMS studies of M1, the resulting descending volleys are recorded non-invasively in a target muscle, instead of the spinal cord, through the activation of motoneurons synapsed to the corticospinal tract. This motor evoked

potential (MEP) can be recorded using electromyography (EMG) and are usually evaluated as the peak-to-peak amplitude in mV. The temporal dispersion of D-waves and I-waves causes phase cancellation of motor unit potentials, due to the asynchronous activation of motoneurons, resulting in MEPs always having smaller amplitudes than compound muscle action potentials (CMAP) recorded from electrical stimulation of peripheral nerves [37]. This highlights the fact that MEPs involve both central and peripheral neurons, therefore any interpretation of results cannot assume purely cortical changes.

2.2.2 Motor Thresholds

Motor thresholds can be determined while the target muscle is at rest referred to as resting motor threshold (RMT), or actively contracting at 10-20% of their maximal voluntary contraction (active motor threshold; AMT), and is defined as the lowest TMS intensity that activates motoneurons to elicit a reliable MEP in the target muscle [37]. RMT and AMT can be determined using the relative frequency method to find the lowest TMS intensity that produces an MEP amplitude greater than 50 μV (RMT) and 200 μV (AMT) in 10 out of 20 trials [37], [40]. Statistical methods such as Parameter Estimation by Sequential Testing and maximum Likelihood Regression (ML-PEST) [41] are also available and provide a more accurate estimation and require a smaller number of test pulse than the relative frequency method [37], [42]. Drug studies determined that motor thresholds are mainly the result of membrane excitability of

intracortical and corticospinal neurons related to voltage-gated Na^+ channels [43]. However, corticospinal synaptic excitability, related to glutamatergic receptors, may also play a role in measured thresholds [43]. RMT is always greater than AMT and there is also roughly a 3ms delay in resting MEPs compared to active [37]. This is a result of many lower motor neuron being in a subliminal state due to the recruitment of motor units, meaning they are close to the threshold of an action potential. This allows an MEP to be easily elicited through further depolarization of these motoneurons by mainly an I1-wave at lower TMS intensities [37], [44]. While the resting state require a larger excitatory input to sufficiently depolarize and recruit lower motor neurons, that can only be achieved by the temporal summation of later I-waves generated from higher TMS intensities.

2.2.3 Motor Evoked Potential

MEP amplitudes at a single TMS intensity provide no information about corticospinal excitability, instead MEPs are recorded as a function of TMS intensity called MEP recruitment curves (RC) or input-output curves (I-O curve). The RC itself is usually a sigmoidal function, with a baseline, steep rising slope and a final plateau [45]. Each of these aspects relate to different mechanisms of excitability, and have been shown to not change together [46]. The baseline, for example, is related to RMT (or AMT for active curves), while the slope of the recruitment curve is indicative of glutamatergic, GABAergic and neuromodulation synaptic excitability of the corticospinal pathway

[43]. The slope is also associated with the recruitment of corticospinal neurons in the cortex, since some components of the corticospinal pathway may require a greater TMS intensity for excitation or may be further away from the coil and require a higher intensity to be reached [45]. The plateau of the recruitment curve is thought to reflect the balance between excitatory and inhibitory synaptic components of the corticospinal volley, but is also associated with the phase cancellation of motor unit potentials due to asynchronous motoneuron activation [37], [47].

2.2.4 Intracortical Circuits

Receptor function of intracortical circuitry of M1 can be indirectly assessed through paired-pulse TMS protocols that delivers a conditioning stimulus (CS) followed by a test stimulus (TS). The TS intensity is set to a reference value of either 1mV or 120% RMT to allow for the observation of facilitation or inhibition [37]. However, using a TS at the inflection point of the RC is ideal as it would allow for equal amounts of facilitation and inhibition [37]. Short-interval intracortical inhibition (SICI) is thought to represent short-lasting or fast inhibitory postsynaptic potentials (IPSPs) mediated by $GABA_A$ receptors that suppress later I-waves (I_2, I_3, I_4), and are modulated by dopamine, nicotine, and noradrenalin [43], [44]. SICI is elicited by a subthreshold CS, followed by a supra-threshold TS at an interstimulus interval (ISI) of 1-5ms [48]. Although, refractory processes of the corticospinal axons are likely responsible for the inhibition seen for ISIs less than 1.5ms [43]. Variations in CS results in a U-shaped

SICI magnitude curve, which means SICI represents a balance between facilitation and inhibition in the corticospinal pathway [43]. On the other hand, long-interval intracortical inhibition (LICI) represents slow IPSPs likely mediated by $GABA_B$ receptors that also suppress later I-waves (I_2, I_3, I_4) [38]. LICI is produced by a supra-threshold CS, followed by a supra threshold TS at an ISI of 50-200ms [37]. At an ISI of 50ms, later I-waves show facilitation although MEPs are inhibited, suggesting the inhibition may occur in the spinal cord [44]. Intracortical facilitation (ICF) represents excitatory postsynaptic potentials (EPSPs) likely mediated by the glutamatergic N-Methyl-D-aspartate (NMDA) receptors, and modulated by norepinephrine [37]. However, there are no changes to the amplitude or number of I-waves with ICF, suggesting that ICF may recruit additional circuits not involved in the production of I-waves [44]. ICF can be evaluated using a sub-threshold CS and a supra-threshold TS similar to the SICI protocol but with a longer ISI of 8-30ms [37]. ICF is also assumed to represent net facilitation due to its pharmacological relationship with SICI [43], which can explain the U-shaped SICI magnitude curve. However, unlike SICI the magnitude of ICF increases with larger CS [37].

2.2.5 Afferent Circuits

The receptor function of afferent circuitry can be evaluated indirectly with peripheral nerve stimulation as the CS preceding single-pulse TMS to the motor cortex as the TS. These circuits likely incorporate projections from the thalamus to the primary

somatosensory cortex (S1), and from S1 to M1 [49]. Short-latency afferent inhibition (SAI) represents fast IPSPs shown to be mediated by both $GABA_A$ [50] and acetylcholine [51] receptors. It is produced by sensory nerve stimulation (e.g. median, ulnar, digital) followed by a supra-threshold TMS stimulus at an ISI around the latency of the N20 event-related potential (20-25ms) plus an additional few milliseconds to account for the conduction time of the afferent potential from S1 to M1 [37]. The N20 latency can be determined through the recording of somatosensory evoked potentials (SEP) using electroencephalography (EEG) over S1, which is located 2 cm posterior to C3 using the international 10-20 system. A recently published study has determined that an ISI of N20+4ms produces a greater depth of inhibition than an ISI of N20+6ms [52]. The magnitude of SAI increases with a stronger CS and has been proven to have a cortical origin since it suppresses later I-waves (I_2, I_3, I_4) similarly to intra-cortical inhibition [44]. Long-latency afferent inhibition (LAI) is elicited using the same procedures as SAI but with an ISI around 200ms [37]. Currently no studies have investigated the effect of LAI on I-waves, but it has been shown that LAI is also mediated by $GABA_A$ receptors [52]. Similarly to SAI, the magnitude of LAI increases with a stronger CS until all sensory afferents are recruited in the median nerve. However, when the digital nerve of the second digit is stimulated, LAI is only present with a CS that activates all sensory afferents and does not change with CS intensity [53]. Both SAI and LAI do not seem to be related to tactile acuity nor motor skills [54], but are attenuated due to painful stimulation [49]. Cutaneous versus mixed nerve

stimulation require different ISIs to evoke both SAI and LAI, but do not affect the magnitude of inhibition [49]. Additionally, nerve stimulation closer to the target muscle for both SAI and LAI allow for greater inhibition, likely due to somatotopic organization in the brain [49].

2.2.6 Interhemispheric Circuits

The receptor function between M1s in both hemispheres can also be assessed through short- and long-latency interhemispheric inhibition (SIHI and LIHI). It is unknown exactly which receptors are involved in SIHI, but it is likely cortical level GABAergic receptors that are able to suppresses later I-waves (I_2, I_3, I_4) through fast IPSPs via a transcallosal route [44]. SIHI is elicited by a supra-threshold CS to the contralateral M1 and a supra-threshold TS to the ipsilateral M1 at an ISI of 8-12ms. LIHI represents slow IPSPs mediated by $GABA_B$ receptors [55] and is elicited by a similar paired-pulsed protocol as SIHI but with an ISI of 40-50ms [37]. Epidural I-waves have not been assessed for LIHI, but it is postulated that the inhibitory circuit includes trans-callosal projections, as well as projections from other motor related cortices such as the contralateral dorsolateral prefrontal cortex, dorsal premotor cortex and S1 [37].

Chapter 3: Literature Review

3.1 Neurotransmission

Chemical synaptic transmission is the primary method for signal transmission between neurons in the CNS and plays a major role in brain function. This form of neurotransmission occurs through the diffusion of neurotransmitters from vesicles in the pre-synaptic terminal to receptors in the membrane of the post-synaptic terminal. An action potential in the pre-synaptic neuron opens voltage-gated Ca^{2+} channels at the terminal, this influx of Ca^{2+} allows for the release of neurotransmitters into the synaptic cleft. They bind to receptors on the post-synaptic membrane that lead to the opening or closing of ion channels, changing the conductance of the post-synaptic neuron to excite or inhibit an action potential. Unlike electrical synapses (e.g. gap-junctions), chemical synapses can only transmit signal in the direction of the axon and cause a delay of about 0.3-5ms. However, chemical transmission is able to alter the magnitude of the signal effortlessly through inhibition or excitation.

3.1.1 Receptors

Numerous neurotransmission systems exist, although the CNS is comprised mainly of glutamatergic excitatory synapses, with about 20-25% of GABAergic synapses in the form of inhibitory interneurons [56]–[60]. There are three major types of ionotropic glutamatergic receptors: α-amino-3-hydroxy-5-methyl-4-isoxazolepropionic acid (AMPA), kainate, and NMDA and one type of metabotropic glutamate receptor (mGlu). The NMDA is one of the most significant glutamatergic receptors as it is thought to be involved in long-term potentiation (LPT) or long-term synaptic plasticity [61]. This ligand-gated channel is only activated in the presence of glycine and if the membrane is initially depolarized by another glutamatergic receptor (e.g. AMPA), which allows Mg^{2+} to be expelled from the NMDA receptor and Na^{+} and Ca^{2+} to enter (while K^{+} exits). The activity of the NMDA receptor has been shown to be highly connected to brain-derived neurotrophic factor (BDNF), which is a protein thought to be involved in activity dependent neural plasticity [20]. Firstly, activation of NMDA receptors and influx of Ca^{2+} lead to expression of BDNF [62]. Intern BDNF can upregulate NMDA receptor activity through phosphorylation, allowing for LTP of glutamatergic function [63].

GABAergic receptors come in two forms: $GABA_A$ and $GABA_B$. The $GABA_A$ receptor is an ionotropic receptor that directly contributes to Cl^{-} influx, while the $GABA_B$ receptor is a metabotropic receptor. The second-messenger cascade of $GABA_B$

indirectly opens K^+ channel that allow inhibition to last longer than with $GABA_A$. Additionally, BDNF is involved in GABAergic activity and has also been shown to decrease inhibition, possibly through $GABA_A$ receptor phosphorylation or transcription [20], [64]. Downregulation of Cl^- transport by BDNF may also decrease GABAergic inhibition [20].

3.1.2 Neurotransmitters

Both GABA and Glu are neurotransmitters that are synthesized from glutamine (Gln) through glutamate-glutamine and GABA-glutamine cycling. Gln is catalyzed by phosphate-activated glutaminase (PAG) in glutamatergic and GABAergic neurons to produce Glu. However, in GABAergic neurons Glu is catalyzed further though a reaction mechanism involving glutamic acid decarboxylase (GAD) to synthesize GABA. Glu that is released from neurons during neurotransmission is taken up by astrocytes and stored as Gln by glutamine synthetase (GS), prior to being recycled back to the neuron. GABA follows a similar recycling path, by being taken up by astrocytes and converted to Gln via the intermediate succinate [65], [66]. Glutamate-glutamine cycling shows the metabolic relationship between neurons and glial cells and is the primary method for the replacement of both Glu and GABA in the neuron. GABAergic and glutamatergic neurons can also up-take both extracellular GABA and Glu, and recycle them by converting them to the correct neurotransmitter needed [67]. This close biochemical and functional relationship between GABA and Glu plays a crucial role in

maintaining the inhibitory and excitatory stability of the brain and managing cortical and corticospinal communication [68]. Synaptic potentiation induced by BDNF does not only occur by modulating receptor function, but also by modulating neurotransmitter release of Glu [69] and synaptic/extrasynaptic clearance of GABA [64].

GABA is the most prevalent inhibitory neurotransmitter found in the mammalian CNS. There are three forms of GABA present in the CNS; vesicular, intracellular and extracellular. The majority of GABA is found in the cytoplasm of neurons (i.e. intracellularly), and is assumed to have a role in metabolism, while vesicular GABA is found in the neuronal synapse and mediates neurotransmission through $GABA_A$ and $GABA_B$ receptors [70]. Free extracellular GABA on the other hand, acts mainly as a neuromodulator on extra-synaptic $GABA_A$ receptors [71], [72]. The concentration of GABA in the brain is about 1 mM/L [73], [74], which is significantly lower than other dominating metabolites and is obscured by more abundant co-resonating metabolites such as creatine (Cr) at 3.0 ppm, Gln and Glu at 2.3 ppm, and N-acetyl aspartate (NAA) at 1.9 ppm in MRS as seen in **Figure 5** [35]. MRS measures of GABA does not differentiate between the different forms of GABA but rather give a total concentration of GABA in a regional volume. However, there is evidence that the MRS GABA measures reflect extracellular GABA rather than vesicular or cytoplasmic [66], [72].

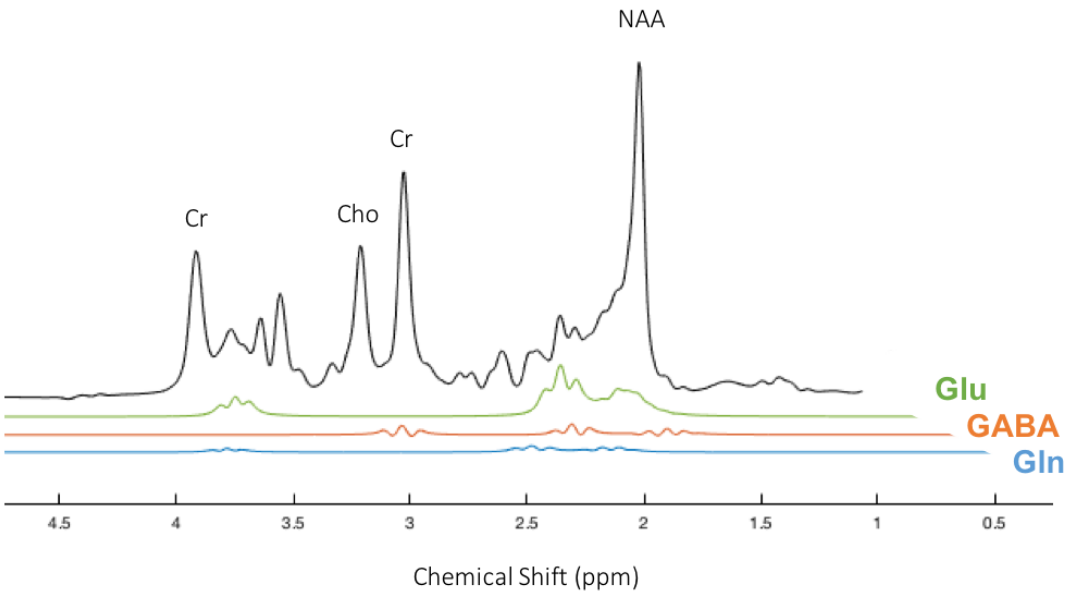

***Figure 5**: A common PRESS spectrum of the brain, along with individual GABA, Glu, and Gln spectra. It is evident that GABA, Glu, and Gln are co-resonating and are obscured by more abundant neurometabolites.*

Glu is the dominant excitatory neurotransmitter in the human brain, and is also found in vesicular, intracellular and extracellular form. Similar to GABA, vesicular Glu is found in the neural synapse and mediates neurotransmission through ionotropic and metabotropic Glu receptors. While the largest concentration of Glu is involved in metabolism in the cytoplasm of GABAergic and glutamatergic neurons and glia. However, due to the neurotoxic potential of Glu only a small portion of Glu is present extracellularly and within the synapse [70]. The concentration of Gln and Glu in the human brain are about 3-6 mM/L and 6-13 mM/L, respectively. Both Glu and Gln have

similar MRS spectra making it difficult to get accurate measures of each separately. Regardless of the high concentration of Glu, its spectra are usually contaminated by other metabolites such as Gln, GABA, and NAA [75]. Note that the concentration of Glu is about 10x the concentration of Gln, and hence the composite Gln + Glu (Glx) measure is primarily driven by Glu [66].

3.2 Exercise-Related Changes to Neurotransmission

3.2.1 Neurotransmitters

In MRS studies of long-term exercise, highly fit individuals have been shown to have lower resting Glu levels in the visual cortex [76]. Conflictingly, more physical activity predicts a higher concentration of Glu in the visual cortex [77]. Although this outcome may, in part, be the result of neural activation from visual stimuli [78]. Effect of acute exercise on Glu levels have not shed any light on the conflicting evidence of long-term changes to neurotransmission. Following an acute bout of exercise Glx has been shown to increase in the visual cortex [77], [78] and in anterior cingulate cortex [77]. This increase in Glx is likely related to the increase of peripheral lactate (Lac) following exercise, which has been shown to be taken up by the brain [79], [80]. Lac does not accumulate in the brain or exit the brain, but instead is used for energy metabolism and synthesis of Glu through the Lac-cycle [77], [78], [81]. Increase in Glu in the visual cortex has also been seen due to neural activation from visual stimuli [78]. A decrease

in absolute Glx concentrations (|Glx|) and no change in Glx:Cr are also seen following acute exercise [76]. However, in this study there was a significant decrease in Cr following acute exercise, which would affect the Glx:Cr ratio calculated. These conflicting results show the need for further investigation into the role of exercise on Glu concentrations.

Currently no studies have investigated the effect of long-term exercise on GABA concentrations in the brain. Primarily due to its small concentration in the brain and difficulty resolving it from the rest of the spectrum. GABA has been shown to increase in the visual cortex after an acute bout of exercise [77]. GABA plays a role in neurotransmission, as well as an intermediate in metabolism. Hence, the increase in GABA levels following acute exercise may just be related to increased cerebral blood flow and metabolic activity. With respect to long-term changes, the question remains whether this increase in GABA is temporary or persists throughout long-term exercise.

3.2.2 Receptors

Very few studies have considered the effect of chronic exercise on corticospinal excitability and receptor function. It has previously been shown that long-term exercisers and sedentary individuals do not differ in RMT [82]–[86], AMT [82], [85], or MEP amplitude [82], [85]. This suggests that exercise does not induce changes in corticospinal excitability of the upper limb, and hence membrane excitability.

However, MEP amplitudes of active lower limb muscles are larger in low physically active individuals compared to highly active adults [87]. This may be caused by differences in the muscle composition (muscle fibre concentrations and area) between physically active individuals, who primarily use their lower limbs during exercise, and sedentary individuals [88]–[90].

Both sedentary and long-term exercisers show similar levels of short-interval intracortical facilitation [82], ICF [82], SICI [82], [85], and contralateral silent period [85], suggesting intracortical receptor function is not affected by long-term aerobic exercise. Measures of trans-callosal inhibition, such as ipsilateral silent period [83], [84], [91] are greater in long-term exercisers, although LIHI is unaffected [84]. This suggests that exercise-induced neuroplastic changes selectively affect certain GABAergic neurons involved in trans-callosal communication. However, not all TMS circuits have been investigated. Afferent circuits such as SAI and LAI may play an important role in exercise-induced potentiation.

Chapter 4: Hypothesis

As discussed in the literature review, BDNF, a modulator of activity dependent neuroplasticity generally downregulates GABAergic function and upregulates Glutamatergic function [20]. Additionally, a number of human studies have seen a decrease in GABA concentrations in the sensorimotor cortex due to endogenous plasticity related to motor learning and ischaemic forearm block [66]. Based on these findings it is hypothesized that GABAergic activity and concentrations will be decreased as a function of fitness/ long-term aerobic exercise, while Glutamatergic function and concentrations will be increased. Previous studies investigating exercise-induced structural changes in the both men and women have shown increases in cortical thickness in areas of the pre-frontal [92], [93] cortex and pre/post central gyrus [92]. Additionally, one study looking at a population of women only saw an increase in GM volume in the pre-frontal cortex as a results of fitness [94]. Numerous studies have also shown that fitness improves WM microstructure in the corpus callosum, corona radiata, cingulum, and superior longitudinal fasciculus [95]–[97]. Therefore, it is hypothesized that results will be similar to previous studies that showed an increase in cortical thickness and improved WM microstructure.

Chapter 5: Experiment 1

The first experiment set out to meet objectives of the primary goal of the thesis. That is to validated GABA measurements by ensuring they are stable over time and comparable to previous literature.

5.1 Introduction

GABA is the most prevalent inhibitory neurotransmitter in the brain. Due to its importance in both normal brain function and in disease, there is considerable interest in reliable non-invasive measurements *in vivo*. The concentration of GABA is significantly lower than other dominating metabolites and is obscured by more abundant co-resonating metabolites such as Cr, NAA and Glu [35]. Thus, it is necessary to ensure precise, consistent and reliable measurements. The purpose of this study was to ensure the stability of the local MR system with respect to GABA measurements using both phantom and human validation. A MRS phantom was developed to ensure the consistency of GABA concentrations, with the goal of long term quality assurance measures. Next, GABA concentrations were verified in human participants using MRS software specifically developed for GABA, to confirm measured concentrations of

GABA are comparable to previous findings in the healthy population. This experiment will lead the way for the development of a daily quality control protocol to ensure future GABA MRS studies using the local MR system are reliable.

5.2 Methods

5.2.1 Phantom Validation

A 20cm diameter spherical container (polyethylene terephthalate) was used as the housing for five 5cm diameter metabolite-containing spheres (polypropylene) fixed in a coplanar fashion in 3% agarose (**Figure 6A**). The size of the phantom allows for adequate loading of the RF head coil which is 30cm in diameter. One of the metabolite spheres was used as a reference based on the "Braino" phantom (GE Healthcare, Milwaukee WI). The other four spheres included 2) Braino + 1mM GABA; 3) 1mM GABA only; 4) Braino + 2mM GABA; and 5) 2mM GABA only. A concentration of 1mM was chosen based on the average concentration in the human brain [73], while 2mM was chosen to improve the resolvability of GABA. A table describing the exact concentrations of metabolite is shown in **Figure 6B**. Metabolites were dissolved in double distilled deionized water containing 50mM KH_2PO_4 (Riedel-de Haen; 04243), 56mM NaOH (Sigma; S0899), 0.10% sodium azide (Sigma-Aldrich; S2002) and 0.10% Omniscan a Gadolinium (Gd) based contrast agent (GE Healthcare Canada Inc; 02172771).

A

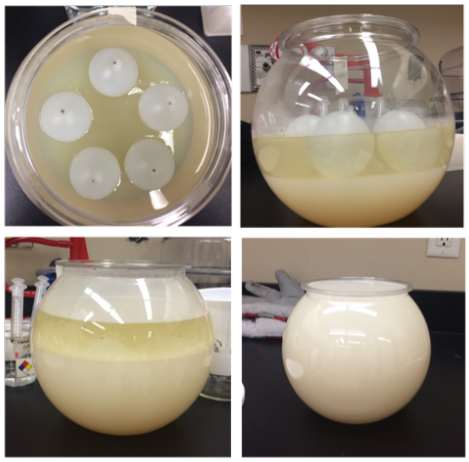

B

Metabolites	Sphere 1 (mM)	Sphere 2 & 4 (mM)	Sphere 3 & 5 (mM)
Creatine (Cr)	10.0	10.0	-
Choline Chloride (Ch)	3.0	3.0	-
myo-Inositol (mI)	7.5	7.5	-
L-Glutamic acid (Glu)	12.5	12.5	-
L-Lactic acid (Lac)	5.0	5.0	-
N-acetyl-L-aspartic acid (NAA)	12.5	12.5	-
γ-aminobutyric acid (GABA)	-	1.0 / 2.0	1.0 / 2.0

Figure 6: *A) Creation of the 20cm phantom. 5 metabolite spheres were embedded in agar. B) The metabolites contained in each of the 5 spheres; Cr (Sigma; C0780), Cho (Sigma; C1879), mI (Fluka; 57570), Glu (Fluka; 49449), Lac (Fluka; 71718), NAA (Fluka; 00920), GABA (Sigma; A2129).*

Single voxel MEGA-PRESS and PRESS spectra were acquired from each sphere in a randomized fashion, with 3 repetitions, during nine sessions using a 3T GE MR750 scanner with a 32-channel phased-array head coil (General Electric Healthcare, Milwaukee, WI). The acquisition parameters used are listed in **Figure 7A**. PRESS spectra were acquired from the reference sphere to confirm other neurometabolites were stable throughout each of the sessions. Room temperature was accounted for using the custom variable tempC during acquisition. Automatic shimming was used to homogenize the field. If spectra had a linewidth above 5 Hz during the pre-scan they were rejected and voxels were either re-positioned within the sphere or higher-order

shimming was implemented. Each spectrum was fitted using Tarquin [26] to provide measures of metabolite concentrations referenced to water. **Figures 7B-D** show sample spectra and fitting generated by Tarquin.

A

Parameters	Spheres Containing GABA	Spheres Without GABA
Sequence	MEGA-PRESS	PRESS
TE/TR	68/2000 ms	35/2000 ms
No. of Averages	360 (160 edited & non-edited)	64
Voxel Size	3x3x3 cm ($27\ cm^3$)	3x3x3 cm ($27\ cm^3$)
Spectral Bandwidth	2000 Hz	2000 Hz
No. of Samples	2048	2048

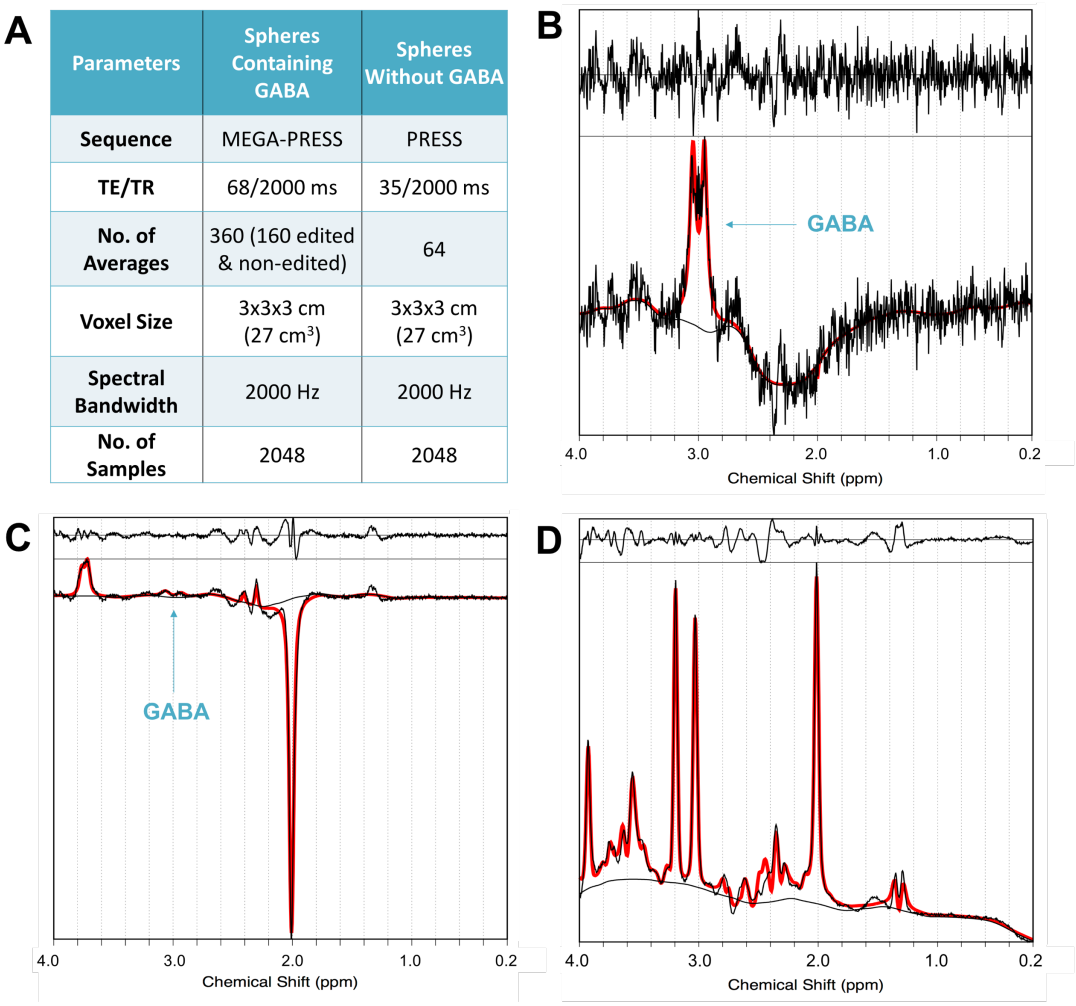

Figure 7: *A) Acquisition parameters used for spheres with and without GABA. B) MEGA-PRESS spectrum of a sphere containing only 1mM of GABA. C) MEGA-PRESS spectrum of sphere containing 'Braino' + 1mM GABA. D) PRESS spectrum of sphere without any GABA.*

System receiver gains (R1 and R2), transmit gain (TG), and linewidth were reviewed to ensure that neither system pre-scan values nor poor spectral acquisition contributed to data variability. Fit quality was assessed in Tarquin using the ratio between the fit residual and spectral noise denoted as Q. The measured GABA concentration were not compared to the known concentration of GABA in the phantom. Due to the low amount of GABA required for each sphere, it is possible that the phantom solutions did not contain the exact GABA concentrations intended due to measurement errors and loss of product during mixing. Instead only the ratio of GABA concentrations (ratio between spheres 2:4 and spheres 3:5) were assessed. A 3-way ANOVA was performed using 'within session', 'between session' and 'presence of Braino' as factors.

5.2.2 Human Validation

Following a 3-plane localizer image and ASSET calibration scan for parallel imaging, an axial T1-weighted fast SPoiled GRadient Echo (fSPGR) structural scan was acquired (TR=7.9ms, TE=3.1ms, flip angle = 12°, matrix=240x240, FoV=24cm, slices= 180, slice thickness=1mm isotropic). Four 3 x 3 x 3 cm (27 cm^3) voxels were placed in the anterior cingulate cortex (ACC), occipital cortex (OCC), hand knob region sensorimotor cortex (SMC) and basal ganglia (BG) of a healthy male participant (age 24), as seen in **Figure 8**. Voxels were rotated to avoid cerebrospinal fluid (CSF) and optimize their placement in a region. Outer volume suppression bands were used to suppress macromolecule and metabolite contamination outside the voxel. The spectra

were acquired using the same MEGA-PRESS sequence as used in the phantom testing. Automatic shimming was used and spectra with linewidth above 12 Hz were re-shimmed if necessary.

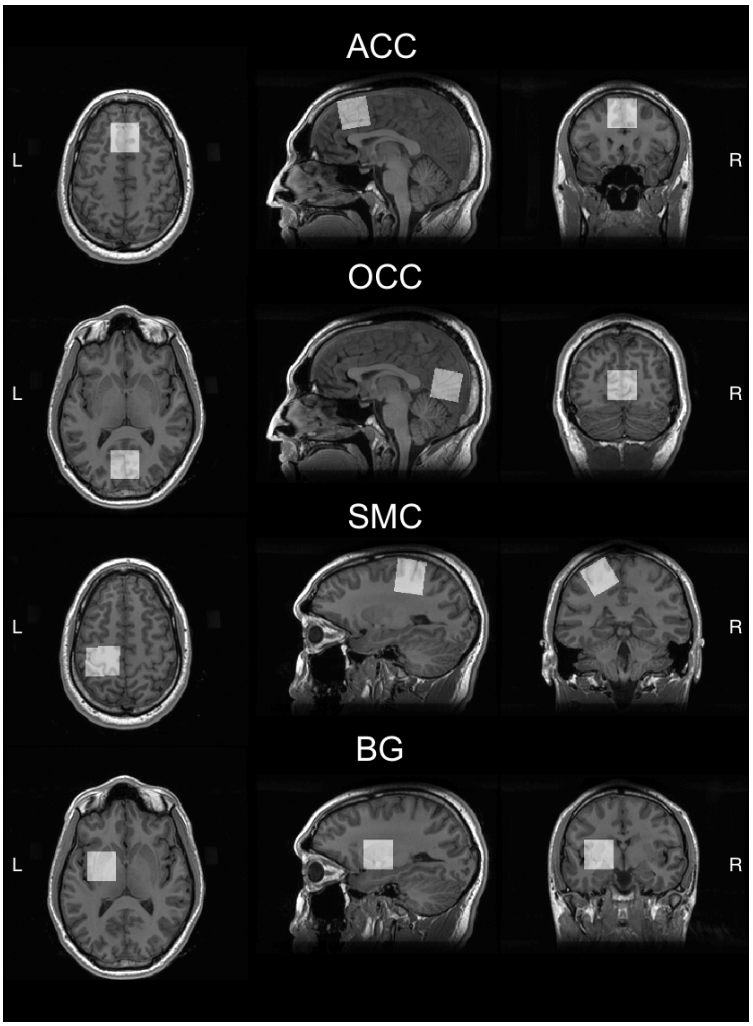

Figure 8: *Voxel placement for human validation of GABA. Anterior medial region to capture the ACC, medial OCC parallel to cerebellum, left hand knob region of the SMC, and left BG.*

GABA concentrations with macromolecule contamination (GABA+) were estimated using a GABA-specific software called Gannet (v3.0), that fits a Lorentzian curve to the GABA peak at 3.0 ppm [98]. Additionally, spectra were corrected for frequency offsets, and normalized for macromolecule contamination and editing efficiency [99]. Spectra were also tissue-corrected for partial volume effects from differences in the concentration of gray matter, white matter and CSF in the voxels of interest. This was accomplished in Gannet by registering the voxel to a T1-weighted image and segmenting into GM, WM, and CSF using SPM 12 [100]. GABA+ was referenced to both water and Cr, the measured values were then compared to GABA+ concentrations of the same regions from studies of healthy participants using MEGA-PRESS on a 3T system. Specifically, measured GABA concentration are considered valid if they fall within 2SD of the concentrations measured in the ACC [101], OCC [102], SMC [103], and BG [104] of previous literature. A summary of previously measured values can be seen in **Table 1**.

Table 1: Previous literature measuring GABA in the brain

	Population	Acquisition	Tissue Composition	GABA Concentrations
ACC (101)	49 males (20-76 years)	- 8-channel head coil - 3 x 3 x 3 cm voxel - 320 scans	GM/ (GM+WM) = 57.85 %	**GABA+/Cr:** 0.265 ± 0.038
OCC (102)	7 males and 8 female (26.1 ± 5.1 years)	- 8-channel head coil - 3 x 3 x 3 cm voxel - 332 scans	No Segmentation	**GABA+/H2O:** 1.13 ± 0.07
SMC (103)	7 males and 1 female (31.4 ± 3.9 years)	- 8-channel head coil - 3 x 3 x 3 cm voxel - 332 scans	GM = 32 ± 3% WM = 54 ± 7% CSF = 14 ± 4%	**GABA+/H2O:** 1.028 ± 0.123
BG (104)	17 males (17) and 12 females (34.0±10.2 years)	- coil not stated - 3 x 3 x 3 cm voxel - 256 scans	GM = 35 ±10% WM = 63 ±11%	**GABA+/H2O:** 1.18 ± 0.2

5.3 Results

5.3.1 Phantom Validation

The results for all 9 sessions can be found in **Figure 9**. There were no significant differences between spheres with and without 'Braino' ($F_{(1,16)} = 1.46$, $p = 0.2448$), and no statistically significant within ($F_{(2,53)} = 1.31$, $p = 0.2985$) or between ($F_{(8,53)} = 2.34$, $p = 0.0707$) session differences in ratios of GABA. However, an interaction effect between session and presence of 'Braino' was evident ($F_{(8,53)} = 4.69$, $p = 0.0042$). To determine the exact interaction a 2-way ANOVA was performed on spheres with and without 'Braino' separately, using 'within session' and 'between session' as factors. The 2-way ANOVA determined that spheres without 'Braino' have an effect session ($F_{(8,26)}$

= 3.31, p = 0.0199), while spheres with 'Braino' do not ($F_{(8,26)}$ = 1.47, p = 0.2423).

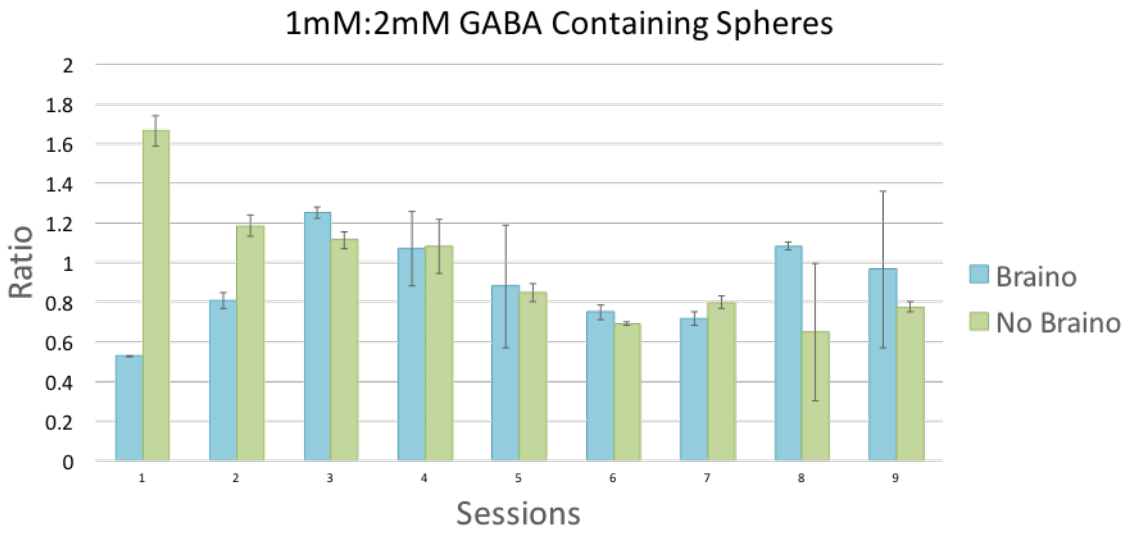

Figure 9: *Mean and SD of GABA ratios for all 9 sessions.*

5.3.2 Human Validation

The GABA measurements for each region can be seen in **Table 2**. None of the measured GABA concentrations were within 2SD of values from previous literature.

Table 2: GABA+ Measurements compared to previous literature

	Previous Literature	Tissue Composition	GABA+/Cr	GABA+/H2O
ACC	**GABA+/Cr:** 0.265 ± 0.038	GM = 59 % WM = 31% CSF = 10 %	0.137 (8.1%)	2.35 (7.8%)
OCC	**GABA+/H2O:** 1.13 ± 0.07	GM = 75% WM = 22% CSF = 3%	0.140 (2.8%)	2.51 (2.6%)
SMC	**GABA+/H2O:** 1.028 ± 0.123	GM = 38% WM = 56% CSF = 6%	0.134 (5.0%)	1.76 (4.7%%)
BG	**GABA+/H2O:** 1.18 ± 0.2	GM = 49% WM = 48% CSF = 3%	0.172 (5.9%)	2.79 (5.8%)

5.4 Discussion

This experiment aimed to validate GABA MRS on a local MR system to ensure reproducible results in future studies. Through phantom work we discovered that GABA measurements, using the methodology stated above, are generally stable over time on this specific MR system. These results ensure that GABA variability will not be directly affected by hardware or sequence instability. Some of the variability between sessions can be attributed to the temperature dependence of phantom work in H^1 MRS [28], since the temperature during each session varied between 18-24ºC. However, MRS in humans is not affected by temperature to such a degree. The interaction effect indicates that quantification of GABA is more variable without the

presence of other neurometabolites. This likely stems from the fact that Tarquin uses other metabolites as references during the pre-processing and quantification of spectra. This lack of metabolites creates an incomplete model, because there are too few degrees of freedom (degree of freedom ≤ number of metabolites. Thus the fit should be compared between different fitting programs, such as LCModel, Gannet and jMRUI. Phantom data was not analyzed with Gannet because at the time of processing Gannet did not have the capability of analyzing phantom spectra. However, recent updates to the software have added these capabilities. In summary, our GABA phantom is stable and has promise as an option for long term quality assurance. However, future work should also assess both B_0 and B_1 differences over time and how these affect GABA consistency in the phantom, since the MEGA-PRESS sequence is susceptible to frequency shifts [105], [106]. It is important to have a quality assurance protocol for the standardization of GABA measurement, thus allowing for multi-centre and longitudinal studies.

Human validation found that none of the regions measured were within 2SD of previous literature. This can be explained by many factors, such as differences in quantification and processing methods. For example, most of the studies used LCModel [101], [103], [104], while only one of the studies used Gannet [102]. LCModel was not developed for the challenges of editing sequences such as MEGA-PRESS, and thus does not correct for frequency shifts which highly effect the editing efficiency of GABA [105],

[106]. Additionally, some studies did not correct for partial volume effects [102], which may have altered their results. Further, this experiment analyzed only one participant at a single time point, which is not enough for proper reproducibility statistics. A minimum of three participants would be needed to evaluate for outliers, as such there is no way of knowing if the participant in question is indeed an outlier due to some unforeseen factors. The low fitting error also points to the fact that the data is adequate but the participant in questions might have just been an outlier compared to previous studies.

Recently published work evaluating the reproducibility of GABA at 24 research sites around the world, including our specific MR site [107], can shed light on the reproducibility of our MR system and how it compares to sites around the world. This multi-site study used the same MEGA-PRESS acquisition and Gannet pipeline as presented in this experiment. GABA concentrations were analyzed in the medial parietal lobe of 12 participants (5 females; 25.50 ± 3.73) at our local MR site and were comparable with measurements from other sites around the world. Although our human validation experiment found that GABA values did not coincide with previous literature, another study analyzing the reproducibility of GABA on our MR system does validate the measures. This experiment also highlights the importance of having standardized acquisition and analyses methods for the detection of GABA.

Chapter 6: Experiment 2

The second experiment sought out to complete the primary and secondary goal of the thesis by investigating how fitness alters both neurophysiological and structural measures.

6.1 Abstract

Previous reports have proven that aerobic exercise has both neuroprotective and neurorehabilitative benefits. However, the underlying mechanisms have not been fully investigated in post-menopausal women, who are more likely to suffer from age-related diseases such as Alzheimer's disease and stroke in their later years. We aimed to define the neurophysiological and structural signatures that differentiate sedentary from highly fit women, in order to improve our understanding of how aerobic exercise can combat age-related disease in females. A total of 35 healthy, right-handed, post-menopausal women were recruited (59.49 ± 3.40 years). Cardiorespiratory fitness was estimated using the Astrand-Ryhming Cycle Ergometer Test (45.89 ± 14.26 mL/kg/min). Transcranial magnetic stimulation (TMS) was used to assess γ-aminobutyric acid (GABA) and glutamate (Glu) receptor function in the primary motor

cortex (M1) and magnetic resonance spectroscopy (MRS) was used to quantify GABA and Glu concentrations in M1. T1-weighted magnetic resonance imaging (MRI) was used to assess cortical thickness (CT) of sensorimotor and frontal regions of interest (ROI), while the microstructure of sensorimotor white matter (WM) tracts and other ROIs was evaluated through diffusion tensor imaging (DTI). Regression analysis found that fitness improves the microstructure in pre-motor and sensory tracts, as well as the hippocampal cingulum in post-menopausal women. There was no effect of fitness on CT nor neurophysiological measures. This suggests cardiorespiratory fitness may preserve motor control and tactile acuity, as well as memory in post-menopausal women via improvements in WM microstructure.

6.2 Introduction

Physical activity is recognized as being one of the most accessible and cost-effective ways to improve health and lower the risk of chronic disease throughout the lifespan. Long-term aerobic exercise has the ability to improve learning, memory and the overall function of the brain, consequently promoting brain health and delaying age-related cognitive decline [2]–[4]. Additionally, exercise accelerates rehabilitation in stroke patients and helps reverse the effects of dementia and Alzheimer′s disease [7], [8]. Previous research focusing on the the effects of long-term exercise on the brain have included both males and females. However, considering the prevalence of Alzheimer′s disease in women [108], [109] and/or major stroke-related disability that is experienced

by women compared to men [110], it is prudent to explore the mechanisms by which aerobic exercise promotes brain health and prevents age-related diseases in women.

Research exploring the role of exercise in women has shown that those with greater cardiorespiratory fitness perform better on cognitive assessments [94], [111]–[114] and demonstrate greater activation in the pre-frontal cortex (PFC) during executive function tasks [111], [113]. There is evidence to suggest these fitness-related effects may be related to structural changes. For example, fit post-menopausal women have greater cortical volume in areas of the PFC and subgenual cortex compared to their low-fit counterparts [94]. High fitness levels in women are also associated with greater volume of pre-frontal white matter (WM) tracts [94]. Further, lower resting mean arterial pressure and greater cerebrovascular conductance in the carotid arteries of fit older women have been reported [112], suggesting improved blood flow to the brain.

There remain several unanswered questions about how long-term aerobic exercise, as represented by cardiorespiratory fitness, influences the female brain. The microstructure of WM tracts has not been explored in women, although fitness has been shown to cause improvements in multiple tracts, including the corpus callosum, cingulum, corona radiata, and superior longitudinal fasciculus [95]–[97], [115]. This information can be acquired through a magnetic resonance (MR) technique called diffusion tensor imaging (DTI), which encodes water diffusivity as a rank-2 tensor.

Neurotransmission, which plays a key role in neural function has also never been investigated with respect to fitness in women. Transcranial magnetic stimulation (TMS) can indirectly assess whether fitness has an effect on GABAergic and glutamatergic receptor function in multiple corticospinal circuits. While magnetic resonance spectroscopy (MRS), another MR technique, is able to measure concentration of neurometabolites. MRS will determine whether concentrations of the most prevalent inhibitory neurotransmitter, γ-aminobutyric acid (GABA), and excitatory neurotransmitter, glutamate (Glu), change as a function of fitness level in females.

The goal of the present study was to provide a comprehensive description of the neurophysiological and structural differences that differentiate fit from sedentary post-menopausal women. Neurophysiological measures were assessed using both TMS and MRS techniques, while structural measures were assessed with standard anatomical MR images (MRI) and DTI. An improved understanding of how aerobic exercise and cardiorespiratory fitness achieve their benefits will aid in the design of effective training programs to help combat ageing-related disease in females.

6.3 Methods

6.3.1 Participants

A total of thirty-five healthy post-menopausal females (59.49 ± 3.40) participated in the study with a subset of twenty-four individuals included in the MRI portion of the study. Participants provided informed written consent approved by the Hamilton Integrated Research Ethics Board (HiREB). Exclusion criteria included significant medical conditions such as chronic pain, Crohn's disease, Celiac disease or diabetes, history of head injuries, neurological or psychological disorders, smoking or certain medications (including hormone replacement therapy). Permitted medications included thyroid hormone replacement (N = 8; Levothyroxine), bone density strengthener (N = 3; Risedronate), cholesterol reducer (N = 2; Rosuvastatin), hypertension therapy (N=2; Candesartan cilexetil, Hydrochlorothiazide, Indapamide, Perindopril), arthritis treatment (N = 1; Tocilizumab) and gastroesophageal reflux treatment (N = 1; Lansoprazole). All participants were right-handed as determined by a modified version of the Edinburgh Handedness Scale [116]. Participants were considered post-menopausal if they had not had a menstrual period in the past 12 months [117]. The Montreal Cognitive Assessment (MOCA) was administered to assess multiple cognitive domains, including attention, concentration, executive functions, memory, language, visuospatial skills, abstraction, calculation and orientation to ensure participants did not have any symptoms of mild-cognitive impairment [118]. Participants were included only if their MOCA scores were greater than 26. Physical

activity as a rate of energy expenditure (MET/min) was determined using the International Physical Activity Questionnaire (IPAQ), which evaluates physical activity over the past week [119]. Body composition was determined by measuring fat-free body mass and percent body fat (%BF) via air-displacement plethysmography using the Bod Pod® Composition System (Life Measurement Inc.; Concord, CA, USA) [120]. Participants were asked to fast for 3 hours prior to the body composition assessment and not to perform any strenuous exercise 12 hours prior to the assessment. Thoracic gas volume was estimated for each body composition test using the algorithm provided in the Bod Pod® software.

Cardiovascular fitness was assessed for each participant. Maximal oxygen consumption (VO_{2max}) in mL/kg/min was estimated using a modified version of the Astrand-Ryhming cycling ergometer protocol [121], [122], which is a widely used submaximal cardiorespiratory fitness assessment for adults [123]. Participants were cleared to participate in the fitness test using the Physical Activity Readiness Questionnaire (PAR-Q) [124]. The protocol involved a 1-minute warm up at a low workload (25-50 W) on a cycle ergometer (Kettler Ergo Race I; Ense, Germany), followed by a 6-minute single stage of continuous cycling (60 RPM at a workload of 50-75W) designed to increase the heart rate (HR) of participants to a target of 60% of their heart rate reserve (HRR). Below is the equation for the target HR (HR_{target}), where the maximal HR (HR_{max}) was determined using the tradition age-predicted formula

(220-age) and the resting HR ($HR_{resting}$) was measured by participants using the radial pulse on the morning of their session before they got out of bed.

$$HR_{target} = 0.6 \times (HRR) = 0.6 \times \left(HR_{max} - HR_{resting}\right)$$

If HR_{target} was less than 120 BPM for a participant it was changed to 120 BPM, a minimum requirement for the accurate estimation of VO_{2max} using the Astrand-Ryhming test. Measurements were taken at the end of every minute for at least 6-minutes using a HR monitor (Polar A3; Lake Success, NY, USA) fitted prior to the fitness assessment. If the target HR was not reached by the 2- and 4-minute mark, the workload was adjusted accordingly. At the 6-minute mark, if the participant had not reached steady-state at the target HR (i.e. within 5 BPM), the intensity was again adjusted and 2 minutes added to the test. This step was repeated until participants reached the target HR at steady-state for two consecutive minutes. The HR and work load at the last 2 minutes of the test, along with the participant's body mass, sex and age, were used to calculate the estimated VO_{2max} using the Astrand-Ryhming nomogram [123], [125]. Maximal oxygen consumption was also adjusted for body composition ($VO_{2max}{}^{ADJ}$) by using fat-free body mass instead of total mass [126].

6.3.2 Electrophysiological Acquisition

Electrophysiological measures were acquired from all participants approximately

23.29 ± 13.72 days from the initial cardiorespiratory fitness test. **Figure 10** gives a summary of the TMS circuits assessed. Participants were asked to refrain from alcohol consumption and strenuous physical exercise 12 hours prior to the session. Electromyography (EMG) was used to record motor evoked potentials (MEPs) over the right and left abductor pollicis brevis (APB) using 9mm diameter Ag-AgCl surface electrodes in a bipolar belly-tendon arrangement. A wet ground electrode was placed around the forearm. EMG recordings were amplified by a gain of x1000, band pass filtered (20Hz—2.5kHz) (Intronix Technologies Corporation Model 2024F with Signal Conditioning; Bolton, ON, Canada), then sampled at 5kHz (Power1401; Cambridge Electronic Design, Cambridge, UK) and collected using Signal software (Cambridge Electronic Design; v6.02).

Compound muscle action potentials (CMAP) were recorded to determine the maximal M-wave (M_{max}). Recordings were acquired from participants that were seated upright in an armchair with their right arm slightly bent resting on a pillow in the supine position. Nerve stimulation was performed with a constant current stimulator (Digitimer DS7AH; Welwyn Garden City, UK) and a bar electrode placed over the median nerve at the wrist with the cathode proximal evoking a response in the APB using square wave pulses of 0.2ms. The nerve stimulator intensity was slowly incremented by 1mA every 5s, until the peak-to-peak amplitude of the M-wave did not change for three consecutive increments of the nerve stimulator intensity.

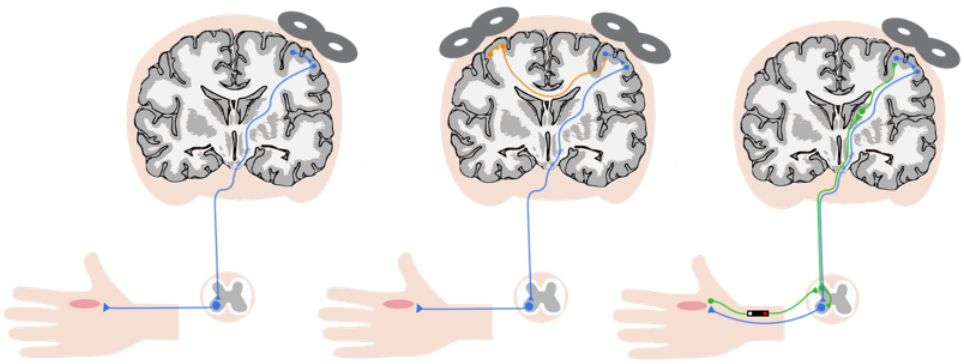

	Intracortical		Interhemispheric		Afferent	
	SICI	ICF	SIHI	LIHI	SAI	LAI
CS	90% AMT	90% AMT	~1mV	~1mV	PNS	PNS
TS	~1mV	~1mV	~1mV	~1mV	~1mV	~1mV
ISI	2ms	12ms	10ms	40ms	24ms	200ms

Figure 10: *An overview of TMS circuits assessed in the study. Intracortical circuits a probed by the TS preceded by a CS at the same location. Interhemispheric circuits are probed by the TS preceded by a CS in the opposite hemisphere. Afferent circuitry is probed by probed by the TS preceded by peripheral nerve stimulation (PNS).*

To determine maximum voluntary contraction (MVC), participants completed three maximal isometric contractions of the right APB against an immovable structure. Each contraction lasted 5s with at least 30s of rest between trials. Amplified and filtered EMG activity was full-wave rectified and fed into an oscilloscope (Tektronix TDS 2004C; Beaverton, OR, United States) to display the magnitude of the contraction to the participant. For a given participant, the greatest maximum EMG activity obtained

from the three trials was considered the MVC. The oscilloscope was set to display a horizontal target line representing the maximum EMG voltage at 10% of MVC. The participant then used visual feedback to match their contraction to the target line during the acquisition of active motor threshold (AMT), which is detailed below.

TMS was performed using a customized figure-of-eight branding coil (50mm diameter), connected to a Magstim Bistim stimulator (Whitland, UK). The motor hotspots of the right and left APB muscles were identified in the left and right hemisphere, respectively, as the cortical location that elicited the largest and most consistent MEP in the relaxed APBs. The coil was orientated at a 45° angle from the sagittal plane to induce a posterior-anterior current. Location and orientation of the motor hotspots were digitally registered using the Brainsight Neuronavigation system (Rogue Research, Montreal, QC, Canada). Resting motor threshold (RMT) and AMT were determined at the motor hotspot for the right APB using the maximum-likelihood parameter estimation by sequential testing (ML-PEST) algorithm found in the TMS Motor Threshold Assessment Tool software (MTAT v2.0) [42]. The motor threshold assessment was run without a priori information and was stopped after 20 stimuli [42]. In the rest condition, a MEP was defined as having a minimum peak-to-peak amplitude of 50μV in the relaxed right APB [37]. In the active condition, a MEP was defined as a minimum of 200μV peak-to-peak, while participants maintained ~10% of their MVC in the right APB using visual feedback from an oscilloscope [37]. All single-pulse and

paired-pulse TMS paradigms were delivered in a randomized fashion at a 5s interval.

MEP recruitment curves (RC) were acquired from the right APB at rest by delivering 8 TMS pulses at TMS intensities in increments of 10% between 90% and 200% RMT. Short intracortical inhibition (SICI) and intracortical facilitation (ICF) were assessed using paired-TMS pulses with an interstimulus interval (ISI) of 2ms [82] and 12ms [46], respectively. The conditioning stimulus (CS) was set to an intensity of 90% AMT and the test stimulus (TS) was set to evoke MEPs with peak-to-peak amplitudes of ~1 mV in the right APB at rest. For each of these measures, 15 conditioned stimuli (CS-TS) and 15 unconditioned stimuli (TS) were randomly delivered.

Short- and long-latency afferent inhibition (SAI, LAI) were assessed by delivering a single TMS pulse over the APB hotspot, preceded by nerve stimulation of the median nerve at the wrist with an ISI of 24ms (SAI) and 200ms (LAI) [54]. Nerve stimulation was performed with a constant current stimulator (Digitimer DS7AH; Welwyn Garden City, UK) and a bar electrode placed over the median nerve at the wrist with the cathode proximal evoking a response in the APB using square wave pulses of 0.2ms in length. The nerve stimulator intensity was set to the motor threshold (MT) of the APB muscle, which was defined as the minimum intensity (in mA) that evoked a visible twitch in the APB. The TS was set to evoke MEPs with peak-to-peak amplitudes of ~1 mV in the right APB at rest. For each circuit, 15 conditioned stimuli using the nerve stimulator

(CS-TS) and 15 unconditioned stimuli (TS) were randomly delivered.

Short- and long-latency interhemispheric inhibition (SIHI, LIHI) were assessed by delivering a CS to the motor hotspot for the left APB and a TS to the right APB hotspot at an ISI of 10ms (SIHI) and 40ms (LIHI) [127]. Both the CS and TS were set to evoke MEPs with peak-to-peak amplitudes of ~1 mV in the left and right APB, respectively. For each circuit, 15 conditioned stimuli (CS-TS) and 15 unconditioned stimuli (TS) were randomly delivered.

6.3.3 MRI Acquisition

A subset of 24 participants were scanned using a 3T GE MR750 scanner with a 32-channel phased-array head coil (General Electric Healthcare, Milwaukee, WI) about 10.46 ± 14.55 days after the TMS session. Participants were asked to refrain from alcohol consumption and strenuous physical exercise 12 hours prior to the session. Following a routine 3-plane localizer image and ASSET calibration scan for parallel imaging, an axial T1-weighted fast SPoiled GRadient Echo (fSPGR) structural scan was acquired (TR=7.9ms, TE=3.1ms, flip angle = 12°, matrix=240x240, FoV=24cm, slices= 180, slice thickness=1mm isotropic).

The structural scan was used to position a 20x20x20 mm^3 voxel of interest (VOI) over the left hand knob area (M1) with the use of two reliable anatomical landmarks [128].

An example of the voxel placement can be seen in **Figure 11A**. The VOI was rotated in the coronal plane to optimize the placement in gray matter (GM), avoiding cerebrospinal fluid (CSF). Outer volume suppression (OVS) bands were placed along the outside of the VOI to suppress macromolecule and metabolite contamination. Automated voxel shimming prior to MRS yielded water-line widths ranging from 3 to 8Hz. MRS of the VOI was performed to quantify GABA using Mescher–Garwood point-resolved spectroscopy (MEGA-PRESS) GABA editing sequence with water suppression [33] (TR=2000ms, TE=68ms, number TE's per scan=2, NEX=8, number of averages=320, data points=2048, receiver bandwidth=2000Hz). Additionally, 16 unsuppressed water reference spectra were acquired. Although the Glu composite Glx (Glu+Gln) can be measured reliably from the MEGA-PRESS sequence [129], the acquisition itself was not designed to measure Glu levels. Therefore, Glu concentrations were acquired from the VOI using a stimulated-echo acquisition mode (STEAM) sequence optimized to resolve Glu from GABA and Gln at 3T (TR=1500ms, TE=72ms, TM=6ms, NEX=8, number of averages=512, data points=2048, receiver bandwidth=5000Hz) [130], based on Hu et al. [36]. The STEAM sequence is ideal for coupled spin systems, such as Glu, and allows for better water and macromolecule suppression then PRESS sequences. An example of MEGA-PRESS and optimized STEAM spectra is shown in **Figure 11B and 11C**, respectively.

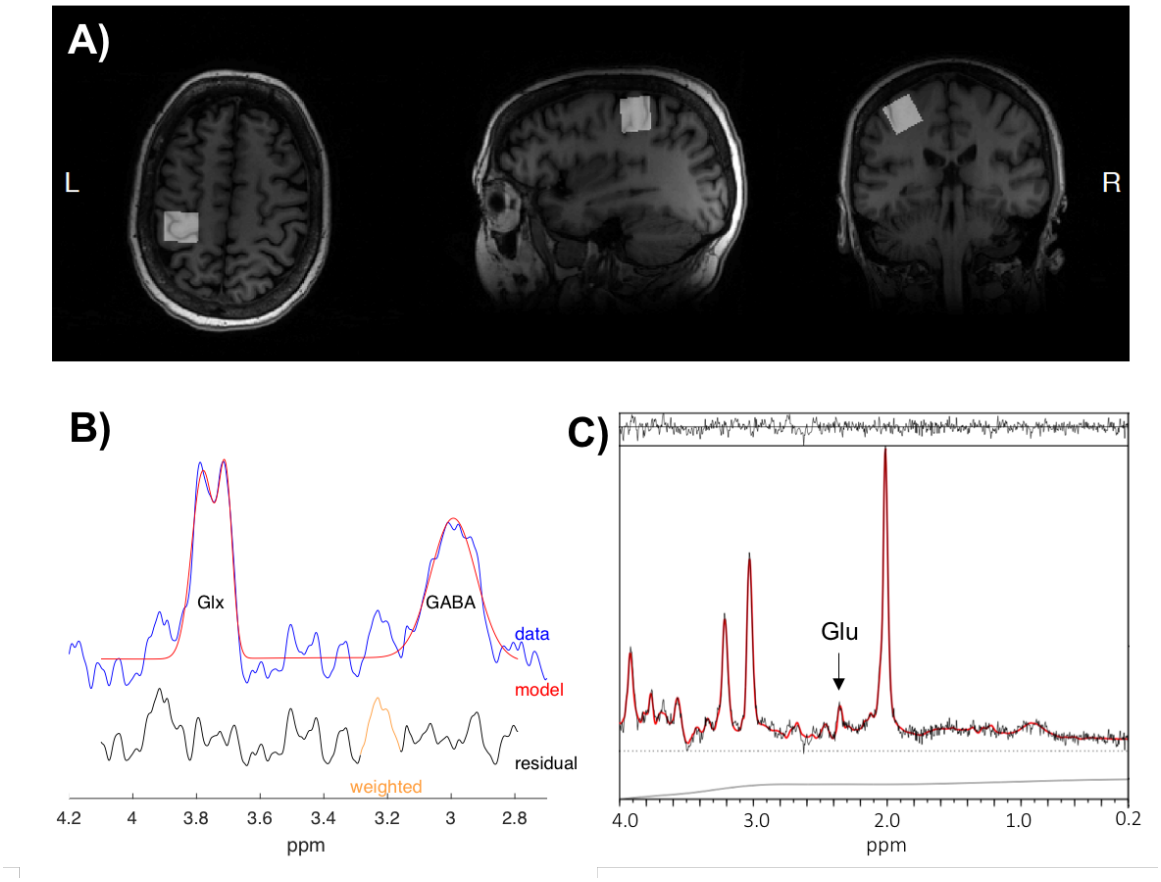

***Figure 11**: A) Depicts the placement of the VOI in the hand-knob region of the primary motor cortex. B) An example MEGA-PRESS spectrum output from Gannet. C) An example STEAM spectrum output from LCModel.*

Finally, axial DTI in 60 non-coplanar directions was carried out to assess white matter microstructure using a dual-echo echo-planar imaging (EPI) sequence (TR=11000ms, TE=87ms, b-value=900s/mm^2, matrix=96x96, slices=50, FOV=23cm, slice thickness=2.9mm, ASSET=2). Diffusion was acquired for all 60 direction using 3 separate scans (19, 20, and 21 directions) with three T2- weighted (b-value=0s/mm^2)

images incorporated at the beginning of each of the acquisitions. Diffusion imaging was acquired last to reduce the effect of frequency offset on MRS measures [105].

6.3.4 Electrophysiological Analysis

All MEPs were inspected for background muscle activity, and trials were discarded if EMG activity exceeded 50μV in the 30ms prior to the TMS stimulus artefact. Data for a given participant was discarded if there were less than 10 trials for paired-pulse paradigms and less than 5 trials for any point on the recruitment curve. For the RC the mean peak-to-peak MEP amplitude was calculated for each %RMT intensity (90–200%). A MATLAB script was then used to fit a Boltzmann sigmoid function to the RC as a percentage of maximal stimulator output (%MSO) using least squares curve-fitting [131]–[133]. The function was bounded by $MEP_{baseline}$ to ensure the fitted curve was non-negative. $MEP_{baseline}$ was considered the minimum noise of the data, which was determined to be 0.013 mV. Below is the Boltzmann sigmoid function:

$$y(x) = MEP_{baseline} + \frac{MEP_{plateau}}{1 + e^{\frac{S_{50} - x}{k}}}$$

An example of the fitted curve from one participant can be seen in **Figure 12**. The fitting process estimated the RC $MEP_{plateau}$ (i.e. maximum peak-to-peak MEP in mV), the inflection point (S_{50}) or stimulus intensity in %MSO required to evoke a MEP equal

to half the plateau, and the Slope (1/k) of the sigmoid function (mV/%MSO). Additionally, $Slope_{peak}$ in mV/%MSO was also determined as the instantaneous slope at S_{50} [87]. Data with an estimated plateau 15% different from the maximum amplitude of the fitted curve were excluded, as this showed that the RC acquired was exponential and has not adequately captured the plateau [131].

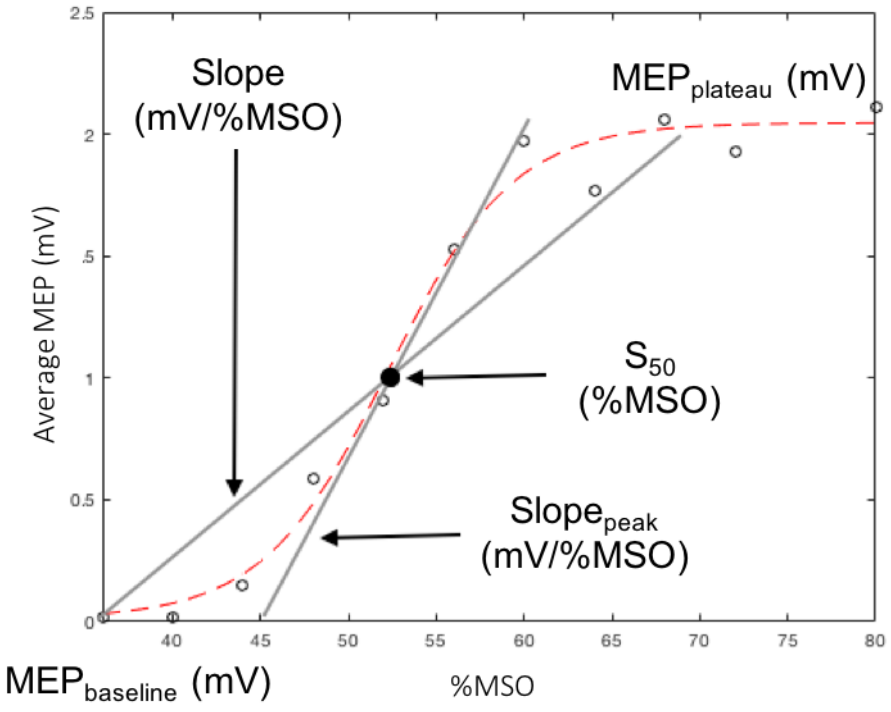

Figure 12: *Example sigmoidal curve fitting to the average MEPs of the recruitment curve.*

For paired-pulse TMS measures, the mean peak-to-peak MEP amplitude was calculated for each CS-TS (paired pulse) and TS, separately. The percentage inhibition and

facilitation was determined as a ratio of conditioned over unconditioned stimulus (CS-TS/TS). Inhibition was evident in a circuit when the CS-TS/TS ratio was ≤0.9, while facilitation was evident when the ratio was ≥1.10.

6.3.5 MRI Analysis

MRS spectra from MEGA-PRESS acquisitions were processed with Gannet (v3.0) [98], a MEGA-PRESS specific analysis software, using default processing parameters. GABA concentrations with macromolecule contamination (GABA+) were referenced to water, corrected for frequency offsets, and normalized for macromolecule contamination and editing efficiency [99]. STEAM spectra were analyzed for Glu with LCModel using basis sets generated through phantom experiments [24], and were also referenced to water. Tissue composition (%GM, %WM, %CSF) in the VOI were estimated using Gannet by registering the VOI to the T1-weighted anatomical image and segmenting the anatomical image into GM, WM, and CSF using SPM 12 [100]. GABA+ and Glu levels were not correlated with tissue content (%Tissue) nor %GM in tissue ($\%GM_{tissue}$), hence concentrations were not partial volume corrected [134]. The quality of all fitted spectra was assessed by analyzing Cramér-Rao lower bounds (CRLBs) of GABA+ and Glu, which take into account differences in both SNR and line-width of each metabolite [135]. If CRLBs were more than 2SD away from the mean of all participant data for a given measure, the data was excluded from statistical analysis [135].

Anatomical images were reconstructed and segmented with the freely available FreeSurfer (v6.0) image analysis suite described in previous literature [136]–[148], using SHARCNET high-performance computing clusters (Shared Hierarchical Academic Research Computing Network and Compute/Calcul Canada). T1 weighted images were first normalized for intensity and skull stripped. White matter and pial surface boundaries were then traced by following T1 tissue intensity gradients. The cortical surface was modelled and cortical thickness measured as the distance between the white matter and pial boundary for each vertex of the model as depicted in **Figure 13A**. All cortical reconstructions and volumetric segmentations were visually inspected for substantial errors but no manual interventions were applied [149]. Regional CT measures are determined by registering the cortical surface folding patterns of the model to a spherical atlas shown in **Figure 13B**, and then by parcellating into specific sulcal and gyral regions. Specifically, the somatosensory (BA 1, 2, 3a,3b), anterior and posterior M1 (BA 4a, 4p), and pre-motor (BA 6) areas in the left hemisphere were determined by mapping the Brodmann areas and thresholding [150]. Additionally, the superior frontal gyrus (SFG), middle frontal gyrus (MFG), inferior frontal gyrus (IFG) and orbitofrontal cortex (OFC) were evaluated as reference ROIs, since areas of the frontal lobe have commonly shown an increase in volume or CT with fitness levels [92], [93], [151], [152]. A MFG ROI was produced by combining the caudal and rostral middle frontal regions from the Desikan–Killiany anatomical atlas [147], [153]. An IFG ROI was produced by combining the pars opercularis, pars triangularis and pars

orbitalis. Lastly, an OFC ROI was produced by combining the lateral and medial orbitofrontal regions. **Figure 13C** and **13D** depicts an example of the sensorimotor and reference ROIs, respectively. CT was not normalized, since it has not been shown to change as a function of brain size [154].

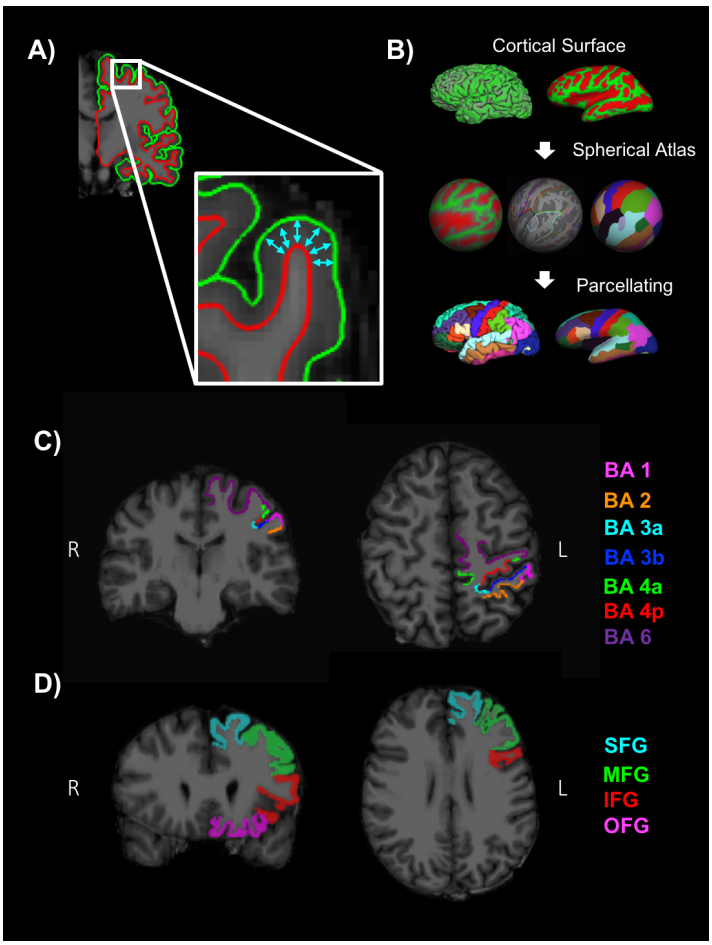

Figure 13: *A) Depiction of the pial (green) and WM (red) boundary. CT is measured between these boundaries. B) Freesurfer determines regions by parcellating the cortical surface model using a spherical atlas. C) Example of sensorimotor and frontal reference D) ROIs used for CT analysis.*

DWI were analyzed using the FMRIB Software Library (FSL; v5.0.11) [155]. Participant data was first skull-stripped using the *Brain Extraction Tool (BET)* [156], then corrected for susceptibility artifacts using B0 field maps and *FUGUE*, and finally corrected for eddy-current distortions and head motion using the *eddy_correct* tool [157]. Using *dtifit* [158], [159] from the FSL Diffusion Toolbox (FDT), diffusion tensors were reconstructed by estimating and fitting a tensor model to the raw diffusion data, producing images of fractional anisotropy (FA), axial diffusion (AD), and mean diffusion (MD). Radial diffusion (RD) was calculated using *fslmath* by averaging the second and third eigenvalues. Tract-Based Spatial Statistics (TBSS) was then used to create a WM skeleton representing WM tracts common to all participants in $1mm^3$ standard Montreal Neurological Institute (MNI152) space using the FMRIB58_FA standard [160]. The WM skeleton was thresholded at an FA of 0.02 and can be seen overlaid on the FMRIB58_FA standard in **Figure 14**. Participant DTI were then aligned to this common space using the individualized transformation matrix produced by the nonlinear registration tool *FNIRT* in TBSS [161]–[163]. Each participant′s aligned DTI data was then masked using the WM skeleton, thereby ensuring every participant had diffusion data from WM common to all participants. Next, ROIs on the WM skeleton were selected using the sensorimotor area tract template (SMATT) [164], which included tracts running between the corticospinal tract and the left M1, dorsal premotor cortex (PMd), ventral premotor cortex (PMv), supplementary motor area (SMA), pre-supplementary motor area (preSMA) and primary somatosensory cortex (S1) as shown

in **Figure 15A**. The corpus callosum (CC), left corona radiate (CR), cingulum, and superior longitudinal fasciculus (SLF) from ICBM-DTI-81 white matter labels atlas [95]–[97], [115] were also selected as ROI references based on numerous studies that found associations between the microstructure of these regions and fitness [95]–[97]. A total of 9 reference ROIs were selected and specified in **Figure 15B**. Subsequently, average FA, AD, RD and MD were calculated for each ROI in every participant.

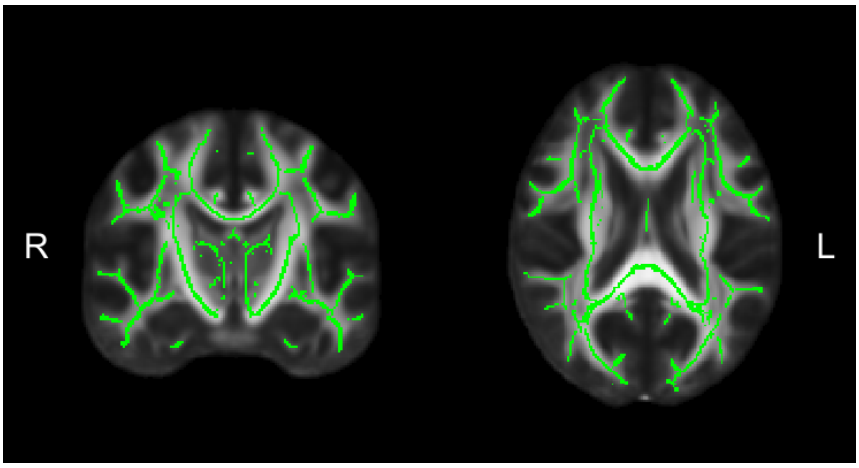

Figure 14: *The WM skeleton projected on a standard FA image. Each of these WM tracts is present in every participant.*

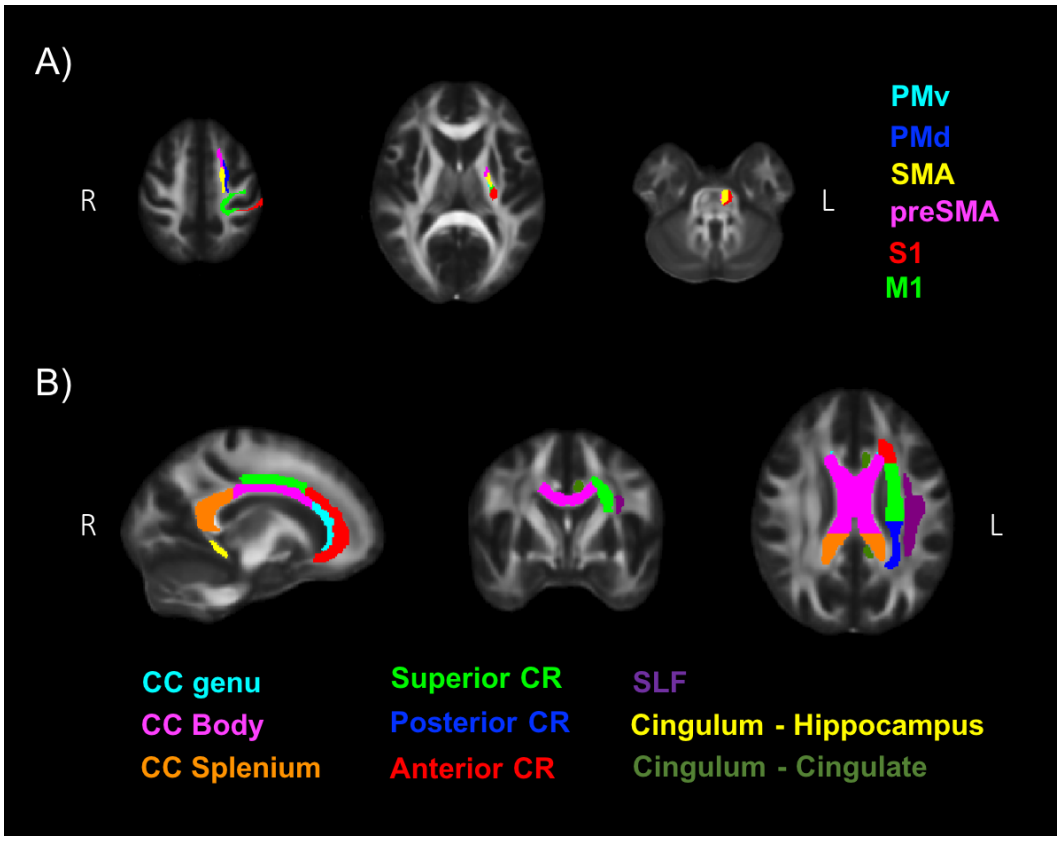

***Figure 15**: Example of A) sensorimotor and B) reference ROIs used for DTI analysis.*

6.3.6 Statistical Analysis

All statistical analyses were carried out using PRISM 6 (GraphPad Software, Inc.; v6.0e) and R software (R Core Team (2018), R Foundation for Statistical Computing; v3.5.0). Normality was assessed using the Shapiro-Wilk test. Outliers were identified using the ROUT method with Q=1% in PRISM [165], which allows for multiple outliers to be detected. Outliers were removed for regression modeling and

correlations. Correlations were analyzed using either Pearson's product moment correlation coefficient r for normally distributed data or Spearman's rank correlation coefficient ρ for non-parametric data.

Multiple linear regression analysis was used to determine if the dependent measures could be modelled using fitness and age. This models a separate linear equation for each dependent measure (Y_d) in 3D space, with the two independent measures (X_i) orthogonal to Y_d. Below is the equation being modelled for each dependent measure:

$$Y_d = \beta_0 + \beta_{Fitness} X_{Fitness} + \beta_{Age} X_{Age} + \varepsilon_i$$

β are the regression coefficients and ε is the error associated with fitting the model. Two independent factors, VO_{2max}^{ADJ} and age, were used without an interaction term. VO_{2max}^{ADJ} was used instead of VO_{2max} to correct for body composition differences. Residuals were plotted against the predicted Y_i to assess the homoscedasticity and were also tested using the Shapiro-Wilk normality test. All tests were considered significant if $p < 0.05$.

6.4 Results

6.4.1 Cardiorespiratory Fitness

Demographics and descriptive information of all participants can be found in **Table 3**. The distribution of VO_{2max} in both TMS and MRI samples is also shown in **Figure 16**. Both samples were composed of low-to-moderately fit and highly fit athletically trained individuals, as described by normative values for the Astrand-Ryhming submaximal test in females between the ages of 50-65 years [166]. VO_{2max} in the TMS sample was normally distributed (skewness = 0.1548, kurtosis = -1.184), although the MRI sample had a non-normal distribution of VO_{2max} (skewness = 0.1653, kurtosis = -1.469).

Table 3: Demographics and descriptive information

	TMS (N=35)	**MRI (N=24)**
Age (years)	59.49 ± 3.40	59.58 ± 3.56
VO_{2MAX} (mL/kg/min)	45.89 ± 14.26	45.38 ± 15.92
VO_{2MAX}^{ADJ} (mL/kg/min)	69.71 ± 14.48	68.50 ± 16.15
IPAQ (MET/min)	5412 ± 4635	5406 ± 4135
%BF	35.24 ± 9.92	35.17 ± 10.35
Weight (kg)	65.42 ± 10.75	68.75 ± 17.00
Education (years)	17.17 ± 2.53	17.50 ± 2.64
MOCA score	28.14 ± 1.52	28.25 ± 1.48

Mean ± SD displayed. VO_{2max}, maximal oxygen consumption; VO_{2max}^{ADJ}, maximal oxygen consumption adjusted for fat-free body mass; %BF, percent body fat; education, full time in years including primary and secondary school; MOCA, Montreal Cognitive Assessment is scored out of 30 possible points.

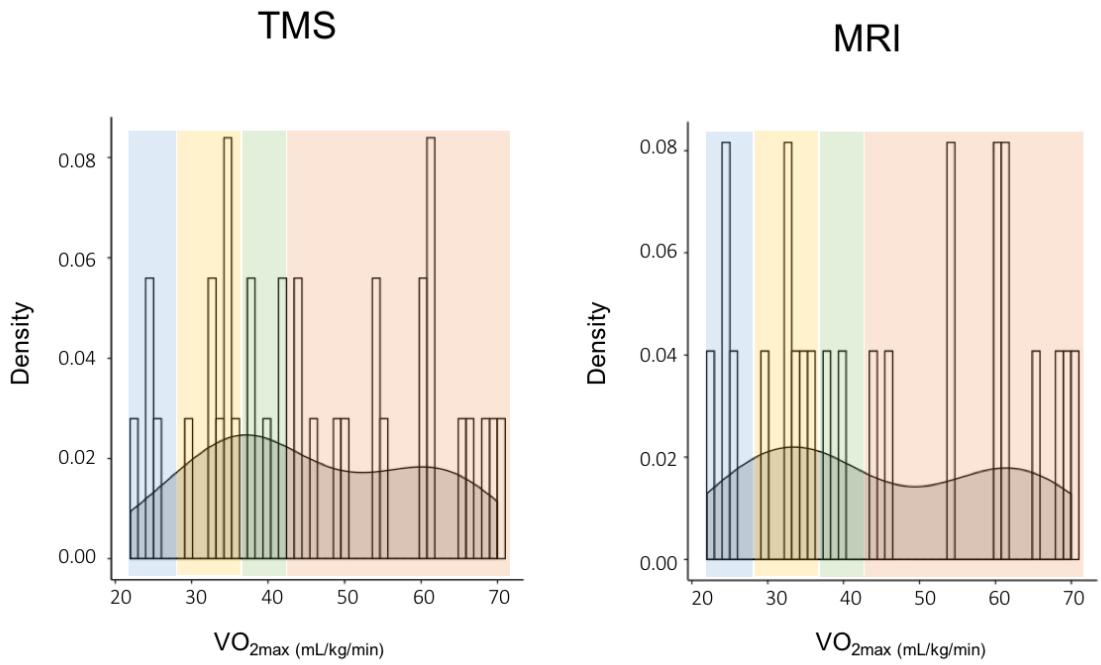

***Figure 16**: Distribution of cardiorespiratory fitness in the TMS and MRI portion of the study. Colours depict below average (blue), average (yellow), high (green) and very high (orange) fitness levels.*

6.4.2 Membrane Excitability

M_{max} was not correlated with fitness (r = 0.267, p = 0.121). **Table 4** shows the regression model for measures of membrane excitability as a factor of fitness and age. One RC was discarded for having less than 5 trials for multiple point on the recruitment curve and a total of 4 RCs were discarded for not adequately capturing the plateau. The goodness of fit of the Boltzmann sigmoid to the RC for the remaining participants (N = 30) was adequate with an R^2 of 0.88 ± 0.15. Three outliers were removed for $Slope_{peak}$ (N = 27) and one for Slope (N = 29) prior to regression analysis. For the remaining

measures of membrane excitability, all participants were included in the statistical analysis (N = 35). There was no relationship between fitness and all the measures of membrane excitability. Age was also not a significant factor in the model. The residuals of $Slope_{peak}$, Slope, $MEP_{plateau}$ and RMT were determined to be non-normal, meaning the data is not fully explained by this linear model.

6.4.3 Neurotransmitter Receptor Function

Table 5 depicts the multiple regression analysis of TMS circuits and the depth of inhibition or facilitation. One outlier was removed from ICF data before the analysis for a total of N = 34 participants. All residuals passed normality testing. There were no significant relationships between fitness nor age and each circuit. For intracortical circuits, 6 participants did not show any facilitation for ICF and 4 participants did not show inhibition for SICI. For interhemispheric circuits only 2 participants did not show any SIHI and 4 participants didn't show any LIHI. When assessing afferent circuitry, 14 participants showed no SAI and 2 participants showed no LAI.

6.4.4 Neurotransmitter Concentrations

One GABA+ and one Glu dataset were poorly fit, with CRLBs 2SD away from the mean, and were discarded. All remaining CRLBs were <20%. One outlier was removed for GABA+ data prior to regression analysis, producing a total sample size of N = 22 for GABA+ and N = 23 for Glu. Water concentrations, which were used as a reference

for both GABA+ and Glu, were found to be stable across all participants regardless of age (r = 0.331, p = 0.143). VOI tissue segmentation revealed average %Tissue of 0.83 ± 0.04 and $\%GM_{tissue}$ of 0.46 ± 0.09. GABA+ was not correlated with %Tissue (ρ = 0.22, p = 0.34) nor $\%GM_{tissue}$ (ρ = 0.39, p = 0.07). Glu concentrations were also not correlated with %Tissue (ρ = 0.31, p = 0.15) nor $\%GM_{tissue}$ (ρ = -0.05, p = 0.82). Coefficient of variation (%CV) were 19.13% for GABA+ and 9.60% for Glu. All residuals passed normality testing. However, no significant relationship existed between fitness nor age and GABA+ or Glu concentrations as seen in **Table 5**.

6.4.5 Cortical Thickness

One participant was an outlier for cortical thickness of BA 4a and excluded from regression modelling. Fitness and age did not significantly model cortical thickness in the sensorimotor area nor the frontal reference ROIs as seen in **Table 6**. However, there was evidence of a trending relationship between age and cortical thickness of BA 1 in S1 (p = 0.06), such that older participants show a decrease in BA 1 cortical thickness. The residuals of BA 4a were determined to be non-normal, meaning the data is not fully explained by this linear model.

6.4.6 White Matter Microstructure

One participant was an outlier for RD and MD of PMd and excluded from regression modelling, while another participant was an outlier for MD in the body of the CC and

excluded from analysis. Fitness was shown to have a significant positive relationship with FA in the PMd ($p = 0.009$) and a significant positive relationship with AD in S1 ($p = 0.04$), as shown in **Table 7** and **Table 9**, respectively. A significant positive relationship between age and RD exists in the preSMA ($p = 0.03$) and S1 ($p = 0.03$), and a trending positive relationship in M1 ($p = 0.05$) and PMd ($p = 0.07$) as seen in **Table 8**. **Table 10** shows no significant relationship between fitness nor age and MD. The residuals of RD in the cingulum cingulate gyrus, AD in the body of the CC, and MD in the S1 were determined to be non-normal, meaning the data is not fully explained by this linear model.

Regression models of the reference ROIs revealed a significant positive relationship between fitness and AD ($p = 0.009$; **Table 9**), and a trending positive relationship between fitness and MD in the part of the cingulum connected to the hippocampus ($p = 0.05$; **Table 10**). A positive trending relationship between fitness and AD of the splenium of the CC was also observed ($p = 0.07$; **Table 9**). There was a significant positive relationship between age and RD in the cingulum connected to the cingulate gyrus ($p = 0.02$) as seen in **Table 8**. A trending negative relationship exists between age and FA in the splenium of the CC ($p = 0.06$; **Table 7),** and a positive relationship between FA and MD in the cingulum connected to the cingulate gyrus ($p = 0.06$; **Table 10**). All residuals passed normality testing.

6.5 Discussion

The present study investigated the neurophysiological and structural biomarkers that may vary as a function of fitness in post-menopausal women. It is the first study to evaluate WM matter microstructure in a sample of post-menopausal females and found that cardiorespiratory fitness increased FA in the PMd, and increases AD in S1 and in the tract of the cingulum connected to the hippocampus. Although previous studies have found fitness-related increases in cortical volume of the PFC in post-menopausal women [94], our results did not show an effect of fitness on CT. This study is also the first to evaluate neurophysiological measures in women as a function of fitness and found no significant effect of fitness on corticospinal excitability or GABAergic and glutamatergic receptor function in the motor cortex. Similarly, we did not observe any significant effect of fitness on the concentration of GABA or Glu within the motor cortex.

The current work determined that cardiorespiratory fitness affects the microstructure of WM tracts travelling between the corticospinal tract and the pre-motor and sensory areas in post-menopausal women. Our results indicate a significant positive relationship between fitness and FA of tracts travelling to the left PMd, such that more fit individuals showed greater FA or better general microstructure in the PMd tract [22]. Similarly, Johnson et al. observed using tractography that the majority of WM tracts stemming from a region of the CC that had a strong relationship with cardiorespiratory

fitness, connected to the pre-motor cortex [115]. The PMd is associated with motor selection and planning using visual and somatosensory integration, thus playing a critical part in motor initiation and learning [167]. One study assessing motor function in aged rhesus monkeys found that faster motor function was associated with greater FA and lower RD in WM tracts contributing to motor processing, such as the internal capsule [168]. Similar results have been seen in humans, where fine finger movement performance has been associated with greater FA and lower MD in the internal capsule [169]. Additionally, 3-weeks of bilateral upper limb training have been shown to increase FA in corticospinal tracts travelling along the internal capsule [170]. Further, following 5-days of motor learning using the non-dominant hand, the magnitude of skill acquisition was positively related to FA of WM tracts between the ipsilateral PMd and SMA, as well as the contralateral M1 [171]. Based on our findings, we suggest that fitness may contribute to improved motor control and learning by promoting pre-motor WM microstructure in post-menopausal women.

We also found an increase in AD of the left S1 tract in fit individuals, which may indicate reduced axonal loss or degradation of the S1 tract with greater levels of fitness [22]. S1 is involved in processing afferent signals and integrating sensory and motor information for the completion of skilled movement [172]. Previous literature has shown that tactile training for 3-weeks increases FA in the WM of S1 [173]. These studies, along with our findings, suggest that cardiorespiratory gains may also yield

greater tactile acuity through improved WM microstructure. Collectively, our findings in the PMd and S1 imply that fitness-related improvements to sensory and pre-motor WM microstructure could promote faster reaction times, as well as better coordination and tactile acuity in post-menopausal women. This is important to consider when it comes to ageing, since aging has been found to decrease reaction time and impair motor coordination [174] and tactile acuity [175]. Promisingly, allowing long-term exercise may preserve these functions.

The present study demonstrates that cardiorespiratory fitness promotes WM integrity in tracts associated with memory function in post-menopausal women. Analysis of our reference ROIs reveal an increase in AD as a function of fitness in the portion of the left cingulum connected to the hippocampus, indicating reduced axonal degradation [22]. Prior research has also reported an improvement in the microstructure of the cingulum associated with fitness levels [95]–[97]. In particular, similar to our study, Tseng et al. observed that Master athletes have lower MD in the left hippocampal cingulum compared to their sedentary counterparts [97]. The hippocampus plays an important role in memory function and has been consistently implicated in the neural plasticity effects of long-term exercise [176], with larger hippocampal volume associated with cardiorespiratory fitness and improved memory [177]. Enhanced cingulum microstructure has also been shown to promote memory function [178]. Based on these findings, it is likely that the fitness-related improvements to the

microstructure of the hippocampal cingulum, as observed in our study, may also contribute to improving memory function.

Contrary to previous studies reporting that fitness increases CT in the left pre-central, post-central gyrus, MFG [92] and in the dorsolateral PFC [93], here we found no significant relationship between fitness and CT in the left sensorimotor area or in frontal reference ROIs in post-menopausal women. This finding is also in contradiction with Erickson et al. who found fitness-related increases in the cortical volume of the PFC in post-menopausal women [94]. Although related, volume is not a direct measure of CT [179], which may explain the differences between our findings. Further, there are differences in the relative fitness of the sample populations, with only one of the studies having a wide range of fitness levels similar to our sample [92].

Our data indicates that cardiorespiratory fitness does not influence corticospinal excitability or GABAergic and glutamatergic receptor function in the motor cortex of post-menopausal women in support of previous findings [82]–[86], [91]. For example, fitness did not alter SICI in the APB [85] and flexor carpi radialis (FCR) [82], which assesses intracortical GABAergic receptor function. Likewise, intracortical glutamatergic receptor function in the form of ICF in the FCR was unaffected by fitness [82]. It was also confirmed that LIHI, which assesses interhemispheric GABAergic receptor function, is unaffected by fitness [84]. Nonetheless, other trans-callosal

circuits such as ipsilateral silent period (iSP) increase with fitness and physical activity [83], [84], [86]. This study also found that afferent circuitry, specifically SAI and LAI, are not affected by fitness. No previous literature has investigated SAI and LAI with respect to long-term exercise, although the magnitude of inhibition is very similar to a previous study that assessed SAI (0.79 ± 0.35) and LAI (0.59 ± 0.38) in the APB using the same methodology [54]. However, almost half of participants did not show inhibition with SAI, suggesting that the ISI of 24ms may not be effective at maximizing inhibition in this population. The magnitude of SAI was actually closer to a study that used an ISI of N20+6ms (0.84 ± 0.22), which produced a lower magnitude of SAI than N20+4ms [52]. Our results further corroborate previous findings demonstrating that membrane excitability of the upper limb is unaffected by physical activity and fitness [82]–[86], [91]. Additionally, the fact that M_{max} does not correlate with fitness suggests there are no training effects on muscle composition (muscle fibre concentrations and area) of the APB that might influence EMG recordings [180].

The current study is the first of its kind to evaluate GABA concentrations as a function of fitness and found that GABA+ in the primary motor cortex was unaffected by fitness level in post-menopausal women. Our study does not support previous research that has shown higher levels of physical activity predict higher resting Glu levels [77], while more fit individuals have lower resting Glu levels [76]. In contrast, it was found that Glu concentrations are unaffected by fitness in post-menopausal women. However,

it is of note that previous studies studies investigated populations including both men and women, and assessed Glu concentrations in the occipital lobe, which may be affected by neural activation from visual stimuli [78].

Age is a variable we and others have included in the regression model [92], [151]. However, age did not have a significant effect on any of the neurophysiological measures nor CT. This is likely due to the narrow age range of participants (52-65 years) and the fact that this age-range does not reflect the age at which age-related decline becomes more apparent. Nonetheless, age had some influence on some structural markers. A significant positive relationship between age and RD existed in the tracts of the left preSMA and S1, as well as in the left cingulum connected to the cingulate. This relationship indicates that aging may cause demyelination of axons in these tracts [22], highlighting the fact that aging interferes with WM structures associated with both sensorimotor and cognitive function in post-menopausal women.

6.5.1 Limitations

One of the major limitations is the macromolecule contamination of the GABA+ signal due to the bandwidth of the editing pulse in MEGA-PRESS, which may play a role in the observed results [34]. Although MEGA-PRESS with macromolecule suppression exists, this method still suffers from high variability of GABA levels due to the influence of frequency drift [107]. It is also important to note that the measures of

GABA+ from the VOI are not strictly from M1, but actually include other areas of the sensorimotor cortex. It is also unknown whether the area being assessed with MRS is the exact same area being assessed with TMS, since the placement of the VOI is based on structural markers while the location of the TMS hotspot is based on a functional analysis. Future studies would benefit from collecting MRI data prior to the TMS assessment, and using the anatomical images to ensure stimulation is applied at the exact area the VOI was placed in. An additional limitation is that SAI was not assessed using measured somatosensory evoked potentials (SEPs) to determine an ISI for each individual based on the N20 component. Hence, the depth of inhibition may not be at its maximum.

DTI results should also be interpreted with caution as crossing fibers may affect the observed values [21]. Our results showed no effect of fitness on neurotransmission. However, these observations are limited to the motor cortex, and are not generalizable to other regions of the brain. As the majority of fitness related changes have been localized to the frontal lobe and hippocampus, it is possible that these areas may show changes in neurotransmission and require future investigation. Lastly, we used a modified version of the Astrand-Ryhming cycling ergometer protocol [121]–[123], a commonly used submaximal cardiorespiratory fitness assessment to estimate VO_{2max} [181], [182]. Estimating VO_{2max} using a sub-maximal test allowed participants who may be at-risk during a maximal fitness test to be included. However, a maximal

cardiorespiratory fitness assessment to directly measure VO_{2max} could be used in future studies to confirm our findings.

6.5.2 Conclusion

This was one of the first studies to comprehensively assess neurophysiological and structural markers as a function of fitness in post-menopausal women. Our results indicate that fitness does not affect GABA or Glu neurotransmission in the motor cortex of post-menopausal women. Whether these findings can be translated to other regions of the brain remains to be investigated. Further, we show fitness-related changes to the microstructure of WM tracts that are associated with both motor control and sensory processing. Future research may probe whether fitness gains are associated with improved motor skill function such as coordination, and tactile perception in post-menopausal women, and last, whether long-term exercise will preserve this sensorimotor function into their senior years.

Table 4: Results of multiple linear regression of corticospinal excitability and TMS circuits against fitness and age

			Coefficients (β)	***SE***	***95% CI***	*p-value*
RMT (%MSO)	N = 35	VO_{2max}^{ADJ}	0.03	0.11	-0.19 : 0.25	0.79
	47.26 ± 9.09	*Age*	0.54	0.46	-0.41 : 1.48	0.26
AMT (%MSO)	N = 35	VO_{2max}^{ADJ}	0.13	0.09	-0.04 : 0.31	0.14
	34.74 ± 7.40	*Age*	0.38	0.37	-0.37 : 1.13	0.31
$MEP_{plateau}$ (mV)	N = 30	VO_{2max}^{ADJ}	-0.02	0.03	-0.08 : 0.03	0.42
	3.11 ± 1.97	*Age*	-0.02	0.11	-0.23 : 0.20	0.87
Slope (mV/%MSO)	N = 29	VO_{2max}^{ADJ}	0.001	0.002	-0.002 : 0.004	0.62
	0.21 ± 0.11	*Age*	-0.005	0.006	-0.02: 0.01	0.42
S_{50} (%MSO)	N = 30	VO_{2max}^{ADJ}	-0.17	0.16	-0.50 : 0.16	0.31
	60.04 ± 12.14	*Age*	0.48	0.63	-0.82 : 1.78	0.45
$Slope_{peak}$ (mV/%MSO)	N = 27	VO_{2max}^{ADJ}	-0.002	0.002	-0.005 : 0.0009	0.15
	0.14 ± 0.11	*Age*	<0.0001	0.006	-0.01 : 0.01	0.99
SICI	N = 35	VO_{2max}^{ADJ}	-0.003	0.004	-0.01 : 0.005	0.41
	0.52 ± 0.32	*Age*	-0.01	0.02	-0.05 : 0.02	0.44
ICF	N = 34	VO_{2max}^{ADJ}	0.007	0.008	-0.009 : 0.02	0.39
	1.64 ± 0.67	*Age*	0.01	0.03	-0.06 : 0.08	0.72
SAI	N = 35	VO_{2max}^{ADJ}	-0.0003	0.004	-0.009 : 0.008	0.94
	0.86 ± 0.35	*Age*	-0.02	0.02	-0.02 : 0.06	0.27
LAI	N = 35	VO_{2max}^{ADJ}	-0.002	0.002	-0.008 : 0.003	0.41
	0.59 ± 0.25	*Age*	-0.02	0.01	-0.04: 0.007	0.15
SIHI	N = 35	VO_{2max}^{ADJ}	0.0004	0.003	-0.006 : 0.007	0.90
	0.52 ± 0.27	*Age*	-0.004	0.01	-0.03 : 0.02	0.79
LIHI	N = 35	VO_{2max}^{ADJ}	0.004	0.003	-0.002 : 0.01	0.21
	0.64 ± 0.27	*Age*	0.004	0.01	-0.02 : 0.03	0.78

Means ± SD displayed. Bolded values indicate significance as shown.

Table 5: Results of multiple linear regression of neurotransmitter concentrations against fitness and age

			Coefficients (β)	***SE***	***95% CI***	*p-value*
GABA+ (mM)	N = 22	VO_{2max}^{ADJ}	0.002	0.004	-0.007 : 0.01	0.66
	1.61 ± 0.31	*Age*	-0.01	0.02	-0.06 : 0.03	0.55
Glu (mM)	N = 23	VO_{2max}^{ADJ}	<0.0001	0.01	-0.02 : 0.02	0.99
	8.58 ± 0.82	*Age*	-0.04	0.05	-0.15 : 0.06	0.42

Means ± SD displayed. Bolded values indicate significance as shown.

Table 6: Results of multiple linear regression of cortical thickness in the sensorimotor area and frontal reference ROIs against fitness and age

		Coefficients (β)	***SE***	***95% CI***	*p-value*
BA 1	VO_{2max}^{ADJ}	-0.0001	0.002	-0.004 : 0.004	0.95
	Age	-0.017	0.009	-0.035 : 0.001	0.06
BA 2	VO_{2max}^{ADJ}	0.0005	0.002	-0.004 : 0.003	0.80
	Age	-0.006	0.009	-0.024 : 0.011	0.47
BA 3a	VO_{2max}^{ADJ}	0.0008	0.001	-0.002 : 0.003	0.55
	Age	-0.004	0.006	-0.016 : 0.009	0.55
BA 3b	VO_{2max}^{ADJ}	0.002	0.002	-0.001 : 0.005	0.23
	Age	0.001	0.007	-0.014 : 0.017	0.84
BA 4a	VO_{2max}^{ADJ}	0.002	0.001	-0.002 : 0.005	0.31
	Age	-0.012	0.006	-0.025 : 0.002	0.09
BA 4p	VO_{2max}^{ADJ}	0.002	0.002	-0.003 : 0.007	0.38
	Age	0.001	0.011	-0.022 : 0.025	0.91
BA 6	VO_{2max}^{ADJ}	-0.001	0.001	-0.004 : 0.002	0.48
	Age	-0.005	0.06	-0.017 : 0.007	0.39
SFG	VO_{2max}^{ADJ}	-0.001	0.001	-0.003 : 0.001	0.32
	Age	-0.003	0.005	-0.013 : 0.008	0.63
MFG	VO_{2max}^{ADJ}	-0.0001	0.001	-0.002 : 0.002	0.95
	Age	-0.007	0.005	-0.017 : 0.003	0.18
IFG	VO_{2max}^{ADJ}	-0.0005	0.001	-0.003 : 0.002	0.70
	Age	-0.003	0.006	-0.015 : 0.010	0.66
OFG	VO_{2max}^{ADJ}	-0.0009	0.001	-0.004 : 0.002	0.57
	Age	-0.004	0.007	-0.018 : 0.010	0.53

Bolded values indicate significance as shown.

Table 7: Results of multiple linear regression of FA in the sensorimotor area and frontal reference ROIs against fitness and age

		Coefficients (β)	***SE***	***95% CI***	*p-value*
M1	VO_{2max}^{ADJ}	0.0004	0.0002	-0.0001 : 0.001	0.09
	Age	-0.002	0.001	-0.004 : 0.0003	0.09
PMv	VO_{2max}^{ADJ}	0.0002	0.0002	-0.0003 : 0.001	0.33
	Age	-0.002	0.001	-0.004 : 0.001	0.14
PMd	VO_{2max}^{ADJ}	0.001	0.0002	0.0002 : 0.001	**0.009**
	Age	-0.001	0.001	-0.004 : 0.001	0.24
SMA	VO_{2max}^{ADJ}	0.0003	0.0003	-0.0003 :0.001	0.30
	Age	-0.001	0.001	-0.004 : 0.002	0.42
preSMA	VO_{2max}^{ADJ}	0.000	0.000	-0.0002 : 0.001	0.767
	Age	-0.002	0.001	-0.004 :0.0001	0.151
S1	VO_{2max}^{ADJ}	0.0003	0.0002	-0.0001 : 0.001	0.15
	Age	-0.002	0.001	-0.004 : 0.0003	0.10
CC Genu	VO_{2max}^{ADJ}	0.0005	0.0004	-0.0003 : 0.001	0.20
	Age	-0.002	0.002	-0.006 : 0.002	0.23
CC Body	VO_{2max}^{ADJ}	0.0001	0.0005	-0.001 : 0.001	0.78
	Age	-0.001	0.002	-0.005 : 0.004	0.70
CC Splenium	VO_{2max}^{ADJ}	0.0003	0.0002	-0.0002 : 0.001	0.29
	Age	-0.002	0.001	-0.004 : 0.001	0.06
Anterior CR	VO_{2max}^{ADJ}	-0.0003	0.0003	-0.001 : 0.0004	0.41
	Age	-0.0006	0.001	-0.003 : 0.002	0.65
Superior CR	VO_{2max}^{ADJ}	<0.0001	0.0002	-0.0004 : 0.001	0.86
	Age	-0.001	0.001	-0.003 : 0.001	0.30
Posterior CR	VO_{2max}^{ADJ}	0.0001	0.0003	-0.0005 : 0.001	0.75
	Age	<0.0001	0.001	-0.003 : 0.003	0.97
Cingulum Hippocampus	VO_{2max}^{ADJ}	0.0005	0.0003	-0.0001 : 0.001	0.10
	Age	-0.001	0.001	-0.005 : 0.002	0.35
Cingulum Cingulate Gyrus	VO_{2max}^{ADJ}	0.0003	0.0003	-0.0004 : 0.001	0.38
	Age	-0.003	0.002	-0.007 : 0.0001	0.06
SLF	VO_{2max}^{ADJ}	<0.0001	0.0002	-0.0002 : 0.001	0.85
	Age	-0.002	0.001	-0.004 : 0.001	0.09

Bolded values indicate significance as shown.

Table 8: Results of multiple linear regression of RD in the sensorimotor area and frontal reference ROIs against fitness and age

		Coefficients (β)	*SE*	*95% CI*	*p-value*
M1	VO_{2max}^{ADJ}	-2.526E-07	2.478E-07	-7.68 : 2.63 E-07	0.32
	Age	23.780E-07	11.240E-07	0.41 : 47.15 E-07	0.05
PMv	VO_{2max}^{ADJ}	-1.581E-07	3.134E-07	-8.10 : 4.94 E-07	0.62
	Age	23.480E-07	14.210E-07	-6.07 : 53.04 E-07	0.11
PMd	VO_{2max}^{ADJ}	-4.463E-07	2.642E-07	-9.97 : 1.03 E-07	0.11
	Age	21.750E-07	11.150E-07	-1.52 : 45.02 E-07	0.07
SMA	VO_{2max}^{ADJ}	-2.503E-07	3.730E-07	-10.26 : 5.25 E-07	0.51
	Age	27.990E-07	16.920E-07	-7.19 : 63.16 E-07	0.11
preSMA	VO_{2max}^{ADJ}	-3.510E-07	3.275E-07	-10.32 : 3.30 E-07	0.30
	Age	33.700E-07	14.850E-07	2.82 : 64.68 E-07	**0.03**
S1	VO_{2max}^{ADJ}	-0.402E-07	2.376E-07	-5.34 : 4.54 E-07	0.87
	Age	24.980E-07	10.780E-07	2.57 : 47.39 E-07	**0.03**
CC Genu	VO_{2max}^{ADJ}	-7.115E-07	5.720E-07	-19.01 : 4.78 E-07	0.23
	Age	41.250E-07	25.940E-07	-12.70 : 95.19 E-07	0.13
CC Body	VO_{2max}^{ADJ}	0.593E-07	7.394E-07	-14.78 : 15.96 E-07	0.94
	Age	31.440E-07	33.530E-07	-38.30 : 101.16 E-07	0.36
CC Splenium	VO_{2max}^{ADJ}	0.769E-07	3.517E-07	-8.08 : 6.54 E-07	0.83
	Age	28.240E-07	15.950E-07	-4.93 : 61.41 E-07	0.09
Anterior CR	VO_{2max}^{ADJ}	2.816E-07	4.186E-07	-5.89 : 11.52 E-07	0.51
	Age	8.677E-07	18.990E-07	-30 .81 : 48.16 E-07	0.65
Superior CR	VO_{2max}^{ADJ}	-0.579E-07	3.184E-07	-7.20 : 6.04 E-07	0.86
	Age	13.680E-07	14.440E-07	-16.35 : 43.71 E-07	0.35
Posterior CR	VO_{2max}^{ADJ}	1.985E-07	4.115E-07	-6.57 : 10.54 E-07	0.63
	Age	0.325E-07	18.660E-07	-38.48 : 39.13 E-07	0.99
Cingulum Hippocampus	VO_{2max}^{ADJ}	2.394E-07	3.578E-07	-5.05 : 9.83 E-07	0.51
	Age	23.820E-07	16.220E-07	-9.92 : 57.56 E-07	0.16
Cingulum Cingulate Gyrus	VO_{2max}^{ADJ}	0.659E-07	4.737E-07	-9.19 : 10.51 E-07	0.89
	Age	53.410E-07	21.480E-07	8.73 : 98.08 E-07	**0.02**
SLF	VO_{2max}^{ADJ}	0.018E-07	3.239E-07	-6.72 : 6.75 E-07	0.99
	Age	26.570E-07	14.690E-07	-39.83 : 57.12 E-07	0.08

Bolded values indicate significance as shown.

Table 9: Results of multiple linear regression of AD in the sensorimotor area and frontal reference ROIs against fitness and age

		Coefficients (β)	*SE*	*95% CI*	*p-value*
M1	VO_{2max}^{ADJ}	6.160E-07	3.452E-07	-1.01 : 13.34 E-07	0.09
	Age	-8.707E-07	15.660E-07	-41.13 : 23.85 E-07	0.58
PMv	VO_{2max}^{ADJ}	3.007E-07	3.732E-07	-4.75 : 10.77 E-07	0.43
	Age	-3.386E-07	16.930E-07	-38.58 : 31.81 E-07	0.84
PMd	VO_{2max}^{ADJ}	2.862E-07	5.573E-07	-8.73 : 14.45 E-07	0.61
	Age	15.250E-07	25.270E-07	-37.30 : 67.81 E-07	0.55
SMA	VO_{2max}^{ADJ}	2.186E-07	4.093E-07	-6.33 : 10.69 E-07	0.60
	Age	21.470E-07	18.560E-07	-17.13 : 60.07 E-07	0.26
preSMA	VO_{2max}^{ADJ}	1.570E-07	5.255E-07	-9.36 : 12.50 E-07	0.77
	Age	14.870E-07	23.830E-07	-34.68 : 64.43 E-07	0.54
S1	VO_{2max}^{ADJ}	8.240E-07	3.761E-07	0.42 : 16.06 E-07	**0.04**
	Age	-27.750E-07	17.060E-07	-38.25 : 32.70 E-07	0.87
CC Genu	VO_{2max}^{ADJ}	0.718E-07	5.430E-07	-10.58 : 12.02 E-07	0.90
	Age	27.160E-07	24.640E-07	-24.08 : 78.41 E-07	0.28
CC Body	VO_{2max}^{ADJ}	6.605E-07	6.266E-07	-6.43 : 19.64 E-07	0.30
	Age	46.400E-07	28.420E-07	-12.70 : 10.55 E-07	0.11
CC Splenium	VO_{2max}^{ADJ}	11.360E-07	6.047E-07	-1.22 : 23.93 E-07	0.07
	Age	7.351E-07	27.430E-07	-49.68 : 64.39 E-07	0.79
Anterior CR	VO_{2max}^{ADJ}	-1.030E-07	3.849E-07	-9.03 : 6.97 E-07	0.79
	Age	4.602E-07	17.460E-07	-31.70 : 40.90 E-07	0.80
Superior CR	VO_{2max}^{ADJ}	-1.340E-07	4.338E-07	-10.36 : 7.68 E-07	0.76
	Age	-12.780E-07	19.670E-07	-53.69 : 28.14 E-07	0.52
Posterior CR	VO_{2max}^{ADJ}	5.691E-07	6.118E-07	-7.03 : 18.41 E-07	0.36
	Age	-9.645E-07	27.740E-07	-67.34 : 48.05 E-07	0.73
Cingulum Hippocampus	VO_{2max}^{ADJ}	19.190E-07	6.632E-07	5.40 : 32.98 E-07	**0.009**
	Age	-3.839E-07	30.070E-07	-66.38 : 58.70 E-07	0.90
Cingulum Cingulate Gyrus	VO_{2max}^{ADJ}	7.325E-07	7.320E-07	-7.90 : 22.55 E-07	0.22
	Age	17.510E-07	33.200E-07	-51.52 : 86.54 E-07	0.60
SLF	VO_{2max}^{ADJ}	-3.753E-07	4.470E-07	-13.05 : 5.54 E-07	0.41
	Age	-4.962E-07	20.270E-07	-47.12 : 37.20 E-07	0.81

Bolded values indicate significance as shown.

Table 10: Results of multiple linear regression of MD in the sensorimotor area and frontal reference ROIs against fitness and age

		Coefficients (β)	***SE***	***95% CI***	*p-value*
M1	VO_{2max}^{ADJ}	0.282E-07	1.912E-07	-3.69 : 4.26 E-07	0.88
	Age	13.190E-07	8.672E-07	-4.85 : 31.22 E-07	0.14
PMv	VO_{2max}^{ADJ}	-0.178E-07	2.880E-07	-6.17 : 5.81 E-07	0.95
	Age	14.320E-07	13.060E-07	-12.84 : 41.48 E-07	0.29
PMd	VO_{2max}^{ADJ}	-0.322E-07	2.630E-07	-5.81 : 5.16 E-07	0.90
	Age	16.780E-07	11.100E-07	-6.38 : 39.94 E-07	0.15
SMA	VO_{2max}^{ADJ}	-0.948E-07	3.182E-07	-7.57 : 5.67 E-07	0.77
	Age	26.270E-07	14.430E-07	-3.74 : 56.29 E-07	0.08
preSMA	VO_{2max}^{ADJ}	-1.984E-07	3.520E-07	-9.31 : 5.34 E-07	0.58
	Age	28.470E-07	15.970E-07	-47.28 : 61.67 E-07	0.09
S1	VO_{2max}^{ADJ}	2.261E-07	2.160E-07	-2.23 : 6.75 E-07	0.31
	Age	16.030E-07	9.794E-07	-4.34 : 36.39 E-07	0.12
CC Genu	VO_{2max}^{ADJ}	-4.475E-07	4.733E-07	-14.32 : 5.37 E-07	0.36
	Age	35.930E-07	21.470E-07	-8.71 : 80.57 E-07	0.11
CC Body	VO_{2max}^{ADJ}	3.615E-07	4.190E-07	-5.13 : 12.35 E-07	0.40
	Age	17.700E-07	19.390E-07	-22.75 : 58.15 E-07	0.37
CC Splenium	VO_{2max}^{ADJ}	3.085E-07	3.637E-07	-4.47 : 10.65 E-07	0.41
	Age	21.070E-07	16.490E-07	-13.23 : 55.36 E-07	0.22
Anterior CR	VO_{2max}^{ADJ}	1.572E-07	3.661E-07	-6.04 : 9.19 E-07	0.67
	Age	7.128E-07	16.600E-07	-27.40 : 41.66 E-07	0.67
Superior CR	VO_{2max}^{ADJ}	-0.733E-07	3.165E-07	-7.31 : 5.85 E-07	0.82
	Age	5.676E-07	14.350E-07	-24.17 : 35.52 E-07	0.70
Posterior CR	VO_{2max}^{ADJ}	3.245E-07	4.341E-07	-5.78 : 12.27 E-07	0.46
	Age	-3.425E-07	19.690E-07	-44.37 : 37.51 E-07	0.86
Cingulum Hippocampus	VO_{2max}^{ADJ}	8.000E-07	3.964E-07	-0.02 : 16.02 E-07	0.05
	Age	15.220E-07	17.480E-07	-21.13 : 51.57 E-07	0.39
Cingulum Cingulate Gyrus	VO_{2max}^{ADJ}	2.815E-07	4.741E-07	-7.04 : 12.67 E-07	0.56
	Age	42.270E-07	21.500E-07	-2.43 : 86.98 E-07	0.06
SLF	VO_{2max}^{ADJ}	-1.149E-07	3.073E-07	-7.54 : 5.24 E-07	0.71
	Age	16.060E-07	13.940E-07	-12.92 : 45.04 E-07	0.26

Bolded values indicate significance as shown.

Chapter 7: Conclusions

GABA concentrations were validated through phantom and human experiments, prior to the assessment of neurotransmission as a function of exercise. These objectives proved that GABA measurements were stable at the local MR site and comparable to other sites *in vivo*. The primary goal of this thesis investigated the effect of long-term aerobic exercise in the form of cardiorespiratory fitness on neurotransmission. Both neurotransmitter receptor function and neurotransmitter concentrations were assessed using TMS and MRS, respectfully. In summary, the findings show that neurotransmission in the motor cortex remains relatively unchanged in healthy post-menopausal women regardless of fitness level. The secondary goal assessed structural changes with respect to exercise, and found that fitness improved WM microstructures localized to sensory, pre-motor and hippocampal tracts in post-menopausal women. Suggesting long-term exercise is able to promote motor control, tactile acuity and memory in post-menopausal women. The results provided in this thesis can improve our understanding of how aerobic exercise and cardiorespiratory fitness achieve their benefits, and contribute to the developing model of exercise-induced neural plasticity [11]. This information is vital in order to fully take advantage of the beneficial effects

of exercise on behavior and cognition. Specifically, it can be used to create efficient training programs to prevent age-related decline and improve prognosis of age-related disease. The limitations and future directions are discussed below.

7.1 Limitations and Future Directions

The lack of results in neurotransmission are limited to the motor cortex, and are not generalizable to other regions of the brain. Fitness-related potentiation may still be evident in regions that have commonly shown changes to function as a results of long-term exercise, or are involved in high-level processing related to memory, executive function, and motor control such as the frontal cortex, hippocampus and basal ganglia [152], [177], [183]–[185]. Future studies should investigate these regions as a function of fitness to get a complete picture of the effect of exercise on neurotransmission.

The specific type of long-term exercise that was completed by active participants might have also contributed to the negative results on the functional measures. One study using pair associative stimulation (PAS) to induce neuroplasticity in the primary motor cortex was able to induce changes to corticospinal excitability only in skill-trained athletes, not endurance-trained athletes nor inactive controls [186]. The majority of long-term aerobic exercisers included in this study participated in endurance activities such as running, cycling, and swimming. This type of training involves repeated movement sequences, rather than skilled movement that is seen with exercises such as

dance, gymnastics, and figure skating [186]. Suggesting skilled-exercise may be more likely to induce changes in potentiation in the motor cortex, compared to endurance-exercise. Future studies can investigate this theory by including both skill-trained and endurance-trained athletes in their population and comparing how their cardiorespiratory fitness affects measures of neurotransmission.

The relationship between structure and neurophysiology was never considered in this thesis. Although it may affect TMS observations and contribute to inconsistencies in results between studies. For examples, greater cortical thickness of M1 and FA of the pyramidal tracts have been correlated with corticospinal excitability [187]. The propagation of TMS-evoked potentials within the cortex is also affected by GM and FA [188]. Furthermore, inter-hemispheric inhibition is associated with WM volume of the corpus collosum [189]. Although we showed no effect of cardiorespiratory fitness on neurophysiological measures, it is still plausible that the results were confounded by structural changes. Considering we did assess structural measures in our participants we can use these values as covariates in our statistical modelling. Specifically, we can determine if the residuals from our regression modelling are correlated with any of the structural measures and include those measures in the regression model to account for structural variability between participants.

The data were acquired in post-menopausal women and the results may not be

applicable to other populations. It is unknown if the same results will be seen in men, or other age-ranges within women. Exercise-induced changes in neurotransmission are under-investigated and futures studies would benefit from applying the methodology present in this thesis to investigate both men and women with a wide age-range. This would allow researchers to determine if biological sex or age has any effect on fitness related potentiation. Having a wide age range would also allow researchers to determine if fitness is able to preserve neurotransmission after a certain age.

Another limitation of the research is the fact that hormone levels were never assessed to confirm post-menopause. As such, it is possible that our highly fit individuals could have athletic amenorrhoea, instead of being post-menopausal. There is also evidence that showed higher estradiol levels help induce neuroplasticity through non-invasive brain stimulation [190], although it is unclear whether fluctuations in hormone levels in this population would affect fitness-related neural plasticity. However, it can be speculated that the low levels of estradiol seen in post-menopausal women may explain why there were no observed changes to potentiation through long-term exercise. Future studies may want to include hormone assessments for their participants, to determine if ovarian hormones play a role in the propensity for neural plasticity.

It is interesting that acute aerobic exercise is able to induce potentiation in the motor cortex [77], [78], [82], [191]. Although, our results show that these changes might be

relatively short-lived and are not present in chronic aerobic exercisers. However, this thesis did not assess short-term plasticity nor the possible relationship between short-term and long-term potentiation due to fitness. For example, long-term exercise and cardiorespiratory fitness are able to amplify or promote neuroplasticity in the motor cortex induced by acute exercise [77], [82], [192], motor learning [193], [194], and even PAS [85]. This suggest that long-term exercise supports other mechanisms that may help facilitate short-term plasticity in the motor cortex, such as improved blood flow and increase in neurotrophic factors [11]. Future studies would benefit from doing a multi-modal assessment of long-term and acute exercise interventions, to get a better grasp of the relationship between short- and long-term neural plasticity.

The role of BDNF in fitness-induced potentiation of the motor cortex is of particular interest due to its close relationship with GABAergic and Glutamatergic function [20], [62]–[64], [69]. However, this relationship was not investigated in this thesis and has actually never been investigated in previous literature. Fitness and long-term exercise has been associated greater peripheral BDNF levels and possible increase in uptake into the CNS [195]. However, this is an indirect measure of BDNF and does not reflect BDNF levels in the CNS. Another option is to directly assess the BDNF gene in each participant through the rs6265 single nucleotide polymorphisms (SNP). The common form of the BDNF SNP is composed of two valine (val) constituents, however a variation called Val66Met replaces one of the val with a methionine (met) constituent.

Val66Met carriers have been shown to have reduced propensity for neuroplasticity related to motor learning compared to non-carriers [196], [197], and did not improve in memory function after a 4-week exercise intervention [198]. Likely due to reduced secretion of BDNF into the CNS [194], [199]. Hence, it would be of interest to investigate the role of the Val66Met polymorphism in fitness-induced changes to neurotransmission.

Appendix

A.1 Recruitment Curve Fitting Script

```
% Script that fits the Boltzmann sigmoidal function to recruitment curve
data (Carroll, 2001; Kukke, 2014; Schambra, 2015)
%   REQUIRES SUBFUNCTION (sigm_fit_MEP.m) and STATISTICS TOOLBOX
%
%
%       - baseline MEP: bottom limit of curve
%       - plateau MEP: top limit of curve
%       - inflection RMT: stimulation intensity that produces an MEP
half-way
%           between baseline & plateau
%       - peak slope: instantaneous slope at the inflection point
(mV/%RMT)
%       - general slope (1/k): change in stimulus intensity from the
inflection point
%           that relates to a 73% change in MEPs? (1/k = mV/%RMT)
%       - full AUC: area under the curve (of fitted sigmoid)
%       - thresholded AUC: area under the curve of slope as % change
from
%           baseline to plataeu (of fitted sigmoid)
%       - bottom and bop AUC Cutoffs (RMT): the RMT range used for
%           thresholded AUC
%       - estimated RMT: x-intercept from the inflection point at peak
slope
%       - R^2 (coefficient of determination): goodness of a fit
%       - Plateau Evident?: less than 10% difference between the
estimated
%           plateau and the last sample of the fitted curve (plateau
found inside
%           the range of data points)

% Average Recruitment Curve Data [MSO MEP]
RC=[58 0.5
    60 0.6
    65 0.8];

% the range used for thresholded AUC (% change from baseline to plataeu)
AUC_thresh_ON = 0; % [1] Perform AUC thresholding; [0] Don't...
```

```
AUC_range = [25,75];


%% ---------------------------------------------------------------------
% MSO or %RMT
MSO=RC(1,:);

% average MEP
MEP=RC(2,:);

% set some parameters (optional)
baselineMEP = 0.013; % <90% RMT or 0.013 (lower noise limit)
satMEP = NaN; % experimental maxMEP or NaN (will estimate max MEP)

% fitting data to Boltzmann sigmoidal function
fixed_params=[baselineMEP, satMEP , NaN , NaN];
[param,stats] =sigm_fit_MEP(MSO,MEP,fixed_params);

satMEP=param(2); % estimated max MEP if no experimental given
AUC=stats.AUC_full; % Area under curve of sigmoidal function
(trapezoidal method)
gen_slope= param(4);

%%% get inflection point from sigmoidal function
inflectionMSO =param(3); % inflection point of sigmoidal function
inflectionMSO_T0ref=inflectionMSO;
inflextionMEP=baselineMEP + (satMEP/(1+exp((inflectionMSO-
inflectionMSO)./gen_slope))) ;
inflextionMEP_T0ref= inflextionMEP;

%%% get peak slope
inflectionINDX1=find(round(stats.x_vector,1)==round(inflectionMSO,1)); %
round to 1 decimal point
% could't find index try rounding to integer
if isempty(inflectionINDX1)
    new_inflectionMSO=round(param(3)); % inflection point of sigmoidal
function
    inflectionINDX1=find(round(stats.x_vector)== new_inflectionMSO);
end
% only use one index if multiple found (usually right next to eachother)
if length(inflectionINDX1)>2
    error('Multiple inflection points found.');
elseif isempty(inflectionINDX1)
    inflectionINDX1 = NaN;
    slopeMEP = NaN;
else
    inflectionINDX1= inflectionINDX1(1);
    inst_slope1=gradient(stats.y_vector);
    slopeMEP=inst_slope1(inflectionINDX1);% mV/MSO
end
```

```
%%% get AUC of slope only (using % change in MEPs at inflection point)
if AUC_thresh_ON == 1

    AUC_top_thresh = inflextionMEP_T0ref*(AUC_range(2)/50);
    AUC_bottom_thresh = inflextionMEP_T0ref*(AUC_range(1)/50);

    % find indx closest to calculated threshold
    [~,topINDX1]=min(abs(stats.y_vector-AUC_top_thresh));
    % top threshold off of plot because inflection point is off plot
    if isnan(inflectionINDX1) && topINDX1==length(stats.y_vector)
        topINDX1=[];
    end
    % only use one index if multiple found (usually right next to
eachother)
    if length(topINDX1)>2
        error('Multiple top thresholds found for T0.');
    elseif length(topINDX1)==2
        topINDX1= topINDX1(end);
    end

    % find indx closest to calculated threshold
    [~,bottomINDX1]=min(abs(stats.y_vector-AUC_bottom_thresh));
    % botom threshold off of plot because inflection point is off plot
    if isnan(inflectionINDX1) && bottomINDX1==length(stats.y_vector)
        bottomINDX1=[];
    end
    % only use one index if multiple found (usually right next to
eachother)
    if length(bottomINDX1)>2
        error('Multiple bottom thresholds found for T0.');
    elseif length(bottomINDX1)==2
        bottomINDX1= bottomINDX1(end);
    end

    if isempty(bottomINDX1) || isempty(topINDX1)
        error('Not able to find thresholds for T0.');
    end

    try

AUC_thresh(1)=trapz(stats.x_vector(bottomINDX1:topINDX1),stats.y_vector(
bottomINDX1:topINDX1));
    catch % error if not able to fit rage for T1
        error('Not able to find thresholded AUC for T0 - out of
range.');
    end
end

%%% estimate RMT
if isnan(inflectionINDX1)
```

```
    est_RMT= NaN;
else
    est_RMT= inflectionMSO-((stats.y_vector(inflectionINDX1)-
0)/slopeMEP);
end
RMT_amp=baselineMEP + (param(2)/(1+exp((param(3)-est_RMT)/param(4))));

% estimate 1mV
if satMEP<1
    est_1mv = NaN;
else
    est_1mv = param(3)-(log((satMEP/(1-baselineMEP))-1)*param(4));
end

% % determine if baseline in MEPS is evident
% first_MEP=stats.y_vector(1);
% if first_MEP > 0.05
%     bsln_cnfm='NO';
% else
%     bsln_cnfm='YES';
% end


%%% determine if plateau in MEPS is evident
last_MEP=stats.y_vector(end-9:end);
percent_change= ((satMEP-last_MEP(end))/satMEP) * 100;
if percent_change==15 || percent_change>15
    plateau_cnfm='NO';
else
    plateau_cnfm='YES';
end


%%% display results
fprintf('RESULTS: \n');
fprintf(['Baseline MEP (mV): \t',num2str(baselineMEP),'\n']);
fprintf(['Plateau MEP (mV): \t',num2str(satMEP),'\n']);
fprintf(['Inflection MSO: \t',num2str(round(inflectionMSO)),'\n']);
fprintf(['Inflection (mV): \t',num2str(inflextionMEP),'\n']);
fprintf(['Peak Slope (mV/MSO): \t',num2str(slopeMEP),'\n']);
fprintf(['General Slope [1/k] (mV/MSO):
\t',num2str(1/gen_slope),'\n\n']);
fprintf(['Full AUC: \t',num2str(AUC),'\n']);
if AUC_thresh_ON == 1
    fprintf(['Thresholded AUC: \t',num2str(AUC_thresh),'\n']);
    fprintf(['Bottom AUC Cutoffs (MSO):
\t',num2str(round(stats.x_vector(bottomINDX1))),'\n']);
    fprintf(['Top AUC Cutoffs (MSO):
\t',num2str(round(stats.x_vector(topINDX1))),'\n\n']);
end
fprintf(['Estimated RMT MSO: \t',num2str(round(est_RMT)),'\n']);
```

```
fprintf(['Estimated RMT Amplitude (mV): \t',num2str(RMT_amp),'\n']);
fprintf(['Estimated 1mV MSO: \t',num2str(round(est_1mv)),'\n\n']);
fprintf(['R^2: \t',num2str(stats.Rsqr),'\n']);
% fprintf(['Baseline Evident?: \t',bsln_cnfm,'\n']);
fprintf(['Plateau Evident?: \t',plateau_cnfm,'\n\n']);



function
[param,stat]=sigm_fit_MEP(x,y,fixed_params,initial_params,plot_flag)
% Optimization of parameters of the sigmoid function
%
% Syntax:
%       [param]=sigm_fit(x,y)
%
%       that is the same that
%       [param]=sigm_fit(x,y,[],[],[])     % no fixed_params, automatic
initial_params
%
%       [param]=sigm_fit(x,y,fixed_params)        % automatic
initial_params
%       [param]=sigm_fit(x,y,[],initial_params)   % use it when the
estimation is poor
%       [param]=sigm_fit(x,y,fixed_params,initial_params,plot_flag)
%
% param = [min, max, x50, slope]
%
% if fixed_params=[NaN, NaN , NaN , NaN]        % or fixed_params=[]
% optimization of "min", "max", "x50" and "slope" (default)
%
% if fixed_params=[0, 1 , NaN , NaN]
% optimization of x50 and slope of a sigmoid of ranging from 0 to 1
%
%
% Additional information in the second output, STAT
% [param,stat]=sigm_fit(x,y,fixed_params,initial_params,plot_flag)
%
%
% Example:
% %% generate data vectors (x and y)
% fsigm = @(param,xval) param(1)+(param(2)-param(1))./(1+10.^((param(3)-
xval)*param(4)))
% param=[0 1 5 1];  % "min", "max", "x50", "slope"
% x=0:0.1:10;
% y=fsigm(param,x) + 0.1*randn(size(x));
%
% %% standard parameter estimation
% [estimated_params]=sigm_fit(x,y)
%
% %% parameter estimation with forced 0.5 fixed min
% [estimated_params]=sigm_fit(x,y,[0.5 NaN NaN NaN])
%
```

```
% %% parameter estimation without plotting
% [estimated_params]=sigm_fit(x,y,[],[],0)
%
%
% Doubts, bugs: rpavao@gmail.com
% Downloaded from
http://www.mathworks.com/matlabcentral/fileexchange/42641-sigmoid-
logistic-curve-fit

% warning off

x=x(:);
y=y(:);

if nargin<=1 %fail
    fprintf('');
    help sigm_fit
    return
end

automatic_initial_params=[quantile(y,0.05) quantile(y,0.95) NaN 1];
if sum(y==quantile(y,0.5))==0
    temp=x(y==quantile(y(2:end),0.5));
else
    temp=x(y==quantile(y,0.5));
end
automatic_initial_params(3)=temp(1);

if nargin==2 %simplest valid input
    fixed_params=NaN(1,4);
    initial_params=automatic_initial_params;
    plot_flag=1;
end
if nargin==3
    initial_params=automatic_initial_params;
    plot_flag=1;
end
if nargin==4
    plot_flag=1;
end

if exist('fixed_params','var')
    if isempty(fixed_params)
        fixed_params=NaN(1,4);
    end
end
if exist('initial_params','var')
    if isempty(initial_params)
        initial_params=automatic_initial_params;
    end
end
```

```
if exist('plot_flag','var')
    if isempty(plot_flag)
        plot_flag=1;
    end
end

%f = @(p,x) p(1) + (p(2)) ./ (1 + exp((p(3)-x)/p(4)));

f_str='f = @(param,xval)';
free_param_count=0;
bool_vec=NaN(1,4);
for i=1:4;
    if isnan(fixed_params(i))
        free_param_count=free_param_count+1;
        f_str=[f_str ' param(' num2str(free_param_count) ')'];
        bool_vec(i)=1;
    else
        f_str=[f_str ' ' num2str(fixed_params(i))];
        bool_vec(i)=0;
    end
    if i==1; f_str=[f_str ' + ('']; end
    if i==2;
        if isnan(fixed_params(1))
            f_str=[f_str ' )./ (   1 + exp( ('];
        else
            f_str=[f_str ' )./ (   1 + exp( ('];
        end
    end
    if i==3; f_str=[f_str ' - xval ) /'']; end
    if i==4; f_str=[f_str ' )   );'']; end
end

disp(' ')
disp(f_str)
disp(' ')
eval(f_str)

% non linear regression
[BETA,RESID,J,COVB,MSE] = nlinfit(x,y,f,initial_params(bool_vec==1));
stat.param=BETA';

% 95 confidence interval of the parameters
stat.paramCI = nlparci(BETA,RESID,'Jacobian',J);

% 95 confidence interval of the estimation
[stat.ypred,delta] = nlpredci(f,x,BETA,RESID,'Covar',COVB);
stat.ypredlowerCI = stat.ypred - delta;
stat.ypredupperCI = stat.ypred + delta;

% plot(x,y,'ko') % observed data
% hold on
```

```
% plot(x,ypred,'k','LineWidth',2)
% plot(x,[lower,upper],'r--','LineWidth',1.5)

free_param_count=0;
for i=1:4;
    if isnan(fixed_params(i))
        free_param_count=free_param_count+1;
        param(i)=BETA(free_param_count);
    else
        param(i)=fixed_params(i);
    end
end

if plot_flag==1
    x_vector= min(x):1:max(x);
    y_vector = f(param(isnan(fixed_params)),x_vector);
    figure;
    plot(x,y,'ko',x_vector,y_vector,'r--')
    xlim([min(x) max(x)])
    xlabel('% MSO');
    ylabel('average MEP (mV)');
end

% full AUC
stat.AUC_full=trapz(x_vector,y_vector);
stat.x_vector=x_vector;
stat.y_vector=y_vector;
stat.residual=RESID;
stat.Rsqr=1-(sum(RESID.^2)/sum((y-mean(y)).^2));
end
```

A.2 DTI Processing Script

```
#!/bin/bash
########################################
# DTI processing in FSL
########################################

echo " "
echo -n "Enter participant directory to process and press [ENTER] : "
read exam_name

echo " "

# 1) --------------------------- PRE-PROCESSING -----------------------
------

# Merge the dti19 , dti20 and dti21 files
# and store in dti merge
# split each file into individual volumes.
# (ie. 22 for 19-dir , 23 for 20-dir , and 24 for 21-dir)
# Want B0 volumes at the start, and B1000 values afterwards

# Make sure the data is in the proper series
# 19 dir --> Ser7
dir1=Ser7
# 20 dir --> Ser8
dir2=Ser8
# 21 dir --> Ser9
dir3=Ser9
# B0 map 1 (TE=5 ms) --> Ser 10
dir4=Ser10
# B0 map 2 (TE=7.3 ms) --> Ser 11
dir5=Ser11

# Convert data to nifti format and process

cd $exam_name
mkdir DTI_processing

cd exam_*
dcm2niix -z y -o ./$dir1 -f dti19 ./$dir1
dcm2niix -z y -o ./$dir2 -f dti20 ./$dir2
dcm2niix -z y -o ./$dir3 -f dti21 ./$dir3
dcm2niix -z y -o ./$dir4 -f B0_5 ./$dir4
dcm2niix -z y -o ./$dir5 -f B0_7.3 ./$dir5
```

```
cd ..
mkdir DTI_processing/DTI_split

# Split the 3 separate DTI scans
fslsplit exam_*/$dir1/dti19.nii.gz DTI_processing/DTI_split/v19_
fslsplit exam_*/$dir2/dti20.nii.gz DTI_processing/DTI_split/v20_
fslsplit exam_*/$dir3/dti21.nii.gz DTI_processing/DTI_split/v21_

echo " "
echo "Done splitting files "
echo " "

mkdir DTI_processing/DTI_merge
cd DTI_processing/DTI_split

# brain extract one b=0 image (doesn't matter which) for use with
correction section
bet2 v19_0000.nii.gz v19_0000_extract -m -f 0.2

# Merge the split DTI scans in the proper order for processing

fslmerge -t ../DTI_merge/dti60.nii \
v19_0000 v19_0001 v19_0002 \
v20_0000 v20_0001 v20_0002 \
v21_0000 v21_0001 v21_0002 \
v19_0003 v19_0004 v19_0005 v19_0006 \
v19_0007 v19_0008 v19_0009 v19_0010 \
v19_0011 v19_0012 v19_0013 v19_0014 \
v19_0015 v19_0016 v19_0017 v19_0018 \
v19_0019 v19_0020 v19_0021 v20_0003 \
v20_0004 v20_0005 v20_0006 v20_0007 \
v20_0008 v20_0009 v20_0010 v20_0011 \
v20_0012 v20_0013 v20_0014 v20_0015 \
v20_0016 v20_0017 v20_0018 v20_0019 \
v20_0020 v20_0021 v20_0022 v21_0003 \
v21_0004 v21_0005 v21_0006 v21_0007 \
v21_0008 v21_0009 v21_0010 v21_0011 \
v21_0012 v21_0013 v21_0014 v21_0015 \
v21_0016 v21_0017 v21_0018 v21_0019 \
v21_0020 v21_0021 v21_0022 v21_0023

echo "Done merging files "
echo " "

# Check that the volumes are in the
# correct order/number (9 B=0's followed by 60 B=900's)
# [depends on sequence parameters]

# Now perform a brain extraction using BET.
# (adjust threshold using -f 0.3)
```

```
# S.M. Smith. Fast robust automated brain extraction.
# Human Brain Mapping, 17(3):143-155 ,
# November 2002.

cd ../DTI_merge
bet2 dti60.nii.gz dti60_ns -m -f 0.3
echo "Done brain extraction "
echo " "

# 2) --------------------------- CORRECTION ----------------------------
--

### If topup not an option use B0 field maps for susceptibility
correction
### requires two scas at different TE's (ex. TE= 5 & 7.3 ms)

mkdir ../B0_maps
cd ../../exam_*

# split B0 image into volumes (CV -> rhrcctrl = 15)
# vol 0 = magnitude (looks like regular image)
# vol 1 = phase - integer format not rad (white noise like checkered
background)
# vol 2 = real (sinusoidal pattern)
# vol 3 = imaginary (sinusoidal pattern)
fslsplit ./$dir4/B0_5.nii.gz ./$dir4/B0_5_
fslsplit ./$dir5/B0_7.3.nii.gz ./$dir5/B0_7.3_

# don't use mag or phase volumes (scaling issues)
# instead calculate mag and phase from complex data...

# create complex volume (merge real and imaginary)
fslcomplex -complex ./$dir4/B0_5_0002.nii.gz ./$dir4/B0_5_0003.nii.gz
./$dir4/B0_5_complx
fslcomplex -complex ./$dir5/B0_7.3_0002.nii.gz
./$dir5/B0_7.3_0003.nii.gz ./$dir5/B0_7.3_complx

# calculate magnitude
fslcomplex -realabs ./$dir4/B0_5_complx.nii.gz ./$dir4/B0_5_mag
fslcomplex -realabs ./$dir5/B0_7.3_complx.nii.gz ./$dir5/B0_7.3_mag

# calculate phase (in radians)
fslcomplex -realphase ./$dir4/B0_5_complx.nii.gz ./$dir4/B0_5_phase
fslcomplex -realphase ./$dir5/B0_7.3_complx.nii.gz ./$dir5/B0_7.3_phase

# if phase is not in radians (0-6.28) have to adjust manually
fslmaths ./$dir4/B0_5_phase.nii.gz -add 3.14159 ./$dir4/B0_5_phase_rad -
odt float
fslmaths ./$dir5/B0_7.3_phase.nii.gz -add 3.14159
./$dir5/B0_7.3_phase_rad -odt float
```

```
# 'unwrap' phase image
prelude -a ./$dir4/B0_5_mag.nii.gz -p ./$dir4/B0_5_phase_rad.nii.gz -o
./$dir4/B0_5_phase_unwrapped
prelude -a ./$dir5/B0_7.3_mag.nii.gz -p ./$dir5/B0_7.3_phase_rad.nii.gz
-o ./$dir5/B0_7.3_phase_unwrapped

# create fieldmaps (in rad/s)
# -div is the the difference between TE's in ms (should be ~2.5 ms for
3T)
fslmaths ./$dir5/B0_7.3_phase_unwrapped.nii.gz -sub
./$dir4/B0_5_phase_unwrapped.nii.gz -mul 1000 -div 2.3
../DTI_processing/B0_maps/fieldmap -odt float

# run brain extraction of mag image - doesn't matter which TE
bet2 ./$dir4/B0_5_mag.nii.gz ../DTI_processing/B0_maps/mag_extract -m -f
0.2

# regularize fieldmap
cd ../DTI_processing/B0_maps
fslmaths fieldmap.nii.gz -mas mag_extract_mask.nii.gz fieldmap_extract #
mask
fugue --loadfmap=fieldmap_extract.nii.gz -s 1 --
savefmap=fieldmap_gauss_smooth # Gaussian filtering
fugue --loadfmap=fieldmap_gauss_smooth.nii.gz --despike --
savefmap=fieldmap_despike # despike (DC removal?)
fugue --loadfmap=fieldmap_despike.nii.gz -m --savefmap=fieldmap_final #
median filter

### Eddy current correction using 'eddy_correct'
### Diffusion - default volume reference = 0
eddy_correct ../DTI_merge/dti60.nii.gz ../DTI_merge/dti60_corr -def
trilinear

## Then Susceptibility correction ('unwarping of the EPI')
# --dwell is the echo spacing in sec (incorporating any acceleration) ->
around 0.5-0.7 ms

# warp mag image to non-regularized fieldmap (don't get why?)
fugue -i mag_extract.nii.gz --unwarpdir=y --dwell=0.000612 --
loadfmap=fieldmap.nii.gz -w mag_extract_warpped
# register warped mag image with b=0 of DTI data
flirt -in mag_extract_warpped.nii.gz -ref
../DTI_split/v19_0000_extract.nii.gz -out mag_extract_warpped_2_dti -
omat fieldmap2dti.mat
# apply transformation to regularized fieldmap
flirt -in fieldmap_final.nii.gz -ref
../DTI_split/v19_0000_extract.nii.gz -applyxfm -init fieldmap2dti.mat -
out fieldmap_final_registered
# undistort DTI with registered fieldmap
fugue -i ../DTI_merge/dti60_corr.nii.gz --icorr --unwarpdir=y --
```

```
loadfmap=fieldmap_final_registered.nii.gz --dwell=0.000612 -u
../DTI_merge/dti60_susc_corr


echo "Done eddy current and susceptibility correction "
echo " "

# 3) ---------------------------- TENSOR RE-CONSTRUCTION ----------------
--------------

# Reconstruct diffusion tensor using
# FDT on the data that has been
# pre-processed (brain extracted) and
# eddy current corrected data

# if the .bvec .bval files were created
#       cp -R dti60.bvec dti60.bval Results
# if not then get matlab to make them... (custom function)
cd ../../exam_*
matlab -nodisplay -r
"merge_bval_bvec({'./$dir1/dti19.bval','./$dir2/dti20.bval','./$dir3/dti
21.bval'},
{'./$dir1/dti19.bvec','./$dir2/dti20.bvec','./$dir3/dti21.bvec'},'../DTI
_processing/DTI_merge/'); exit"

cd ../DTI_processing
mkdir Results
cd DTI_merge
dtifit \
-k dti60_susc_corr.nii.gz \
-o ../Results/dti60_corr_final \
-m dti60_ns_mask.nii.gz \
-r dti60.bvec \
-b dti60.bval

# Calculate the RD image L2+L3/2 from
# the fit diffusion tensors

cd ../Results
fslmaths dti60_corr_final_L2.nii.gz \
-add dti60_corr_final_L3.nii.gz sum
fslmaths sum.nii.gz \
-div 2 dti60_corr_final_RD

# rename L1 = AD
cp  dti60_corr_final_L1.nii.gz dti60_corr_final_AD.nii.gz


# Copy FA to white matter skeleton analysis folder
mkdir ../../../study_WM_mask
```

```
cp dti60_corr_final_FA.nii.gz
../../../study_WM_mask/dti60_corr_final_FA_$exam_name.nii.gz

echo "Done reconstructing diffusion tensors."
echo " "


#!/bin/bash
##########################################
# DTI ROI Analysis
##########################################

cd study_WM_mask

# Create study derived white matter skeleton which represents
# the centres of all tracts common to the group (warped to standard
MNI152 space)
tbss_1_preproc *.nii.gz
tbss_2_reg -T
tbss_3_postreg -S

echo "Done creating study derived white matter mask "
echo " "

# project participant data onto white matter skeleton
echo " "
echo -n "Compare mean_FA_skeleton to all_FA; Enter threshold (0.2)
[ENTER] : "
read FA_thr
echo " "
tbss_4_prestats $FA_thr # make sure threshold works for data

# Create mask for each ROI using:
# fslmaths JHU-ICBM-labels-1mm.nii.gz -thr inx# -uthr inx#
~/Desktop/Thesis/DATA/MRI/ICBM-DTI-81_labels/ROI_name
# Directory for masks:
mask_dir=~/Desktop/Thesis/DATA/MRI

# Make sure there is a text file with a list of all the ROI names
# (names used for naming conventions - no spaces)
roi_names1=$mask_dir/ICBM-DTI-81_labels.txt
roi_names2=$mask_dir/SMATT.txt

# For each participant....
cd ..
for d in * ; do

    if [ "$d" == "study_WM_mask" ] ; then
        continue;
    fi
```

```
    subj=$d
    echo "$subj"
    echo " "

    cd $subj/DTI_processing/Results
    mkdir ../ROI_analysis
    mkdir ../ROI_Results

    # Warp and apply study WM mask to FA/AD/RD/MD subject data
    #FA
    applywarp -r ${FSLDIR}/data/standard/FMRIB58_FA_1mm.nii.gz \
    -i dti60_corr_final_FA.nii.gz \
    -w
../../../study_WM_mask/FA/dti60_corr_final_FA_"$subj"_FA_to_target_warp.
nii.gz \
    -o dti60_corr_final_FA_norm

    fslmaths dti60_corr_final_FA_norm.nii.gz \
    -mul ../../../study_WM_mask/stats/mean_FA_skeleton_mask.nii.gz \
    dti60_corr_final_FA_norm_skeleton

    #AD
    applywarp -r ${FSLDIR}/data/standard/FMRIB58_FA_1mm.nii.gz \
    -i dti60_corr_final_AD.nii.gz \
    -w
../../../study_WM_mask/FA/dti60_corr_final_FA_"$subj"_FA_to_target_warp.
nii.gz \
    -o dti60_corr_final_AD_norm

    fslmaths dti60_corr_final_AD_norm.nii.gz \
    -mul ../../../study_WM_mask/stats/mean_FA_skeleton_mask.nii.gz \
    dti60_corr_final_AD_norm_skeleton

    #RD
    applywarp -r ${FSLDIR}/data/standard/FMRIB58_FA_1mm.nii.gz \
    -i dti60_corr_final_RD.nii.gz \
    -w
../../../study_WM_mask/FA/dti60_corr_final_FA_"$subj"_FA_to_target_warp.
nii.gz \
    -o dti60_corr_final_RD_norm

    fslmaths dti60_corr_final_RD_norm.nii.gz \
    -mul ../../../study_WM_mask/stats/mean_FA_skeleton_mask.nii.gz \
    dti60_corr_final_RD_norm_skeleton

    #MD
    applywarp -r ${FSLDIR}/data/standard/FMRIB58_FA_1mm.nii.gz \
    -i dti60_corr_final_MD.nii.gz \
    -w
```

```
../../../study_WM_mask/FA/dti60_corr_final_FA_"$subj"_FA_to_target_warp.
nii.gz \
    -o dti60_corr_final_MD_norm

    fslmaths dti60_corr_final_MD_norm.nii.gz \
    -mul ../../../study_WM_mask/stats/mean_FA_skeleton_mask.nii.gz \
    dti60_corr_final_MD_norm_skeleton

    echo "Done projecting participant data onto white matter mask "
    echo " "

    echo "ROI Analysis starting... "
    echo " "

    # Apply ROI masks to FA/AD/RD/MD subject data
    # find avaerage FA/AD/RD/MD per ROI and create a text file

    echo -e "ROI Name\t Average FA" > ../ROI_Results/FA_avg.txt
    echo -e "ROI Name\t Average AD" > ../ROI_Results/AD_avg.txt
    echo -e "ROI Name\t Average RD" > ../ROI_Results/RD_avg.txt
    echo -e "ROI Name\t Average MD" > ../ROI_Results/MD_avg.txt

    # ATLAS 1
    while IFS='' read -r line || [[ -n "$line" ]]; do

        echo "ROI: $line"

        # FA

        fslmaths dti60_corr_final_FA_norm_skeleton.nii.gz \
        -mas $mask_dir/ICBM-DTI-81_labels/$line.nii.gz \
        ../ROI_analysis/FA_$line

        temp=$(fslstats ../ROI_analysis/FA_$line.nii.gz -M)
        echo -e "$line\t $temp" >> ../ROI_Results/FA_avg.txt

        # AD

        fslmaths dti60_corr_final_AD_norm_skeleton.nii.gz \
        -mas $mask_dir/ICBM-DTI-81_labels/$line.nii.gz \
        ../ROI_analysis/AD_$line

        temp=$(fslstats ../ROI_analysis/AD_$line.nii.gz -M)
        echo -e "$line\t $temp" >> ../ROI_Results/AD_avg.txt

        # RD

        fslmaths dti60_corr_final_RD_norm_skeleton.nii.gz \
        -mas $mask_dir/ICBM-DTI-81_labels/$line.nii.gz \
```

```
    ../ROI_analysis/RD_$line

    temp=$(fslstats ../ROI_analysis/RD_$line.nii.gz -M)
    echo -e "$line\t $temp" >> ../ROI_Results/RD_avg.txt

    # MD

    fslmaths dti60_corr_final_MD_norm_skeleton.nii.gz \
    -mas $mask_dir/ICBM-DTI-81_labels/$line.nii.gz \
    ../ROI_analysis/MD_$line

    temp=$(fslstats ../ROI_analysis/MD_$line.nii.gz -M)
    echo -e "$line\t $temp" >> ../ROI_Results/MD_avg.txt

done < "$roi_names1"

# ATLAS 2
while IFS='' read -r line || [[ -n "$line" ]]; do
    echo "ROI: $line"

    # FA

    fslmaths dti60_corr_final_FA_norm_skeleton.nii.gz \
    -mas $mask_dir/SMATT/$line.nii.gz \
    ../ROI_analysis/FA_$line

    temp=$(fslstats ../ROI_analysis/FA_$line.nii.gz -M)
    echo -e "$line\t $temp" >> ../ROI_Results/FA_avg.txt

    # AD

    fslmaths dti60_corr_final_AD_norm_skeleton.nii.gz \
    -mas $mask_dir/SMATT/$line.nii.gz \
    ../ROI_analysis/AD_$line

    temp=$(fslstats ../ROI_analysis/AD_$line.nii.gz -M)
    echo -e "$line\t $temp" >> ../ROI_Results/AD_avg.txt

    # RD

    fslmaths dti60_corr_final_RD_norm_skeleton.nii.gz \
    -mas $mask_dir/SMATT/$line.nii.gz \
    ../ROI_analysis/RD_$line

    temp=$(fslstats ../ROI_analysis/RD_$line.nii.gz -M)
    echo -e "$line\t $temp" >> ../ROI_Results/RD_avg.txt

    # MD
```

```
        fslmaths dti60_corr_final_MD_norm_skeleton.nii.gz \
        -mas $mask_dir/SMATT/$line.nii.gz \
        ../ROI_analysis/MD_$line

        temp=$(fslstats ../ROI_analysis/MD_$line.nii.gz -M)
        echo -e "$line\t $temp" >> ../ROI_Results/MD_avg.txt

    done < "$roi_names2"

    echo " "
    echo "Done ROI analysis for $subj"
    echo " "

    cd ../../../

done

    echo "ROI Analysis complete."
```

References

[1] D. E. R. Warburton and S. S. D. Bredin, "Reflections on Physical Activity and Health: What Should We Recommend?," *Can. J. Cardiol.*, vol. 32, no. 4, pp. 495–504, Apr. 2016.

[2] J. E. Ahlskog, Y. E. Geda, N. R. Graff-Radford, and R. C. Petersen, "Physical exercise as a preventive or disease-modifying treatment of dementia and brain aging," *Mayo Clin Proc*, vol. 86, no. 9, pp. 876–884, Sep. 2011.

[3] S. Colcombe and A. F. Kramer, "Fitness effects on the cognitive function of older adults: a meta-analytic study," *Psychol Sci*, vol. 14, no. 2, pp. 125–130, 2003.

[4] K. I. Erickson *et al.*, "Exercise training increases size of hippocampus and improves memory," *Proc Natl Acad Sci U S A*, vol. 108, no. 7, pp. 3017–3022, 2011.

[5] L. L. Craft and F. M. Perna, "The Benefits of Exercise for the Clinically Depressed," *Prim Care Companion J Clin Psychiatry*, vol. 6, no. 3, pp. 104–111, 2004.

[6] A. Ströhle, "Physical activity, exercise, depression and anxiety disorders," *J. Neural Transm.*, vol. 116, no. 6, pp. 777–784, Jun. 2009.

[7] S. Gallanagh, T. J. Quinn, J. Alexander, and M. R. Walters, "Physical activity in the prevention and treatment of stroke," *ISRN Neurol*, vol. 2011, p. 953818, 2011.

[8] P. Heyn, B. C. Abreu, and K. J. Ottenbacher, "The effects of exercise training on elderly persons with cognitive impairment and dementia: a meta-analysis," *Arch*

Phys Med Rehabil, vol. 85, no. 10, pp. 1694–1704, 2004.

[9] "Statistics Canada (2015). Table 117-0019 – Distribution of the household population meeting/not meeting the Canadian physical activity guidelines, by sex and age group, occasional (percentage)."

[10] M. S. Tremblay, R. C. Colley, T. J. Saunders, G. N. Healy, and N. Owen, "Physiological and health implications of a sedentary lifestyle," *Appl. Physiol. Nutr. Metab.*, vol. 35, no. 6, pp. 725–740, Dec. 2010.

[11] J. El-Sayes, D. Harasym, C. V. Turco, M. B. Locke, and A. J. Nelson, "Exercise-Induced Neuroplasticity: A Mechanistic Model and Prospects for Promoting Plasticity," *Neurosci.*, pp. 1–21, Apr. 2018.

[12] S. J. Colcombe *et al.*, "Aerobic exercise training increases brain volume in aging humans," *J Gerontol A Biol Sci Med Sci*, vol. 61, no. 11, pp. 1166–1170, 2006.

[13] J. C. Smith *et al.*, "Interactive effects of physical activity and APOE-epsilon4 on white matter tract diffusivity in healthy elders," *Neuroimage*, vol. 131, pp. 102–112, 2016.

[14] B. Zimmerman *et al.*, "Cardiorespiratory fitness mediates the effects of aging on cerebral blood flow," *Front Aging Neurosci*, vol. 6, p. 59, 2014.

[15] E. Bullitt *et al.*, "The effect of exercise on the cerebral vasculature of healthy aged subjects as visualized by MR angiography," *AJNR Am J Neuroradiol*, vol. 30, no. 10, pp. 1857–1863, 2009.

[16] A. G. Thomas, A. Dennis, P. A. Bandettini, and H. Johansen-Berg, "The effects of aerobic activity on brain structure," *Front Psychol*, vol. 3, p. 86, 2012.

[17] C. Rosano *et al.*, "Psychomotor speed and functional brain MRI 2 years after completing a physical activity treatment," *J Gerontol A Biol Sci Med Sci*, vol. 65, no. 6, pp. 639–647, 2010.

[18] P. J. Magistretti and I. Allaman, "A cellular perspective on brain energy metabolism and functional imaging," *Neuron*, vol. 86, no. 4, pp. 883–901, 2015.

[19] K. D. Singh, "Which 'neural activity' do you mean? fMRI, MEG, oscillations

and neurotransmitters," *Neuroimage*, vol. 62, no. 2, pp. 1121–1130, 2012.

[20] D. K. Binder and H. E. Scharfman, "Brain-derived neurotrophic factor," *Growth Factors*, vol. 22, no. 3, pp. 123–131, 2004.

[21] J. M. Soares, P. Marques, V. Alves, and N. Sousa, "A hitchhiker's guide to diffusion tensor imaging.," *Front. Neurosci.*, vol. 7, p. 31, 2013.

[22] A. L. Alexander, J. E. Lee, M. Lazar, and A. S. Field, "Diffusion tensor imaging of the brain.," *Neurotherapeutics*, vol. 4, no. 3, pp. 316–29, Jul. 2007.

[23] C. Gasparovic *et al.*, "Use of tissue water as a concentration reference for proton spectroscopic imaging," *Magn. Reson. Med.*, vol. 55, no. 6, pp. 1219–1226, Jun. 2006.

[24] S. W. Provencher, "Automatic quantitation of localized in vivo 1H spectra with LCModel," *NMR Biomed*, vol. 14, no. 4, pp. 260–264, 2001.

[25] S. W. Provencher, "Estimation of metabolite concentrations from localized in vivo proton NMR spectra," *Magn Reson Med*, vol. 30, no. 6, pp. 672–679, 1993.

[26] M. Wilson, G. Reynolds, R. A. Kauppinen, T. N. Arvanitis, and A. C. Peet, "A constrained least-squares approach to the automated quantitation of in vivo (1)H magnetic resonance spectroscopy data," *Magn Reson Med*, vol. 65, no. 1, pp. 1–12, 2011.

[27] A. Naressi *et al.*, "Java-based graphical user interface for the MRUI quantitation package," *Magma*, vol. 12, no. 2–3, pp. 141–152, 2001.

[28] D. J. Drost, W. R. Riddle, G. D. Clarke, and A. M. T. Group, "Proton magnetic resonance spectroscopy in the brain: report of AAPM MR Task Group #9," *Med Phys*, vol. 29, no. 9, pp. 2177–2197, 2002.

[29] R. A. de Graaf, *In Vivo NMR Spectroscopy: Principles and Techniques: 2nd Edition*. 2007.

[30] C. T. Moonen *et al.*, "Comparison of single-shot localization methods (STEAM and PRESS) for in vivo proton NMR spectroscopy," *NMR Biomed*, vol. 2, no. 5–6, pp. 201–208, 1989.

[31] A. Haase, J. Frahm, W. Hanicke, and D. Matthaei, "1H NMR chemical shift selective (CHESS) imaging," *Phys Med Biol*, vol. 30, no. 4, pp. 341–344, 1985.

[32] M. Mescher, A. Tannus, M. O. Johnson, and M. Garwood, "Solvent Suppression Using Selective Echo Dephasing," *J. Magn. Reson. Ser. A*, vol. 123, no. 2, pp. 226–229, 1996.

[33] M. Mescher, H. Merkle, J. Kirsch, M. Garwood, and R. Gruetter, "Simultaneous in vivo spectral editing and water suppression," *NMR Biomed*, vol. 11, no. 6, pp. 266–272, 1998.

[34] P. G. Mullins *et al.*, "Current practice in the use of MEGA-PRESS spectroscopy for the detection of GABA," *Neuroimage*, vol. 86, pp. 43–52, 2014.

[35] N. A. Puts and R. A. Edden, "In vivo magnetic resonance spectroscopy of GABA: a methodological review," *Prog Nucl Magn Reson Spectrosc*, vol. 60, pp. 29–41, 2012.

[36] J. Hu, S. Yang, Y. Xuan, Q. Jiang, Y. Yang, and E. M. Haacke, "Simultaneous detection of resolved glutamate, glutamine, and gamma-aminobutyric acid at 4 T," *J Magn Reson*, vol. 185, no. 2, pp. 204–213, 2007.

[37] P. M. Rossini *et al.*, "Non-invasive electrical and magnetic stimulation of the brain, spinal cord, roots and peripheral nerves: Basic principles and procedures for routine clinical and research application. An updated report from an I.F.C.N. Committee," *Clin Neurophysiol*, vol. 126, no. 6, pp. 1071–1107, 2015.

[38] V. Di Lazzaro *et al.*, "The physiological basis of transcranial motor cortex stimulation in conscious humans.," *Clin. Neurophysiol.*, vol. 115, no. 2, pp. 255–66, Feb. 2004.

[39] V. Di Lazzaro *et al.*, "I-wave origin and modulation," *Brain Stimul*, vol. 5, no. 4, pp. 512–525, 2012.

[40] S. Groppa, M. Muthuraman, B. Otto, G. Deuschl, H. R. Siebner, and J. Raethjen, "Subcortical substrates of TMS induced modulation of the cortico-cortical connectivity," *Brain Stimul*, vol. 6, no. 2, pp. 138–146, 2013.

[41] F. Awiszus, "TMS and threshold hunting," *Suppl Clin Neurophysiol*, vol. 56, pp. 13–23, 2003.

[42] C. B. Ah Sen, H. J. Fassett, J. El-Sayes, C. V Turco, M. M. Hameer, and A. J. Nelson, "Active and resting motor threshold are efficiently obtained with adaptive threshold hunting.," *PLoS One*, vol. 12, no. 10, p. e0186007, 2017.

[43] U. Ziemann *et al.*, "TMS and drugs revisited 2014," *Clin Neurophysiol*, vol. 126, no. 10, pp. 1847–1868, 2015.

[44] V. Di Lazzaro, U. Ziemann, and R. N. Lemon, "State of the art: Physiology of transcranial motor cortex stimulation," *Brain Stimul.*, vol. 1, no. 4, pp. 345–362, Oct. 2008.

[45] H. R. Siebner and J. Rothwell, "Transcranial magnetic stimulation: new insights into representational cortical plasticity," *Exp Brain Res*, vol. 148, no. 1, pp. 1–16, 2003.

[46] K. Dyke *et al.*, "Comparing GABA-dependent physiological measures of inhibition with proton magnetic resonance spectroscopy measurement of GABA using ultra-high-field MRI," *Neuroimage*, vol. 152, pp. 360–370, 2017.

[47] H. Devanne, B. A. Lavoie, and C. Capaday, "Input-output properties and gain changes in the human corticospinal pathway," *Exp Brain Res*, vol. 114, no. 2, pp. 329–338, 1997.

[48] T. Kujirai *et al.*, "Corticocortical inhibition in human motor cortex," *J Physiol*, vol. 471, pp. 501–519, 1993.

[49] C. V. Turco, J. El-Sayes, M. J. Savoie, H. J. Fassett, M. B. Locke, and A. J. Nelson, "Short- and long-latency afferent inhibition; uses, mechanisms and influencing factors," *Brain Stimul.*, vol. 11, no. 1, pp. 59–74, Jan. 2018.

[50] V. Di Lazzaro *et al.*, "Effects of lorazepam on short latency afferent inhibition and short latency intracortical inhibition in humans," *J Physiol*, vol. 564, no. Pt 2, pp. 661–668, 2005.

[51] V. Di Lazzaro *et al.*, "Muscarinic receptor blockade has differential effects on

the excitability of intracortical circuits in the human motor cortex," *Exp Brain Res*, vol. 135, no. 4, pp. 455–461, 2000.

[52] C. V. Turco, J. El-Sayes, M. B. Locke, R. Chen, S. Baker, and A. J. Nelson, "Effects of lorazepam and baclofen on short- and long-latency afferent inhibition," *J. Physiol.*, vol. 596, no. 21, pp. 5267–5280, Nov. 2018.

[53] C. V Turco, J. El-Sayes, H. J. Fassett, R. Chen, and A. J. Nelson, "Modulation of long-latency afferent inhibition by the amplitude of sensory afferent volley.," *J. Neurophysiol.*, vol. 118, no. 1, pp. 610–618, Jul. 2017.

[54] C. V Turco, M. B. Locke, J. El-Sayes, M. Tommerdahl, and A. J. Nelson, "Exploring Behavioral Correlates of Afferent Inhibition.," *Brain Sci.*, vol. 8, no. 4, Apr. 2018.

[55] K. Irlbacher, J. Brocke, J. V Mechow, and S. A. Brandt, "Effects of GABA(A) and GABA(B) agonists on interhemispheric inhibition in man," *Clin Neurophysiol*, vol. 118, no. 2, pp. 308–316, 2007.

[56] G. Buzsaki, K. Kaila, and M. Raichle, "Inhibition and brain work," *Neuron*, vol. 56, no. 5, pp. 771–783, 2007.

[57] S. H. Hendry, H. D. Schwark, E. G. Jones, and J. Yan, "Numbers and proportions of GABA-immunoreactive neurons in different areas of monkey cerebral cortex," *J Neurosci*, vol. 7, no. 5, pp. 1503–1519, 1987.

[58] J. S. Isaacson and M. Scanziani, "How inhibition shapes cortical activity," *Neuron*, vol. 72, no. 2, pp. 231–243, 2011.

[59] G. Losi, L. Mariotti, and G. Carmignoto, "GABAergic interneuron to astrocyte signalling: a neglected form of cell communication in the brain," *Philos Trans R Soc L. B Biol Sci*, vol. 369, no. 1654, p. 20130609, 2014.

[60] S. Sahara, Y. Yanagawa, D. D. O'Leary, and C. F. Stevens, "The fraction of cortical GABAergic neurons is constant from near the start of cortical neurogenesis to adulthood," *J Neurosci*, vol. 32, no. 14, pp. 4755–4761, 2012.

[61] C. Lüscher and R. C. Malenka, "NMDA receptor-dependent long-term

potentiation and long-term depression (LTP/LTD).," *Cold Spring Harb. Perspect. Biol.*, vol. 4, no. 6, Jun. 2012.

[62] R. A. Crozier, C. Bi, Y. R. Han, and M. R. Plummer, "BDNF modulation of NMDA receptors is activity dependent.," *J. Neurophysiol.*, vol. 100, no. 6, pp. 3264–74, Dec. 2008.

[63] M. P. Mattson, "Glutamate and neurotrophic factors in neuronal plasticity and disease," *Ann N Y Acad Sci*, vol. 1144, pp. 97–112, 2008.

[64] C. Porcher, I. Medina, and J.-L. Gaiarsa, "Mechanism of BDNF Modulation in GABAergic Synaptic Transmission in Healthy and Disease Brains," *Front. Cell. Neurosci.*, vol. 12, p. 273, Aug. 2018.

[65] L. K. Bak, A. Schousboe, and H. S. Waagepetersen, "The glutamate/GABA-glutamine cycle: aspects of transport, neurotransmitter homeostasis and ammonia transfer," *J Neurochem*, vol. 98, no. 3, pp. 641–653, 2006.

[66] C. J. Stagg, "Magnetic Resonance Spectroscopy as a tool to study the role of GABA in motor-cortical plasticity," *Neuroimage*, vol. 86, pp. 19–27, 2014.

[67] O. A. Petroff, "GABA and glutamate in the human brain," *Neuroscientist*, vol. 8, no. 6, pp. 562–573, 2002.

[68] T. Klausberger *et al.*, "Brain-state and cell-type specific firing of hippocampal interneurons in vivo," *Nature*, vol. 421, no. 6925, pp. 844–848, 2003.

[69] P. Kowiański, G. Lietzau, E. Czuba, M. Waśkow, A. Steliga, and J. Moryś, "BDNF: A Key Factor with Multipotent Impact on Brain Signaling and Synaptic Plasticity.," *Cell. Mol. Neurobiol.*, vol. 38, no. 3, pp. 579–593, Apr. 2018.

[70] H. S. Waagepetersen, U. Sonnewald, and A. Schousboe, "Compartmentation of glutamine, glutamate, and GABA metabolism in neurons and astrocytes: functional implications," *Neuroscientist*, vol. 9, no. 5, pp. 398–403, 2003.

[71] L. Chang, C. C. Cloak, and T. Ernst, "Magnetic resonance spectroscopy studies of GABA in neuropsychiatric disorders," *J Clin Psychiatry*, vol. 64 Suppl 3, pp. 7–14, 2003.

[72] C. J. Stagg, V. Bachtiar, and H. Johansen-Berg, "What are we measuring with GABA magnetic resonance spectroscopy?," *Commun Integr Biol*, vol. 4, no. 5, pp. 573–575, 2011.

[73] Y. Ke, B. M. Cohen, J. Y. Bang, M. Yang, and P. F. Renshaw, "Assessment of GABA concentration in human brain using two-dimensional proton magnetic resonance spectroscopy," *Psychiatry Res*, vol. 100, no. 3, pp. 169–178, 2000.

[74] D. L. Rothman, O. A. Petroff, K. L. Behar, and R. H. Mattson, "Localized 1H NMR measurements of gamma-aminobutyric acid in human brain in vivo," *Proc Natl Acad Sci U S A*, vol. 90, no. 12, pp. 5662–5666, 1993.

[75] S. Ramadan, A. Lin, and P. Stanwell, "Glutamate and glutamine: a review of in vivo MRS in the human brain," *NMR Biomed*, vol. 26, no. 12, pp. 1630–1646, 2013.

[76] A. Dennis *et al.*, "An Ultra-High Field Magnetic Resonance Spectroscopy Study of Post Exercise Lactate, Glutamate and Glutamine Change in the Human Brain," *Front Physiol*, vol. 6, p. 351, 2015.

[77] R. J. Maddock, G. A. Casazza, D. H. Fernandez, and M. I. Maddock, "Acute Modulation of Cortical Glutamate and GABA Content by Physical Activity," *J Neurosci*, vol. 36, no. 8, pp. 2449–2457, 2016.

[78] R. J. Maddock, G. A. Casazza, M. H. Buonocore, and C. Tanase, "Vigorous exercise increases brain lactate and Glx (glutamate+glutamine): a dynamic 1H-MRS study," *Neuroimage*, vol. 57, no. 4, pp. 1324–1330, 2011.

[79] L. Hertz and M. Fillenz, "Does the 'mystery of the extra glucose' during CNS activation reflect glutamate synthesis?," *Neurochem Int*, vol. 34, no. 1, pp. 71–75, 1999.

[80] H. S. Waagepetersen, I. J. Bakken, O. M. Larsson, U. Sonnewald, and A. Schousboe, "Comparison of lactate and glucose metabolism in cultured neocortical neurons and astrocytes using 13C-NMR spectroscopy," *Dev Neurosci*, vol. 20, no. 4–5, pp. 310–320, 1998.

[81] L. Hertz and G. A. Dienel, "Lactate transport and transporters: general principles and functional roles in brain cells," *J Neurosci Res*, vol. 79, no. 1–2, pp. 11–18, 2005.

[82] T. Lulic, J. El-Sayes, H. J. Fassett, and A. J. Nelson, "Physical activity levels determine exercise-induced changes in brain excitability," *PLoS One*, vol. 12, no. 3, p. e0173672, 2017.

[83] K. M. McGregor *et al.*, "Physical activity and neural correlates of aging: a combined TMS/fMRI study," *Behav Brain Res*, vol. 222, no. 1, pp. 158–168, 2011.

[84] K. M. McGregor, B. Crosson, K. Mammino, J. Omar, P. S. García, and J. R. Nocera, "Influences of 12-Week Physical Activity Interventions on TMS Measures of Cortical Network Inhibition and Upper Extremity Motor Performance in Older Adults-A Feasibility Study.," *Front. Aging Neurosci.*, vol. 9, p. 422, 2017.

[85] J. Cirillo, A. P. Lavender, M. C. Ridding, and J. G. Semmler, "Motor cortex plasticity induced by paired associative stimulation is enhanced in physically active individuals," *J Physiol*, vol. 587, no. Pt 24, pp. 5831–5842, 2009.

[86] K. M. McGregor *et al.*, "Aging, aerobic activity and interhemispheric communication," *Brain Sci*, vol. 2, no. 4, pp. 634–648, 2012.

[87] H. Hassanlouei, C. W. Sundberg, A. E. Smith, A. Kuplic, and S. K. Hunter, "Physical activity modulates corticospinal excitability of the lower limb in young and old adults," *J Appl Physiol*, vol. 123, no. 2, pp. 364–374, 2017.

[88] G. Distefano *et al.*, "Physical activity unveils the relationship between mitochondrial energetics, muscle quality, and physical function in older adults.," *J. Cachexia. Sarcopenia Muscle*, vol. 9, no. 2, pp. 279–294, Apr. 2018.

[89] S. Trappe, N. Luden, K. Minchev, U. Raue, B. Jemiolo, and T. A. Trappe, "Skeletal muscle signature of a champion sprint runner.," *J. Appl. Physiol.*, vol. 118, no. 12, pp. 1460–6, Jun. 2015.

[90] Z. Kazior *et al.*, "Endurance Exercise Enhances the Effect of Strength Training on Muscle Fiber Size and Protein Expression of Akt and mTOR.," *PLoS One*, vol. 11, no. 2, p. e0149082, 2016.

[91] K. M. McGregor *et al.*, "Effects of aerobic fitness on aging-related changes of interhemispheric inhibition and motor performance," *Front Aging Neurosci*, vol. 5, p. 66, 2013.

[92] K. N. Wood, R. Nikolov, and J. K. Shoemaker, "Impact of Long-Term Endurance Training vs. Guideline-Based Physical Activity on Brain Structure in Healthy Aging," *Front Aging Neurosci*, vol. 8, p. 155, 2016.

[93] L. S. Jonasson, L. Nyberg, A. F. Kramer, A. Lundquist, K. Riklund, and C. J. Boraxbekk, "Aerobic Exercise Intervention, Cognitive Performance, and Brain Structure: Results from the Physical Influences on Brain in Aging (PHIBRA) Study," *Front Aging Neurosci*, vol. 8, p. 336, 2016.

[94] K. I. Erickson *et al.*, "Interactive effects of fitness and hormone treatment on brain health in postmenopausal women," *Neurobiol. Aging*, vol. 28, no. 2, pp. 179–185, Feb. 2007.

[95] B. L. Marks, L. M. Katz, M. Styner, and J. K. Smith, "Aerobic fitness and obesity: relationship to cerebral white matter integrity in the brain of active and sedentary older adults," *Br J Sport. Med*, vol. 45, no. 15, pp. 1208–1215, 2011.

[96] L. E. Oberlin *et al.*, "White matter microstructure mediates the relationship between cardiorespiratory fitness and spatial working memory in older adults," *Neuroimage*, vol. 131, pp. 91–101, 2016.

[97] B. Y. Tseng *et al.*, "White matter integrity in physically fit older adults," *Neuroimage*, vol. 82, pp. 510–516, 2013.

[98] R. A. Edden, N. A. Puts, A. D. Harris, P. B. Barker, and C. J. Evans, "Gannet: A batch-processing tool for the quantitative analysis of gamma-aminobutyric acid-edited MR spectroscopy spectra," *J Magn Reson Imaging*, vol. 40, no. 6, pp. 1445–1452, 2014.

[99] A. D. Harris, N. A. J. Puts, and R. A. E. Edden, "Tissue correction for GABA-edited MRS: Considerations of voxel composition, tissue segmentation, and tissue relaxations," *J Magn Reson Imaging*, vol. 42, no. 5, pp. 1431–1440, 2015.

[100] J. Ashburner and K. J. Friston, "Unified segmentation," *Neuroimage*, vol. 26, no. 3, pp. 839–851, Jul. 2005.

[101] F. Gao *et al.*, "Edited magnetic resonance spectroscopy detects an age-related decline in brain GABA levels," *Neuroimage*, vol. 78, pp. 75–82, 2013.

[102] M. Mikkelsen, K. D. Singh, P. Sumner, and C. J. Evans, "Comparison of the repeatability of GABA-edited magnetic resonance spectroscopy with and without macromolecule suppression," *Magn Reson Med*, vol. 75, no. 3, pp. 946–953, 2016.

[103] C. J. Evans, D. J. McGonigle, and R. A. Edden, "Diurnal stability of gamma-aminobutyric acid concentration in visual and sensorimotor cortex," *J Magn Reson Imaging*, vol. 31, no. 1, pp. 204–209, 2010.

[104] S. Tayoshi *et al.*, "GABA concentration in schizophrenia patients and the effects of antipsychotic medication: A proton magnetic resonance spectroscopy study," *Schizophr. Res.*, vol. 117, no. 1, pp. 83–91, Mar. 2010.

[105] A. D. Harris *et al.*, "Impact of frequency drift on gamma-aminobutyric acid-edited MR spectroscopy," *Magn Reson Med*, vol. 72, no. 4, pp. 941–948, 2014.

[106] S. Y. Tsai, C. H. Fang, T. Y. Wu, and Y. R. Lin, "Effects of Frequency Drift on the Quantification of Gamma-Aminobutyric Acid Using MEGA-PRESS," *Sci Rep*, vol. 6, p. 24564, 2016.

[107] M. Mikkelsen *et al.*, "Big GABA: Edited MR spectroscopy at 24 research sites," *Neuroimage*, vol. 159, pp. 32–45, 2017.

[108] M. M. Mielke, P. Vemuri, and W. A. Rocca, "Clinical epidemiology of Alzheimer's disease: assessing sex and gender differences," in *Clin Epidemiol*, vol. 6, 2014, pp. 37–48.

[109] M. T. Ferretti *et al.*, "Sex differences in Alzheimer disease — the gateway to

precision medicine," *Nat. Rev. Neurol.*, Jul. 2018.

[110] R. W. Persky, L. C. Turtzo, and L. D. McCullough, "Stroke in women: disparities and outcomes," *Curr Cardiol Rep*, vol. 12, no. 1, pp. 6–13, 2010.

[111] C. T. Albinet, K. Mandrick, P. L. Bernard, S. Perrey, and H. Blain, "Improved cerebral oxygenation response and executive performance as a function of cardiorespiratory fitness in older women: a fNIRS study," *Front Aging Neurosci*, vol. 6, p. 272, 2014.

[112] A. D. Brown *et al.*, "Effects of cardiorespiratory fitness and cerebral blood flow on cognitive outcomes in older women," *Neurobiol Aging*, vol. 31, no. 12, pp. 2047–2057, Dec. 2010.

[113] O. Dupuy *et al.*, "Higher levels of cardiovascular fitness are associated with better executive function and prefrontal oxygenation in younger and older women," *Front Hum Neurosci*, vol. 9, p. 66, Feb. 2015.

[114] J. Weuve, J. H. Kang, J. E. Manson, M. M. Breteler, J. H. Ware, and F. Grodstein, "Physical activity, including walking, and cognitive function in older women," *Jama*, vol. 292, no. 12, pp. 1454–1461, 2004.

[115] N. F. Johnson, C. Kim, J. L. Clasey, A. Bailey, and B. T. Gold, "Cardiorespiratory fitness is positively correlated with cerebral white matter integrity in healthy seniors," *Neuroimage*, vol. 59, no. 2, pp. 1514–1523, 2012.

[116] R. C. Oldfield, "The assessment and analysis of handedness: the Edinburgh inventory.," *Neuropsychologia*, vol. 9, no. 1, pp. 97–113, Mar. 1971.

[117] Z. Al-Safi and N. Santoro, *The Postmenopausal Woman*. MDText.com, Inc., 2000.

[118] Z. S. Nasreddine *et al.*, "The Montreal Cognitive Assessment, MoCA: A Brief Screening Tool For Mild Cognitive Impairment," *J. Am. Geriatr. Soc.*, vol. 53, no. 4, pp. 695–699, Apr. 2005.

[119] C. L. Craig *et al.*, "International Physical Activity Questionnaire: 12-Country Reliability and Validity," *Med. Sci. Sport. Exerc.*, vol. 35, no. 8, pp. 1381–1395,

Aug. 2003.

[120] S. D. Ball, "Interdevice variability in percent fat estimates using the BOD POD," *Eur. J. Clin. Nutr.*, vol. 59, no. 9, pp. 996–1001, Sep. 2005.

[121] P.-O. Åstrand and I. Ryhming, "A Nomogram for Calculation of Aerobic Capacity (Physical Fitness) From Pulse Rate During Submaximal Work," *J. Appl. Physiol.*, vol. 7, no. 2, pp. 218–221, Sep. 1954.

[122] S. F. Siconolfi, E. M. Cullinane, R. A. Carleton, and P. D. Thompson, "Assessing VO2max in epidemiologic studies: modification of the Astrand-Rhyming test," *Med Sci Sport. Exerc*, vol. 14, no. 5, pp. 335–338, 1982.

[123] L. S. Pescatello, A. Ross, R. Deborah, and P. D. Thompson, *ACSM's Guidelines for Exercise Testing and Prescription 9th Ed. 2014*, 9th ed. Philadelphia: Wolters Kluwer/Lippincott Williams & Wilkins, 2014.

[124] D. E. R. Warburton *et al.*, "Evidence-based risk assessment and recommendations for physical activity clearance: Consensus Document 2011.," *Appl. Physiol. Nutr. Metab.*, vol. 36, no. S1, pp. S266–S298, Jul. 2011.

[125] A. Macsween, "The reliability and validity of the Astrand nomogram and linear extrapolation for deriving VO2max from submaximal exercise data.," *J. Sports Med. Phys. Fitness*, vol. 41, no. 3, pp. 312–7, Sep. 2001.

[126] U. Ekelund, P. W. Franks, N. J. Wareham, and J. Åman, "Oxygen Uptakes Adjusted for Body Composition in Normal-Weight and Obese Adolescents," *Obes. Res.*, vol. 12, no. 3, pp. 513–520, Mar. 2004.

[127] L. Hermans *et al.*, "GABA levels and measures of intracortical and interhemispheric excitability in healthy young and older adults: an MRS-TMS study," *Neurobiol Aging*, vol. 65, pp. 168–177, 2018.

[128] T. A. Yousry *et al.*, "Localization of the motor hand area to a knob on the precentral gyrus. A new landmark," *Brain*, vol. 120, no. 1, pp. 141–157, 1997.

[129] F. Sanaei Nezhad, A. Anton, E. Michou, J. Y. Jung, L. M. Parkes, and S. R. Williams, "Quantification of GABA, glutamate and glutamine in a single

measurement at 3 T using GABA-edited MEGA-PRESS," *NMR Biomed.*, vol. 31, no. 1, 2018.

[130] P. W. Sheffield, "Quantification of GLX and STK spin systems in brain at 3T," 2009.

[131] H. M. Schambra *et al.*, "The reliability of repeated TMS measures in older adults and in patients with subacute and chronic stroke," *Front Cell Neurosci*, vol. 9, no. September, p. 335, 2015.

[132] T. J. Carroll, S. Riek, and R. G. Carson, "Reliability of the input-output properties of the cortico-spinal pathway obtained from transcranial magnetic and electrical stimulation," *J. Neurosci. Methods*, vol. 112, no. 2, pp. 193–202, Dec. 2001.

[133] S. N. Kukke, R. W. Paine, C. C. Chao, A. C. de Campos, and M. Hallett, "Efficient and reliable characterization of the corticospinal system using transcranial magnetic stimulation," *J Clin Neurophysiol*, vol. 31, no. 3, pp. 246–252, 2014.

[134] W. Bogner *et al.*, "In vivo quantification of intracerebral GABA by single-voxel (1)H-MRS-How reproducible are the results?," *Eur J Radiol*, vol. 73, no. 3, pp. 526–531, 2010.

[135] R. Kreis, "The trouble with quality filtering based on relative Cramér-Rao lower bounds," *Magn. Reson. Med.*, vol. 75, no. 1, pp. 15–18, Jan. 2016.

[136] B. Fischl, M. I. Sereno, A. M. Dale, B. Fischl, and M. I. Sereno, "Cortical Surface-Based Analysis," *Neuroimage*, vol. 9, no. 2, pp. 179–194, Feb. 1999.

[137] A. M. Dale and M. I. Sereno, "Improved Localizadon of Cortical Activity by Combining EEG and MEG with MRI Cortical Surface Reconstruction: A Linear Approach," *J. Cogn. Neurosci.*, vol. 5, no. 2, pp. 162–176, Apr. 1993.

[138] B. Fischl, M. I. Sereno, R. B. Tootell, and A. M. Dale, "High-resolution intersubject averaging and a coordinate system for the cortical surface.," *Hum. Brain Mapp.*, vol. 8, no. 4, pp. 272–84, 1999.

[139] X. Han *et al.*, "Reliability of MRI-derived measurements of human cerebral cortical thickness: The effects of field strength, scanner upgrade and manufacturer," *Neuroimage*, vol. 32, no. 1, pp. 180–194, Aug. 2006.

[140] J. Jovicich *et al.*, "Reliability in multi-site structural MRI studies: Effects of gradient non-linearity correction on phantom and human data," *Neuroimage*, vol. 30, no. 2, pp. 436–443, Apr. 2006.

[141] F. Ségonne *et al.*, "A hybrid approach to the skull stripping problem in MRI," *Neuroimage*, vol. 22, no. 3, pp. 1060–1075, Jul. 2004.

[142] M. Reuter, H. D. Rosas, and B. Fischl, "Highly accurate inverse consistent registration: a robust approach.," *Neuroimage*, vol. 53, no. 4, pp. 1181–96, Dec. 2010.

[143] M. Reuter, N. J. Schmansky, H. D. Rosas, and B. Fischl, "Within-subject template estimation for unbiased longitudinal image analysis.," *Neuroimage*, vol. 61, no. 4, pp. 1402–18, Jul. 2012.

[144] B. Fischl and A. M. Dale, "Measuring the thickness of the human cerebral cortex from magnetic resonance images.," *Proc. Natl. Acad. Sci. U. S. A.*, vol. 97, no. 20, pp. 11050–5, Sep. 2000.

[145] B. Fischl, A. Liu, and A. M. Dale, "Automated manifold surgery: constructing geometrically accurate and topologically correct models of the human cerebral cortex," *IEEE Trans. Med. Imaging*, vol. 20, no. 1, pp. 70–80, Jan. 2001.

[146] B. Fischl *et al.*, "Whole brain segmentation: automated labeling of neuroanatomical structures in the human brain.," *Neuron*, vol. 33, no. 3, pp. 341–55, Jan. 2002.

[147] B. Fischl *et al.*, "Automatically parcellating the human cerebral cortex.," *Cereb. Cortex*, vol. 14, no. 1, pp. 11–22, Jan. 2004.

[148] B. Fischl *et al.*, "Sequence-independent segmentation of magnetic resonance images," *Neuroimage*, vol. 23, pp. S69–S84, Jan. 2004.

[149] C. S. McCarthy, A. Ramprashad, C. Thompson, J.-A. Botti, I. L. Coman, and W.

R. Kates, "A comparison of FreeSurfer-generated data with and without manual intervention.," *Front. Neurosci.*, vol. 9, p. 379, 2015.

[150] B. Fischl *et al.*, "Cortical folding patterns and predicting cytoarchitecture.," *Cereb. Cortex*, vol. 18, no. 8, pp. 1973–80, Aug. 2008.

[151] M. A. Fletcher *et al.*, "Comparing Aging and Fitness Effects on Brain Anatomy," *Front Hum Neurosci*, vol. 10, p. 286, 2016.

[152] A. M. Weinstein *et al.*, "The association between aerobic fitness and executive function is mediated by prefrontal cortex volume," *Brain Behav Immun*, vol. 26, no. 5, pp. 811–819, 2012.

[153] R. S. Desikan *et al.*, "An automated labeling system for subdividing the human cerebral cortex on MRI scans into gyral based regions of interest," *Neuroimage*, vol. 31, no. 3, pp. 968–980, Jul. 2006.

[154] K. Im, J.-M. Lee, O. Lyttelton, S. H. Kim, A. C. Evans, and S. I. Kim, "Brain Size and Cortical Structure in the Adult Human Brain," *Cereb. Cortex*, vol. 18, no. 9, pp. 2181–2191, Sep. 2008.

[155] M. Jenkinson, C. F. Beckmann, T. E. J. Behrens, M. W. Woolrich, and S. M. Smith, "FSL," *Neuroimage*, vol. 62, no. 2, pp. 782–790, Aug. 2012.

[156] S. M. Smith, "Fast robust automated brain extraction," *Hum. Brain Mapp.*, vol. 17, no. 3, pp. 143–155, Nov. 2002.

[157] J. L. R. Andersson and S. N. Sotiropoulos, "An integrated approach to correction for off-resonance effects and subject movement in diffusion MR imaging.," *Neuroimage*, vol. 125, pp. 1063–1078, Jan. 2016.

[158] T. E. J. Behrens *et al.*, "Characterization and propagation of uncertainty in diffusion-weighted MR imaging," *Magn. Reson. Med.*, vol. 50, no. 5, pp. 1077–1088, Nov. 2003.

[159] T. E. J. Behrens, H. J. Berg, S. Jbabdi, M. F. S. Rushworth, and M. W. Woolrich, "Probabilistic diffusion tractography with multiple fibre orientations: What can we gain?," *Neuroimage*, vol. 34, no. 1, pp. 144–155, Jan. 2007.

[160] S. M. Smith *et al.*, "Tract-based spatial statistics: Voxelwise analysis of multi-subject diffusion data," *Neuroimage*, vol. 31, no. 4, pp. 1487–1505, Jul. 2006.

[161] J. L. R. Andersson, M. Jenkinson, S. Smith, and J. Andersson, "Non-linear optimisation FMRIB Technial Report TR07JA1," 2007.

[162] J. L. R. Andersson, M. Jenkinson, and S. Smith, "Non-linear registration, aka Spatial normalisation FMRIB technical report TR07JA2," 2007.

[163] D. Rueckert, L. I. Sonoda, C. Hayes, D. L. G. Hill, M. O. Leach, and D. J. Hawkes, "Nonrigid registration using free-form deformations: application to breast MR images," *IEEE Trans. Med. Imaging*, vol. 18, no. 8, pp. 712–721, Aug. 1999.

[164] D. B. Archer, D. E. Vaillancourt, and S. A. Coombes, "A Template and Probabilistic Atlas of the Human Sensorimotor Tracts using Diffusion MRI," *Cereb. Cortex*, vol. 28, no. 5, pp. 1685–1699, May 2018.

[165] H. J. Motulsky and R. E. Brown, "Detecting outliers when fitting data with nonlinear regression - a new method based on robust nonlinear regression and the false discovery rate.," *BMC Bioinformatics*, vol. 7, p. 123, Mar. 2006.

[166] I. Astrand, "Aerobic work capacity in men and women with special reference to age.," *Acta Physiol. Scand. Suppl.*, vol. 49, no. 169, pp. 1–92, 1960.

[167] S. S. Kantak, J. W. Stinear, E. R. Buch, and L. G. Cohen, "Rewiring the brain: potential role of the premotor cortex in motor control, learning, and recovery of function following brain injury.," *Neurorehabil. Neural Repair*, vol. 26, no. 3, pp. 282–92, 2012.

[168] A. Sridharan *et al.*, "Brain volumetric and microstructural correlates of executive and motor performance in aged rhesus monkeys.," *Front. Aging Neurosci.*, vol. 4, p. 31, 2012.

[169] E. V Sullivan, T. Rohlfing, and A. Pfefferbaum, "Quantitative fiber tracking of lateral and interhemispheric white matter systems in normal aging: relations to timed performance.," *Neurobiol. Aging*, vol. 31, no. 3, pp. 464–81, Mar. 2010.

[170] X. Wang, M. Casadio, K. A. Weber, F. A. Mussa-Ivaldi, T. B. Parrish, and T. B. Parrish, "White matter microstructure changes induced by motor skill learning utilizing a body machine interface.," *Neuroimage*, vol. 88, pp. 32–40, 2014.

[171] R. Schulz, M. Zimerman, J. E. Timmermann, M. J. Wessel, C. Gerloff, and F. C. Hummel, "White matter integrity of motor connections related to training gains in healthy aging," *Neurobiol. Aging*, vol. 35, no. 6, pp. 1404–1411, Jun. 2014.

[172] M. R. Borich, S. M. Brodie, W. A. Gray, S. Ionta, and L. A. Boyd, "Understanding the role of the primary somatosensory cortex: Opportunities for rehabilitation.," *Neuropsychologia*, vol. 79, no. Pt B, pp. 246–55, Dec. 2015.

[173] W. Debowska, T. Wolak, A. Nowicka, A. Kozak, M. Szwed, and M. Kossut, "Functional and Structural Neuroplasticity Induced by Short-Term Tactile Training Based on Braille Reading.," *Front. Neurosci.*, vol. 10, p. 460, 2016.

[174] R. D. Seidler *et al.*, "Motor control and aging: links to age-related brain structural, functional, and biochemical effects.," *Neurosci. Biobehav. Rev.*, vol. 34, no. 5, pp. 721–33, Apr. 2010.

[175] T. Kalisch, P. Ragert, P. Schwenkreis, H. R. Dinse, and M. Tegenthoff, "Impaired Tactile Acuity in Old Age Is Accompanied by Enlarged Hand Representations in Somatosensory Cortex," *Cereb. Cortex*, vol. 19, no. 7, pp. 1530–1538, Jul. 2009.

[176] K. I. Erickson, R. L. Leckie, and A. M. Weinstein, "Physical activity, fitness, and gray matter volume," *Neurobiol. Aging*, vol. 35, pp. S20–S28, Sep. 2014.

[177] K. I. Erickson *et al.*, "Aerobic fitness is associated with hippocampal volume in elderly humans," *Hippocampus*, vol. 19, no. 10, pp. 1030–1039, 2009.

[178] K. Kantarci *et al.*, "Diffusion tensor imaging and cognitive function in older adults with no dementia.," *Neurology*, vol. 77, no. 1, pp. 26–34, Jul. 2011.

[179] A. M. Winkler *et al.*, "Cortical thickness or grey matter volume? The importance of selecting the phenotype for imaging genetics studies.," *Neuroimage*, vol. 53, no. 3, pp. 1135–46, Nov. 2010.

[180] C. J. Molin and A. R. Punga, "Compound Motor Action Potential:

Electrophysiological Marker for Muscle Training," *J. Clin. Neurophysiol.*, vol. 33, no. 4, pp. 340–345, Aug. 2016.

[181] T. Kawagoe, K. Onoda, and S. Yamaguchi, "Associations among executive function, cardiorespiratory fitness, and brain network properties in older adults," *Sci Rep*, vol. 7, p. 40107, 2017.

[182] H. Guiney, S. J. Lucas, J. D. Cotter, and L. Machado, "Evidence cerebral blood-flow regulation mediates exercise-cognition links in healthy young adults," *Neuropsychology*, vol. 29, no. 1, pp. 1–9, 2015.

[183] T. D. Verstynen *et al.*, "Caudate Nucleus Volume Mediates the Link between Cardiorespiratory Fitness and Cognitive Flexibility in Older Adults," *J Aging Res*, vol. 2012, p. 939285, 2012.

[184] S. M. Hayes, J. P. Hayes, V. J. Williams, H. Liu, and M. Verfaellie, "FMRI activity during associative encoding is correlated with cardiorespiratory fitness and source memory performance in older adults," *Cortex*, vol. 91, pp. 208–220, 2017.

[185] K. Holzschneider, T. Wolbers, B. Roder, and K. Hotting, "Cardiovascular fitness modulates brain activation associated with spatial learning," *Neuroimage*, vol. 59, no. 3, pp. 3003–3014, 2012.

[186] S. Kumpulainen *et al.*, "Differential modulation of motor cortex plasticity in skill- and endurance-trained athletes," *Eur J Appl Physiol*, vol. 115, no. 5, pp. 1107–1115, 2015.

[187] J. List *et al.*, "Relationship between excitability, plasticity and thickness of the motor cortex in older adults," *Neuroimage*, vol. 83, pp. 809–816, Dec. 2013.

[188] T. E. Kearney-Ramos, D. H. Lench, M. Hoffman, B. Correia, L. T. Dowdle, and C. A. Hanlon, "Gray and white matter integrity influence TMS signal propagation: a multimodal evaluation in cocaine-dependent individuals," *Sci. Rep.*, vol. 8, no. 1, p. 3253, Dec. 2018.

[189] M. R. Borich, J. L. Neva, and L. A. Boyd, "Evaluation of differences in brain

neurophysiology and morphometry associated with hand function in individuals with chronic stroke.," *Restor. Neurol. Neurosci.*, vol. 33, no. 1, pp. 31–42, 2015.

[190] M. Inghilleri, A. Conte, A. Curra, V. Frasca, C. Lorenzano, and A. Berardelli, "Ovarian hormones and cortical excitability. An rTMS study in humans," *Clin Neurophysiol*, vol. 115, no. 5, pp. 1063–1068, 2004.

[191] A. M. Singh, R. E. Duncan, J. L. Neva, and W. R. Staines, "Aerobic exercise modulates intracortical inhibition and facilitation in a nonexercised upper limb muscle," *BMC Sport. Sci Med Rehabil*, vol. 6, p. 23, 2014.

[192] C. L. Tsai, C. Y. Pan, F. C. Chen, C. H. Wang, and F. Y. Chou, "Effects of acute aerobic exercise on a task-switching protocol and brain-derived neurotrophic factor concentrations in young adults with different levels of cardiorespiratory fitness," *Exp Physiol*, vol. 101, no. 7, pp. 836–850, 2016.

[193] A. M. Singh, J. L. Neva, and W. R. Staines, "Aerobic exercise enhances neural correlates of motor skill learning," *Behav Brain Res*, vol. 301, pp. 19–26, 2016.

[194] C. S. Mang, K. L. Campbell, C. J. Ross, and L. A. Boyd, "Promoting neuroplasticity for motor rehabilitation after stroke: considering the effects of aerobic exercise and genetic variation on brain-derived neurotrophic factor," *Phys Ther*, vol. 93, no. 12, pp. 1707–1716, 2013.

[195] T. Huang, K. T. Larsen, M. Ried-Larsen, N. C. Moller, and L. B. Andersen, "The effects of physical activity and exercise on brain-derived neurotrophic factor in healthy humans: A review," *Scand J Med Sci Sport.*, vol. 24, no. 1, pp. 1–10, 2014.

[196] J. A. Kleim *et al.*, "BDNF val66met polymorphism is associated with modified experience-dependent plasticity in human motor cortex," *Nat. Neurosci.*, vol. 9, no. 6, pp. 735–737, Jun. 2006.

[197] S. A. McHughen *et al.*, "BDNF Val66Met Polymorphism Influences Motor System Function in the Human Brain," *Cereb. Cortex*, vol. 20, no. 5, pp. 1254–1262, May 2010.

[198] M. E. Hopkins, F. C. Davis, M. R. Vantieghem, P. J. Whalen, and D. J. Bucci, "Differential effects of acute and regular physical exercise on cognition and affect.," *Neuroscience*, vol. 215, pp. 59–68, Jul. 2012.

[199] M. F. Egan *et al.*, "The BDNF val66met polymorphism affects activity-dependent secretion of BDNF and human memory and hippocampal function," *Cell*, vol. 112, no. 2, pp. 257–269, 2003.